Microwave Absorption of Multifunctional Graphene Based Polylactide Acid Composites: Experimental and Numerical Study

by

Mahima Dua

A thesis submitted in partial fulfillment of the requirements for the degree of

Master of Science

Department of Mechanical Engineering

University of Alberta

Abstract

Thermoplastic polymer piping is increasingly used in a variety of industries. Thermoplastics permit fusion bonding for the joining of pipe sections, which can be performed using joule heating. However, embedding heating wires into the plastic adds fabrication complexity and expenditure. Moreover, joule heating enables only localized heat input that requires moderation to avoid damage in polymers. Another key factor linked to failure with this joining method is joint misalignment. Microwave heating may compensate for these inadequacies, resulting in shorter fusing times, improved heating uniformity, and lower electricity use. This study explores the use of pure graphene nanoplatelets (pGNP) and functionalized GNP (fGNP) to create multifunctional polylactide acid (PLA) composites for high microwave absorption. GNP was treated with tannic acid to produce fGNP. A two-step scalable fabrication procedure, consisting of solution blending followed by hot compression molding was used to obtain the pGNP/PLA and fGNP/PLA composites. The concentration of GNP and fGNP in the composites ranged from 0 to 8 wt%. The resulting composites were characterized for their heat capacity, thermal and electrical conductivity, and complex permittivity. Thermal imaging was used to investigate the efficacy of microwave heating in pGNP/PLA and fGNP/PLA samples as a function of microwave power and filler weight fractions. Multi-physics finite element software was used to explore and simulate the microwave heating mechanism in GNP composites. The experimental results were compared to numerical model predictions for maximum temperature and microwave energy absorbed. The produced nanocomposites were found to exhibit strong microwave absorption and thus rapid heating, making this type of composite a promising candidate for gasket materials that facilitate fusion bonding in thermoplastic-based piping via localized heating.

Acknowledgements

I would like to offer my deepest gratitude to my supervisor, Dr. Pierre Mertiny, for his unwavering support and guidance throughout the course of this program. I acknowledge him for offering me this wonderful opportunity, which has aided in my development as a learner and researcher. Thank you, for supporting every trivial idea that I had no matter what the cost was. Thank you, for letting me learn from my own mistakes. In addition, I want to thank you for all your assistance in writing this thesis and the research papers. Moreover, I am extremely appreciative for the many opportunities you have given me to present my work at many venues. I am sure no other supervisor would have supported their students to this extent. I look forward to continuing working with you on my PhD project.

I would like to express my thanks to Shawcor Ltd., the Natural Sciences and Engineering Research Council of Canada (NSERC), and MITACS for providing the financial support for the project. This project enriched my experience by involving me in an exciting product development project but also introduced me to a team of knowledgeable and passionate people.

I offer my enduring gratitude to the faculty, staff, and my fellow students at University of Alberta, who have inspired me to continue my work in this field. Thank you, Drs. Miles Skinner and Hadi Nazaripoor, for the fruitful discussions that inspired many new ideas for this research work. Thank you, Dr. Balakrishnan Nagaranjan, for training me on the Thermtest machine and providing me with guidance. I truly lost track of all your support throughout the duration of this project.

I would also like to express my appreciation to Drs. Ramin Khosravi and Rashid Mirzavand (University of Alberta) and Drs. Bahram Mirkhani and Uttandaraman Sundararaj (University of Calgary) for their assistance with assessing complex permittivity, and specific heat capacity and electrical conductivity, respectively.

Finally, I would like to thank my friends and family for their unconditional support and continuous encouragement. Thank you to all my friends who have assisted me in my endeavor; without their assistance and companionship, I would not have been able to progress. My family deserves special recognition for their unfailing love and support, and for never giving up on me. I would not be who I am now without their endless support.

Table of Contents

List of Tables

List of Figures

List of Symbols

β: Propagation constant

ΔT: Change in temperature

ε: Permittivity of the material

ε_0: Permittivity of the material in air

$\varepsilon''_{\text{eff}}$: Effective relative dielectric loss factor

ε': Dielectric constant

ε'': Dielectric loss factor

ε^*: Complex permittivity of the material

ε_r: Relative permittivity

λ: Wavelength in free space

μ: Magnetic permeability

μ_0: Magnetic permeability of air

μ': Permeability of material

μ_{r}: Relative permeability

ρ: Density of the sample

ρ_{c}: Density of nanocomposite

ρ_{f}: Density of fillers

ρ_{m}: Density of matrix

σ: Electrical conductivity

ω: Angular frequency of microwaves

%: Percentage

A: Magnetic vector potential

c: Speed of light

c_0: Speed of light in vacuum

C_p: Specific heat of the material

B: Magnetic flux density

D: Electric displacement

E: Electric field component

E_{rms}: Root mean square of the electric field

E_s: Source electric field

f: Frequency

f_c: Cut-off frequency

h = Planck's Constant

H: Magnetic field component

J: Current density

j: Imaginary unit

J_e: Experimental microwave energy absorbed

J_s: Simulated microwave energy absorbed

k: Thermal Conductivity of the sample

M: Magnetization vector

m: Mass of the material

m_1 and n_1: Mode numbers

n: unit normal to the surface

n_2: outward normal from medium

P_{ABS}: Absorbed power per unit volume

P_v: Electric polarization vector

P_e: Electric power

P_h: Resistive loss

P_m: Magnetic power

P_r: Radiative loss

P: Microwave power absorbed

Q: Heat Source

Q_{rh}: Resistive losses

Q_{ml}: Magnetic losses

S: closed boundary of computation domain

S_P: Poynting vector

t: Microwave exposure time

T: Temperature

$tan\delta$: Dissipation factor

V: computation domain

V_m: Volume of the material

Ve: Electrical scalar potential

W_e: Electric energy

w_f: Weight fraction of the filler

W_m: Magnetic energy

w_{m}: Weight fraction of the matrix

List of Abbreviations

ABS: Acrylonitrile butadiene styrene

CMC: Ceramic matrix composites

CNS: Carbon nanostructures

CNT: Carbon nanotube

Dp: Penetration depth

EM: Electromagnetic

FEM: Finite element method

fGNP: Functionalized graphene nanoplatelets

GC: Graphite coating

GF: Glass fiber

GP: Graphite powder

HDPE: High-density polyethylene

IR: Infrared

LDPE: Low-density polyethylene

MMC: Metal Matrix Composite

MWCNT: Multi-walled carbon nanotube

pGNP: Pure graphene nanoplatelets

PLA: Polylactic acid or polylactide

PMC: Polymer matrix composites

PMMA: Polymethmethyacrylate

PP: Polypropylene

PS: Polystyrene

PTFE: Polytetrafluoroethylene

PU: Polyurethane

SE: Shielding effectiveness

SiC: Silicon carbide

TA: Tannic acid

TC: Critical temperature

TE Mode: Transverse electric mode

TEM Mode: Transverse electromagnetic wave

T_g: Glass transition temperature

TM Mode: Transverse magnetic mode

Wt: Weight

Chapter 1: Introduction

Aspects of the material discussed in this chapter have been presented in the proceedings of The Canadian Society for Mechanical Engineering (CSME) International Congress, University of Alberta, Edmonton, Canada, June 5 - 8, 2022 and published in the proceedings of The Canadian-International Conference on Composites (CANCOM) International Congress, Fredericton-Moncton, NB, Canada, July 12-15, 2022.

1.1 Motivation

Despite international attempts to increase renewable energy generation, the oil and gas sector supplies more than half of the world's total energy demand [1]. Offshore oil and gas production will play a crucial part in the world's future energy supply as more offshore hydrocarbon reserves are discovered. As such, the safe and sustainable transportation of hydrocarbon products remains a critical issue. Offshore pipelines are often regarded as one of the most cost-effective forms of oil and gas transportation because they are thought to be more energy-efficient than other modes of transportation. Metallic piping has a long history, with the oldest known use dating back to the third century in ancient Greece [2]. More recently, thermoplastic polymer piping is emerging as a viable alternative as it provides various advantages over metal pipes, including improved corrosion and fatigue resistance, chemical inertness, flexibility, a higher stiffness-to-weight ratio, and reduced installation and maintenance costs [2]–[4].

As shown in Figure 1, thermoplastic polymer piping for high-pressure service is typically composed of an inner thermoplastic liner, a helically wrapped continuous reinforcement phase, and a thermoplastic outer jacket. The reinforcement phase, which can be dry fiber reinforcement or a polymer composite bonded or unbonded to the inner and outer thermoplastic layers, is the main load-bearing component of the thermoplastic polymer pipe. Common reinforcements are glass or carbon fibers, as well as metallic wires or bands [3]. The pipe is protected from external damage by the polymer outer covering, known as a jacket.

Electrofusion welding via Joule heating is a method used for joining thermoplastic polymer pipes [5]. As shown in Figure 2, this method entails utilizing couplings or fittings to surround the joint to be fused. An electric current passed through metal coils inserted into the fittings generates heat and melts a section of the pipes, leading to the formation of a joint upon solidification. However, incorporating the metal coils into pipe components introduces complexity into the manufacturing process. Failure mechanisms associated with electrofusion joints include misalignment of joints, incorrect dwell time for heating and cooling, and unsuitable welding, cooling, and warming temperatures [6], [7]. In electrofusion welding of thermoplastic polymer pipes, it is recommended to work at temperatures above -15°C. As a result, in cold weather, this operation must be carried out in shelters with temperatures kept within an acceptable range, resulting in additional costs and time-consuming processes [5]. Due to these limitations, innovative procedures are sought-after to effectively and expediently join piping made of advanced materials.

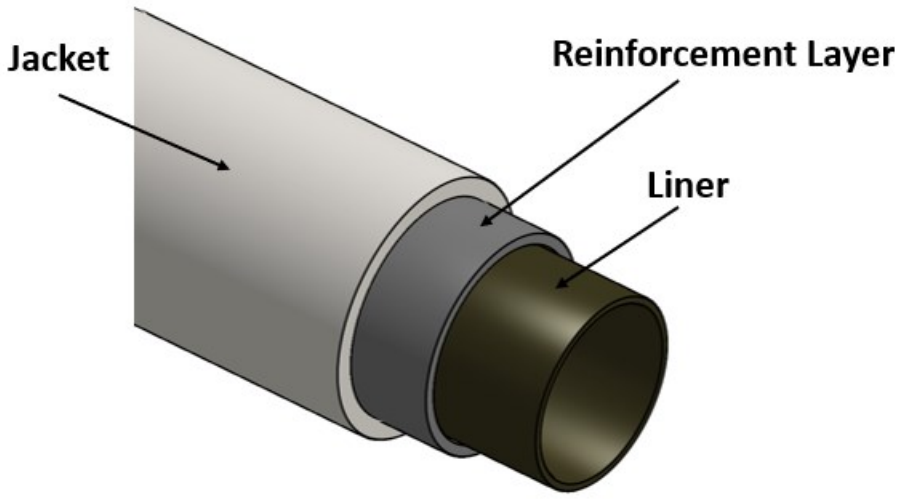

Figure 1: Structure of a Thermoplastic Polymer Pipe (reproduced based on image in [8])

Microwave processing of materials is one such approach. Microwaves were first used for communication purposes [9]. Percy Spencer's 1946 study pioneered the use of microwave radiation to heat surfaces [10]. In the late 1990s, microwave energy became a well-known method

for material processing [11]. Ever since, researchers have used this less-explored source of energy to process important engineering materials, including metals, ceramics, polymers, and their composites [12]. Processing of materials via microwave energy has been proven to be a viable method for sintering [13], [14], drilling [15]–[17], cladding [18], [19], casting [20], [21], and joining [22], [23]. Microwave joining is a type of direct bonding technology that can offer various benefits over traditional joining methods, including quick processing, homogeneous temperature distribution, energy savings, environmental friendliness, welding of complicated geometries, high strength and enhanced joint microstructure [24]–[26].

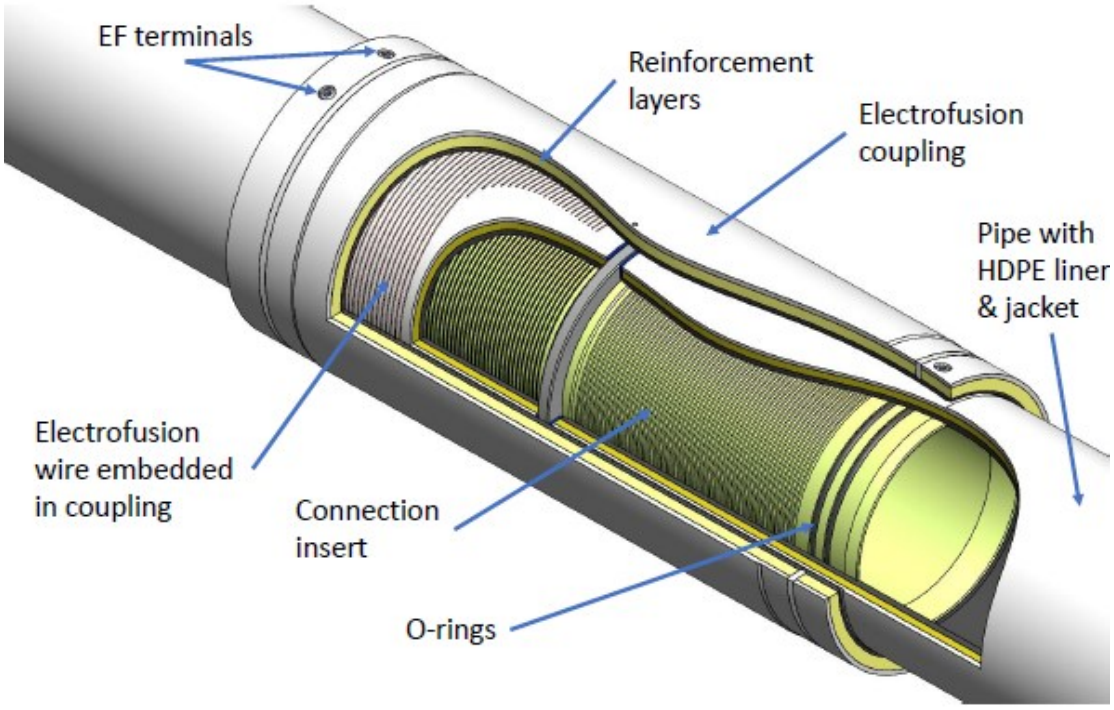

Figure 2: Electrofusion Welding in Thermoplastics

1.2 Thesis Objective

This thesis work is part of a larger collaboration with an industrial partner. The Advanced Composites Materials Engineering Group at the University of Alberta took on the task of exploring the use of pure graphene nanoplatelets (GNP) and modified GNP (fGNP) to create multifunctional

thermoplastic composites for high microwave absorption. Polylactide acid (PLA) was used in this study as a surrogate for the range of thermoplastic polymers used in industrial applications, such as high-density polyethylene (HDPE). The findings provided by this research are used by the industrial partner as an input to guide future process developments for the design and fabrication of polymer-based piping. The underlying research hypothesis is that GNP/PLA composites can be used as a susceptor to facilitate joining of thermoplastic components using microwave irrigation.

To test the above hypothesis, four objectives are considered for this thesis work:

1) Preparation of pGNP/PLA and fGNP/PLA composites by solution mixing. The GNP content in both the materials is varied from 0 to 8 wt% (percentage by weight)

2) Sample characterization of a variety of physical properties, including complex permittivity and permeability, heat capacity, and electrical and thermal conductivity

3) Thermal imaging of samples to investigate the efficacy of microwave heating in pGNP/PLA and fGNP/PLA samples as a function of microwave power and filler weight fractions

4) Explore the microwave heating mechanism in GNP composites using a multi-physics finite element software

1.3 Structure of Thesis

The thesis is divided into six chapters. The first chapter provides motivation behind this work and the second chapter discusses the microwave heating mechanism and earlier works. Material preparation, and experimental set-ups and characterizations are described in Chapter 3. Chapter 4 introduces the numerical modeling set up. Results are presented and discussed in Chapter 5. Model predictions are compared to the experimental results to understand the microwave energy

absorbing property of each specimen type. Chapter 6 summarizes the achievements of this study and makes recommendations for future work.

Chapter 2: Microwave Heating Mechanism

Aspects of the material discussed in this chapter have been presented in the proceedings of The Canadian Society for Mechanical Engineering (CSME) International Congress, University of Alberta, Edmonton, Canada, June 5 - 8, 2022 and published in the proceedings of The Canadian-International Conference on Composites (CANCOM) International Congress, Fredericton-Moncton, NB, Canada, July 12-15, 2022.

2.1 Fundamentals of Microwaves

Microwaves are electromagnetic waves; hence it is essential to first understand electromagnetic waves and the electromagnetic spectrum. Electromagnetic waves are self-propagating waves having electric (E) and magnetic (H) field components that oscillate in phase and perpendicular to each other as well as perpendicular to the propagation direction [27], as illustrated in Figure 3. Electromagnetic waves propagate in a vacuum or in matter and exhibit properties comparable to ordinary waves such as reflection, refraction, diffraction, interference, absorption, and so on.

In vacuum, electromagnetic waves have a constant speed, which includes a relationship between frequency and wavelength (Equation (1)). The Planck equation, Equation (2), may thus be used to predict the energy carried by a certain frequency of an electromagnetic wave [28].

$$c_0 = \lambda \cdot f \tag{1}$$

$$E = h \cdot f \tag{2}$$

where, c_0= speed of light in vacuum, 3.0×10^8 m/s

λ = wavelength in free space (m)

f = frequency (Hz)

h = Planck's Constant, 6.626×10^{-34} Js

Electromagnetic waves are categorized by wavelength into radio waves, microwaves, infrared, light waves, ultraviolet, X-rays, and gamma rays. Figure 4 depicts the electromagnetic spectrum. Microwaves are in the electromagnetic spectrum between infrared radiation and radio frequencies, with a frequency range of around 300 MHz to 300 GHz with a wavelength of 1mm to 1m in vacuum.

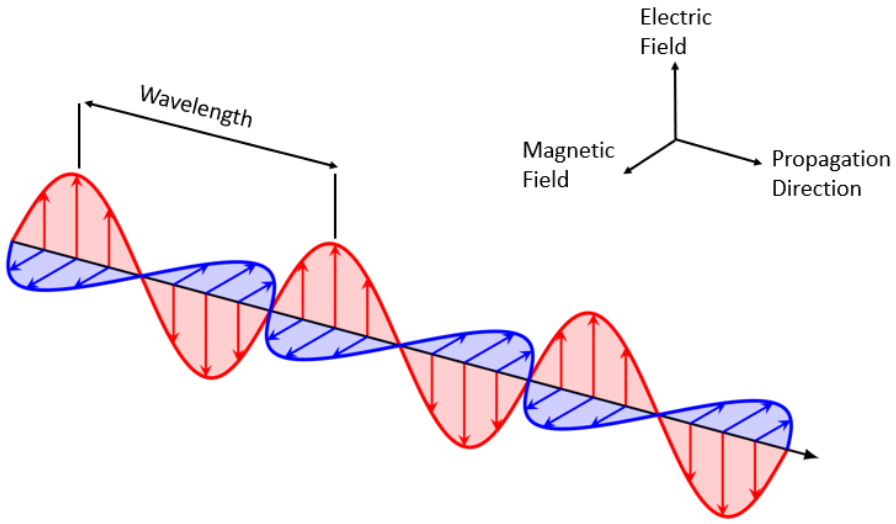

Figure 3: Electric and Magnetic Components of Electromagnetic Waves (reproduced based on image in [29])

According to the Federal Communications Commission [29]–[33], frequencies of 915±25, 2450±13, 5800±75, and 22,125±125 MHz can be utilized for industrial, scientific, and medical purposes. For home and laboratory usage, the most common frequency is 2450 MHz, which has a wavelength of 12.2cm according to Equation 1.

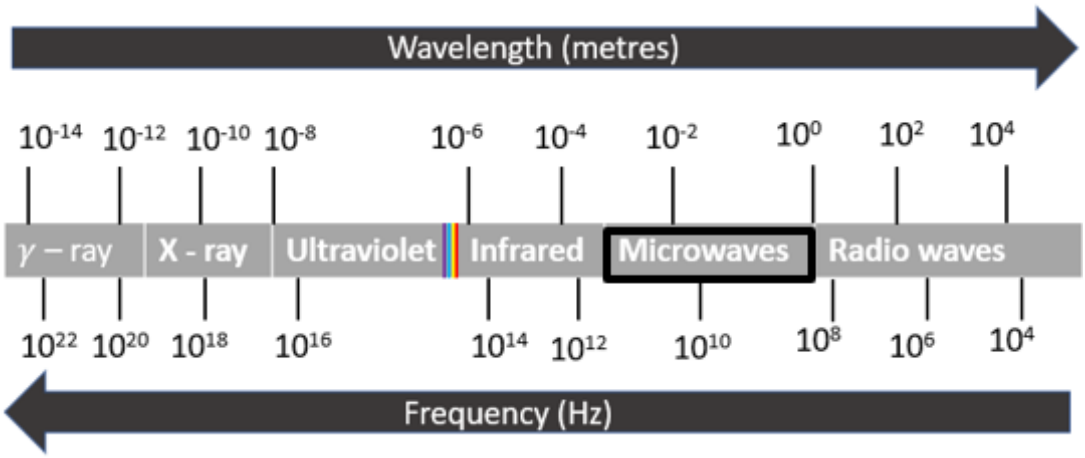

Figure 4: The electromagnetic spectrum depicting the location of microwaves (reproduced based on image in [29])

2.2 Microwave Propagation

Microwaves are generated by a magnetron and transmitted into the chamber of a microwave oven through a waveguide, as shown in Figure 5. The metal walls of the microwave oven act as a Faraday cage. The glass front door and the light bulb chamber are both covered with metal grids. Because the grid holes are small in comparison to the microwave wavelength, they function similarly to metal plates [34]. Once microwaves have been transmitted into the chamber, the metallic walls effectively reflect the microwave radiation. Finally, for the monitoring and adjustment of power to the heated material, a control system is utilized. The cavity shape and size, as well as the applicator type (single mode or multi-mode), have a direct impact on microwave heating efficiency [35]. Most common types of cavities, waveguides, and applicators are discussed in this section.

2.2.1 Cavities

Microwave cavities are structures that are often utilized for electromagnetic wave irradiation of materials. It is a closed structure made up of reflective high-conductivity metal borders for confining electromagnetic energy. Waveguide feeds excite microwave cavities, which support

standing waves. Cavities come in a range of shapes, including rectangular, circular [36], [37], spherical [38], and hexagonal [39], [40].

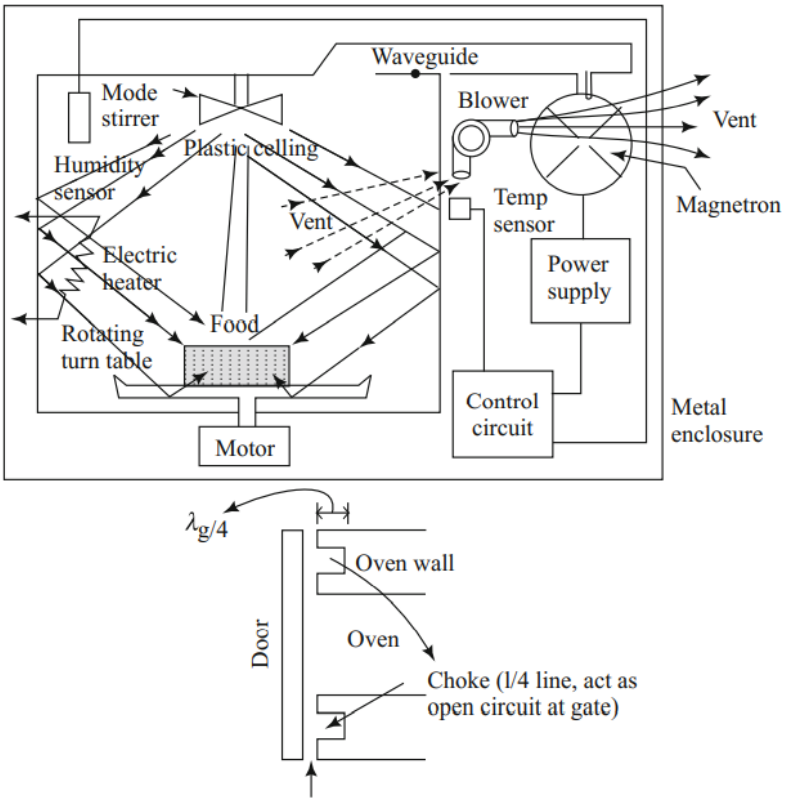

Figure 5: A standard microwave oven's schematic design (reprinted/ adapted by permission from [41] Copyright 2018)

2.2.2 Waveguide modes

Electromagnetic energy is transmitted in waves, which may flow through waveguides in a variety of modes. These distinct forms of waves correlate to the various constituents of an electromagnetic wave. Waveguide modes are as follows:

1) **TE Mode:** Transverse Electric (TE) mode is based on transverse electric waves, often known as H waves. It is distinguished by the fact that the electric field is transverse to the

propagation direction while the magnetic field is normal to the propagation direction. Thus, in the TE mode, the electric field along the propagation direction is zero.

2) **TM Mode:** Transverse magnetic waves, also known as E waves, are differentiated by the fact that the magnetic field is transverse to the direction of propagation, but the electric field is normal to the direction of propagation. Thus, in TM mode, the magnetic field along the propagation path is zero.

3) **TEM Mode:** A transverse electromagnetic wave (or TEM wave) has an electric vector (E vector) and a magnetic vector (H vector) that are both perpendicular to the propagation direction. TEM mode is not achievable in waveguides; it is only possible in coaxial cable and in free space.

2.2.3 Applicators

Applicators are microwave processing chambers. The applicators are categorised as single mode or multi-modal depending on the modes of microwave frequencies emitted by the source.

1) **Single-mode Applicator:** Mono-mode or single-mode microwave ovens can produce a standing wave model, which is caused by the interference of fields with the same amplitude but distinct oscillation orientations. This interface creates a set of nodes with zero microwave energy intensity and a group of antinodes with maximum microwave energy magnitude. The fast rate of heating [42], superior control over microwave system parameters [35], and provision of selective or localised heating [43] are some of the benefits of single-mode equipment. The disadvantages of single-mode equipment are that only one vessel may be irradiated at a time [42], it requires careful component selection to minimise power loss [35], and it is a costly procedure [43].

2) **Multi-Mode Applicator:** This category includes both early microwave ovens and modern home microwave ovens. Multiple modes are induced within a multimode cavity, and the most essential aspect of a multimode device is the deliberate avoidance of developing a standing wave pattern inside the oven cavity. This is done to increase the amount of chaos inside the cavity. The higher the chaos, the larger the dispersion of radiation, which increases the effective heating area [42]. A major limitation of multi-mode equipment is inappropriate sample heating control due to a lack of temperature uniformity. This is partly related to the chaotic nature of the waves, which makes it difficult to evenly heat the samples held inside the oven, thereby resulting in hot and cold areas in the material. However, because of the existence of mode stirrers, multi-mode cavity designs provide a more homogenous electric field and, as a result, more uniform heating inside the cavity [44].

2.3 Fundamentals of Microwave Material Interaction

During the interaction of materials with microwaves, the electrical and magnetic components of microwaves play a significant role in heat generation at the atomic level. The microwave absorption of a material is dependent on its dielectric and magnetic properties because the electric and magnetic field components interact with the substance during irradiation [11], [12]. As a result, the physics of interaction phenomena and the relationships of material properties with microwave electromagnetic properties are crucial in microwave processing. The mathematical model for estimating power absorption, governing equations, and the fundamentals of microwave material interactions are briefly discussed in the following section.

2.3.1 Maxwell's Equations

Maxwell's equations [45] govern the interaction of microwaves with a material [46]. These equations ensure that the electric and magnetic fields vary over time by updating the essential material characteristics involved in energy absorption. The equations are as follows:

$$\nabla \circ E = 0 \tag{3}$$

$$\nabla \circ H = 0 \tag{4}$$

$$\nabla \times E = -j\omega\varepsilon H \tag{5}$$

$$\nabla \times H = j\omega\varepsilon E \tag{6}$$

where, E = electric field vector (Fm^{-1})

H = magnetic field vector (Am^{-1})

ε = permittivity of the material (Fm^{-1})

ω = angular frequency of microwaves (s^{-1})

j = imaginary unit

The complex permittivity (ε*), see Equation (7), is the primary characteristic that describes the energy propagation of the electrical component of electromagnetic radiation within a material [9], [11]. The dielectric constant (ε') is the real part of the complex permittivity, and it represents a material's ability of being polarized by the microwave electric field, thus storing electric energy within the material. The dielectric loss factor (ε'') is the imaginary portion of the complex permittivity, and it represents the material's capacity to dissipate microwave energy into heat. The ability of a material to convert electromagnetic energy into heat is conveniently characterized by the dissipation factor or loss tangent, tan δ, see Equation (8) [47]. The phase difference between the oscillating electric field and the material's polarization is represented by angle δ.

$$\varepsilon* = \varepsilon' - j\varepsilon'' \tag{7}$$

$$\tan\delta = \varepsilon''/\varepsilon' \tag{8}$$

To determine the electric and magnetic field distributions inside a microwave applicator, the Maxwell equations can be solved analytically or numerically with appropriate boundary conditions [48]. Understanding electromagnetic field distribution inside an applicator helps in the appropriate positioning of the material to be heated, resulting in quicker processing [49]. These locations have a strong electromagnetic field strength, which allows microwaves to better couple with materials [27], [48], [49].

2.3.2 Penetration Depth and Power Absorbed

The microwave power absorbed in a material is the power dissipated owing to the electric and magnetic fields of microwave energy, which can be represented as energy changed inside a heated material. Thus, the depth to which radiations enter a material has a considerable impact on the power absorbed by it. Microwaves, however, cannot penetrate within all materials in the same way. Microwave penetration in a non-metallic material is measured in terms of Penetration Depth (*Dp*). It is the distance from the material's surface at which the magnitude of field strength reduces to 1/e or 0.368 of its value at the surface. Mathematically it is represented as [9], [11], [43], [50]:

$$D_P = \frac{1}{\omega \sqrt{\left[0.5\mu_0\mu'\varepsilon_0\varepsilon' \left\{\sqrt{\left(1+\left(\frac{\varepsilon''_{eff}}{\varepsilon'}\right)^2\right)}-1\right\}\right]}} \tag{9}$$

where, μ_0 = magnetic permeability of air (Hm^{-1})

ε_0 = permittivity of the material in air (Fm^{-1})

μ' = permeability of material (Hm^{-1})

ε''_{eff} = effective relative dielectric loss factor

The power absorbed during microwave irradiation must thus be determined by the target material's electromagnetic properties as well as its thickness. The absorbed power per unit volume (Wm^{-3}) of thin non-magnetic materials can be calculated as follows:

$$P_{ABS} = 2\pi f \varepsilon_0 \varepsilon'' E_{rms}^2 \tag{10}$$

where, E_{rms} = root mean square of the electric field (Vm^{-1})

The variation in electric and magnetic field strengths with temperature and time makes experimental measurements of absorbed power inside a material within a microwave cavity extremely challenging [11]. However, using an empirical technique, energy balance may be used to estimate the power component as follows [51]–[53]:

$$mC_p\Delta T = 2\pi f \varepsilon_0 \varepsilon'' E_{rms}^2 V_m t \tag{11}$$

where, m = mass of the material (kg)

C_p= specific heat of the material ($J\ K^{-1}\ kg^{-1}$)

ΔT = change in temperature (°C)

V_m = volume of the material (m^3)

t = microwave exposure time (s)

2.3.3 Microwave – Material Interaction

Due to variations in electric (E) and magnetic field (M) strengths across the material thickness, different materials display variable microwave absorption characteristics during contact with microwaves. Figure 6 depicts the fluctuation of E and H field strength with material thickness. The E and H field strength decreases with material thickness. P denotes the microwave energy absorbed per unit volume of material. The fluctuation of the energy absorbed per unit volume as a function of loss factor (ε'') in thin nonmagnetic materials is given by Equation (10). D denotes the depth of penetration (see Equation (9)).

Materials may be categorized into four major types based on their microwave energy absorption properties [11], [12]:

1) **Transparent**: Microwaves pass through transparent or low-loss insulator materials without being absorbed, as seen in Figure 5. Polytetrafluoroethylene (PTFE) and quartz are two examples of such materials. The decline in E and H field strength with thickness in the materials is almost non-existent. These materials have the lowest loss factor (ε''), can absorb a little amount of microwave energy per unit volume, and have the maximum penetration depth.

2) **Absorber**: The absorber materials are high loss insulators, or dielectric materials that absorb microwaves completely (depending on the value of the dielectric loss factor), as illustrated in Figure 5. Examples of these materials are water and silicon carbide (SiC). The E and H field strength falls as the dielectric loss factor of these materials rises. Furthermore, raising the loss factor improves energy absorption (flat portion of the P curve in Figure 5) while lowering penetration depth. After a critical value of loss factor, at which the energy absorbed per unit volume is maximum, the energy absorbed per unit volume and

penetration depth decrease as the energy conversion inside the material diminishes due to molecular structure in materials [11].

3) **Opaque**: Microwaves are reflected without or with minimum energy absorption in no-loss insulators (opaque materials), which have a low penetration depth and low energy absorption, as seen in category-3 in Figure 6. Metals are an example of these materials. For a few micrometers of thickness, these materials can experience a slight decline in E and H field strength.

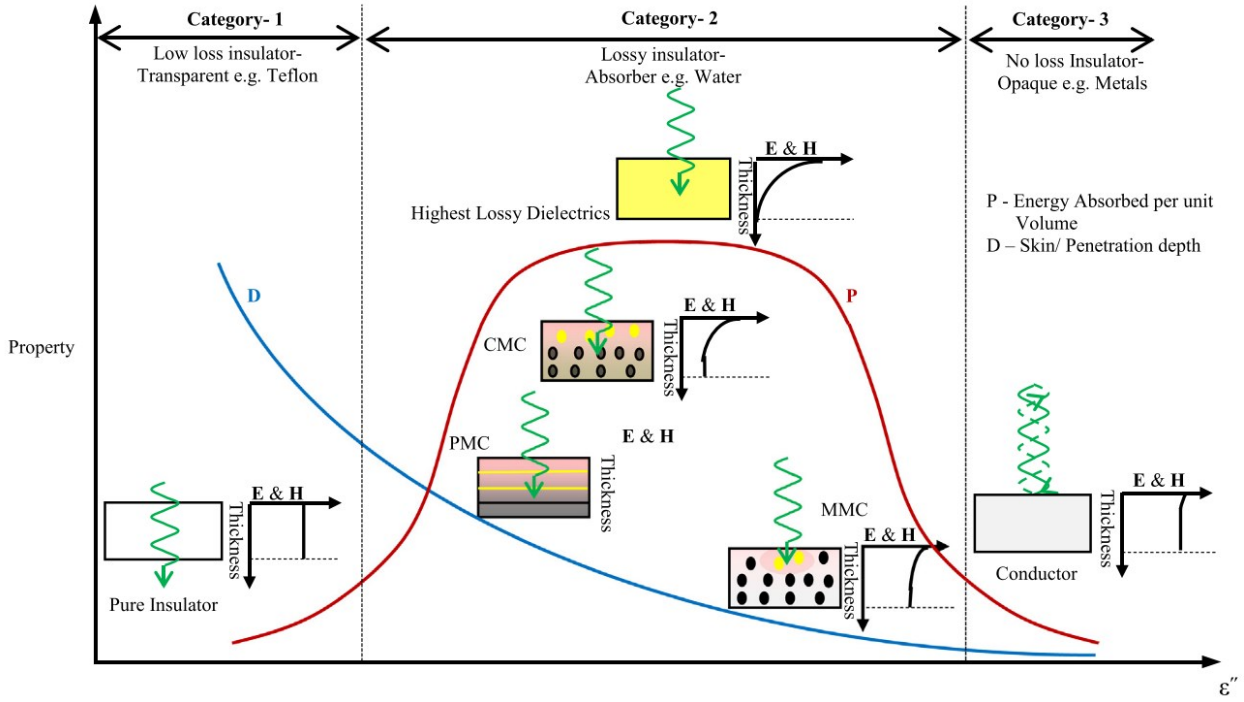

Figure 6: Interaction of Microwaves with Materials (reprinted from [11] with permission from Elsevier)

4) **Mixed – Absorber**: One or more phases of advanced materials, such as composite or multi-phase materials, are high loss insulators, whereas the others are low loss insulators. Microwaves are absorbed by this class of materials by transforming energy locally. Polymer Matrix Composites (PMCs), Ceramic Matrix Composites (CMCs), and Metal Matrix Composites (MMCs) are examples of these materials. Figure 6 depicts the partial

absorption of microwaves by different materials. Localized selective heating and hybrid heating are two important aspects of microwave processing of mixed absorbers [11], [12]. Microwaves are absorbed by the component with high dielectric loss while passing through the low loss material with negligible energy loss. In these materials, heating a specific component while keeping the surrounding material essentially unaffected is possible. This targeted heating procedure is not achievable in conventional heating setups [12].

2.4 Fundamentals of Microwave Heating

When a material interacts with microwaves, the electric and magnetic field components of the microwave impact the material depending on the material type, as illustrated in Figure 7. Heating in non-magnetic materials is impacted by the microwave's electric field component. Examples of such materials are aluminum, copper, water, polymers, and ceramics. Dipolar and conduction losses are the two primary loss processes in non-magnetic materials like the ones mentioned above. In metallic and high conductivity materials, conduction losses are dominant, whereas dipolar losses are dominant in dielectric insulators. Given that PMC are heated by dipolar loss [43], it will be covered in this section.

Magnetic materials such as iron, nickel, and cobalt are influenced by both the electric and magnetic field components of microwaves. The magnetic field influences the electron spin, domain wall, and domain orientation, whereas the electric field controls free electron mobility. Conduction losses, as well as other magnetic losses including hysteresis, eddy current, domain wall resonance, and electron spin resonance, are all part of the heat loss mechanisms in magnetic materials [11], [54], [55].

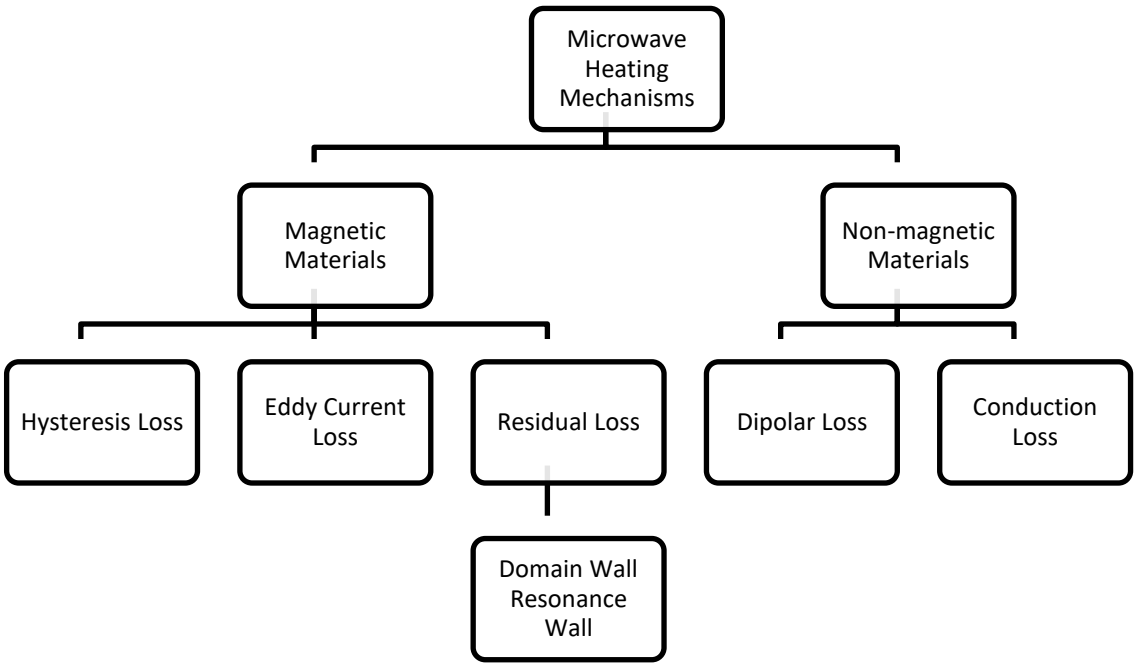

Figure 7: Heating Mechanisms in Materials

2.4.1 Dipolar Loss

Dipolar loss is more effective in dielectric insulator materials (water, ceramics, food items, hydrogen chloride, polymers, etc.). In the absence of an electric field, the molecules in the material are randomly orientated due to thermal activation, and there is no net dipole moment. However, when an oscillating electric field comes into touch with molecular dipoles in these materials, it causes them to agitate, resulting in dipoles. Figure 8 illustrates dipolar loss mechanism in water with positive polarity on the hydrogen atom and negative polarity on the oxygen atom. The molecular dipoles in water respond to the alternating electric field by spinning to align with it at microwave frequencies. Inertial, elastic, frictional, and molecular contact forces oppose these frequent changes in molecule orientation, which increase molecular kinetic energy and cause volumetric heating of the material. The increase in kinetic energy of all dipoles in the material rapidly raises the temperature of the material [11], [12], [27], [43], [46], [51].

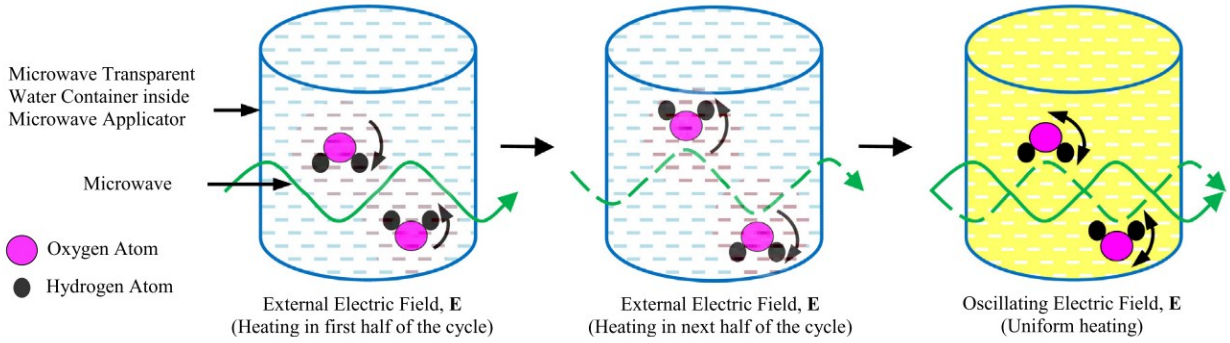

Figure 8: Heating Mechanism via Dipolar Loss (reprinted from [11] with permission from Elsevier)

2.5 Additional Aspects to Consider in Microwave Heating

Depending on the characteristics of a material, the interaction of microwaves with the material generates heat because of electromagnetic interaction. The temperature rise of materials is influenced by dielectric loss, specific heat capacity, and the strength of the applied field. But apart from these properties, there are other phenomena that affect microwave assisted heating of a material. These include the variation of dielectric properties with temperature, frequency, moisture content, microwave power, purity, presence of defects, chemical state, manufacturing method, and the influence of sample size and shape [33], [43], [51]. In the following section variation of dielectric properties is discussed.

2.5.1 Effect of temperature

Dielectric properties of a material vary with temperature as well as frequency. Figure 9 shows the variation of dielectric loss factor and dielectric constant of water with frequency and temperature. When microwaves are used to heat solids with very low dielectric loss, their electromagnetic energy absorption rises fast with temperature. This occurs because of temperature-related changes in dielectric loss values. This mechanism produces accelerated heating, known as thermal runaway, and experiments have been published demonstrating microwave-aided melting of transparent materials such as quartz and polyether ether ketone when heated by microwaves. The

temperature can be stabilized in these situations if heat can be released at a high enough rate or if the microwave power is limited [33], [56]–[58].

2.5.2 Effect of frequency

It is quite evident that the dielectric constant of water drops as temperature and frequency rise. In another work [51], it has been reported that the maximum absorption by water is seen to be around 20 °C when exposed to microwaves at 18 GHz. Another example is Silicon Carbide (SiC), which has a loss factor of 1.71 at ambient temperature but increases to 27.99 when treated with microwave radiation at 2.45 GHz frequency [11].

2.5.3 Effect of Moisture Content

Moisture content has a substantial influence on dielectric properties since water has a dielectric constant of 77 [59] and a loss of 12 [60]. Because the dielectric constant and loss of the material to be treated are frequently substantially lower, such as 3.1 and 0.076 for epoxy polymer [60], the dielectric constant will grow if water is added to the substance [61]. Moisture, on the other hand, can degrade a polymer's physical and mechanical qualities [62], therefore mixing water into a resin to improve microwave heating capabilities is not a possibility. Unfortunately, moisture absorption from the environment can cause some materials to contain moisture, and this must be considered if the material is to be microwave heated by ensuring a consistent environment for handling, storing, and processing.

2.5.4 Effect of Microwave Power and Material Composition

The electric field and the number of polarized dipoles increase as microwave power increases. As a result, the dielectric loss factor of a material rises as microwave power increases [61]. The ability of a substance to absorb microwaves, on the other hand, is limited. As long as free dipoles are accessible to interact with microwaves, microwave-assisted heating will continue to increase.

Moreover, in composite materials the volume composition and orientation of a reinforcement play an important effect, especially when the material is formed of two or more elements [27].

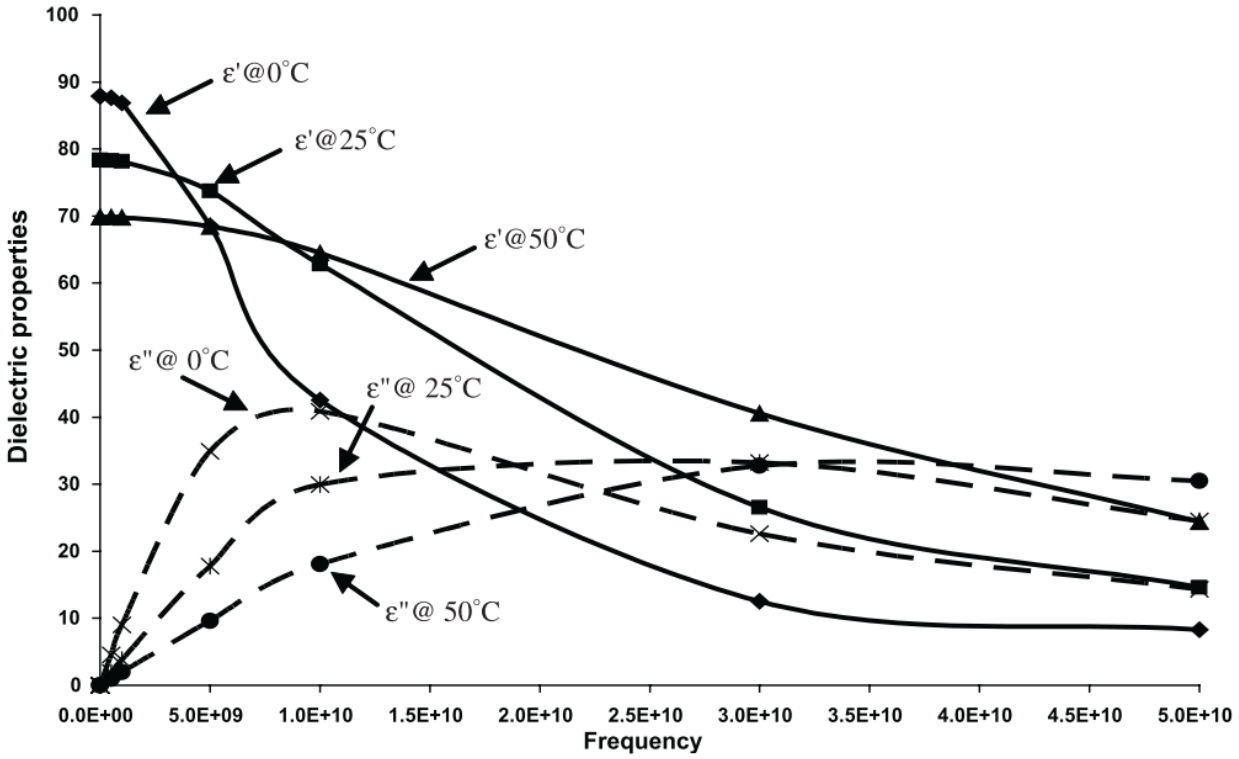

Figure 9: Variation of di-electric properties of water with frequency and temperature (reprinted from [43] with permission from John Wiley and Sons)

2.6 Microwave Absorption in Polymer Matrix Composites

Microwaves do not interact with most polymeric materials due to their low dielectric loss factor. This necessitates the addition of appropriate phases, such as fibers as reinforcement or susceptors. PMCs are made up of two phases: matrix and reinforcement. On irradiation, a material with a high dielectric constant absorbs more microwaves and heats up; the heat is then transferred to a substance with a low dielectric constant via conduction [24], [63]. This is known as a selective mode of heating and is differentiated as a suitable approach for processing PMCs due to its unique volumetric and uniform heating features when compared to conventional processing procedures.

In microwave-assisted heating of PMCs, the structure of the molecular dipole, heating temperature, conductivity, frequency, and dielectric properties of the material components all play a role [11]. The next section will concentrate on thermoplastic-based PMCs.

2.6.1 Thermoplastics-based Polymer Matrix Composites

Interaction of thermoplastic-based polymer composites with microwaves is complex. Heating semicrystalline thermoplastics in the microwave can be challenging until a threshold temperature is achieved, at which time the loss factor increases dramatically [64]. The critical temperature is associated with greater molecular mobility; however, it is not always the same as the polymer's glass transition temperature (Tg). If the critical temperature is higher than Tg, fast heating rates can be achieved until the polymer's melting point is attained. Amorphous polymers can usually be heated more efficiently than semicrystalline polymers. The explanation is that molecules in amorphous polymers are not constrained by the crystal lattice and are hence more mobile [65]. Heating of thermoplastics is primarily governed by three parameters: thermoplastic crystallinity, temperature, and fiber conductivity [11], [24].

The behavior of a thermoplastic with a degree of crystallinity more than 45 percent is virtually transparent to microwaves due to the limitation of dipole reorientation in an alternating electric field. Only a reinforcement would absorb microwaves in this situation, and heat is then transmitted to the matrix material by conduction. However, once the matrix reaches a temperature above critical temperature (TC), it will absorb microwaves and contribute to uniform heating. As seen in Figure 10, microwave radiation is absorbed by both the matrix and the reinforcement in thermoplastics with a degree of crystallinity below 45 percent. The dielectric loss factors of each component influence the percentage of energy absorbed [11], [24], [63], [64]. Despite several processing challenges, microwave processing of polymer composites has advantages over standard processing processes.

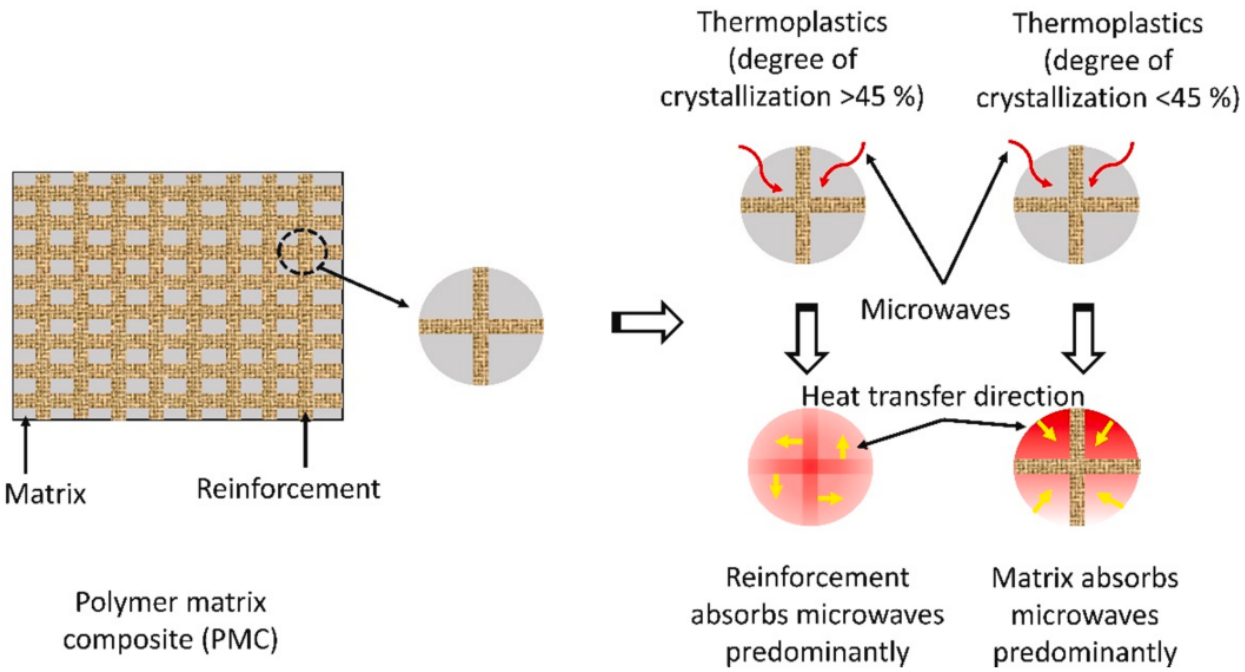

Figure 10: Microwave energy absorption of thermoplastic-based PMCs (reprinted from [24] with permission from Elsevier)

2.7 Previous Research on Microwave Heating

Many applications seeking ultralight, excellent quality, durability, and chemical resistance favor advanced polymer composites reinforced with fibers such as carbon, aramid, glass, and others [66]–[68]. In conventional heating, heat is supplied to a material and circulated by conduction, convection, and radiation. When a material is heated, its area or volume may get overheated or damaged, but the volume of the material that remains heated for a long duration of time may show a coarse grain structure [24]. This affects the crystallization or microstructure of the material, as well as its intrinsic properties.

Since crystallization of thermoplastics is complicated and sensitive to cooling rates, higher cooling rates lead to decreased crystallinity, which results in less molecular chain change and hence impacts material properties [69], [70]. Traditional thermoplastic composite manufacturing procedures have several drawbacks, including fiber burning, non-uniform temperature

distribution, fiber damage, prolonged curing times, thermal gradients, low efficiency, high energy consumption, waste production, and expensive equipment [71]. As a result, innovative approaches to process advanced materials effectively and productively must be developed. Microwave processing of materials is one such technique, which has advantages such as lower power usage, quicker processing, and environmental friendliness.

Microwave radiation has been used in a wide range of applications throughout the last 65 years. In recent years, the focus of microwave energy research has changed from food to advanced materials processing applications, such as synthesis, drying, sintering, cladding, coating, melting, casting and joining [35], [44]. The current review will focus on microwave assisted heating of thermoplastic composites.

2.7.1 Microwave Heating of Thermoplastics

Foong et al. [72] used multi-walled carbon nanotubes (MWCNTs) as a susceptor to microwave weld HDPE. An 800 W domestic oven was used to apply microwave radiation. They studied the effect of MWCNT concentration and microwave heating duration on the tensile strength of the welded sample. To investigate the effect of heating duration, a sample containing 0.5 wt% MWCNTs was heated in the microwave for 2 to 10 seconds. The tensile strength of the welded sample improved when the heating period was raised from 2 to 8 seconds; however, when the heating duration was increased further to 10 seconds, it decreased. When 10 s was used, a void formed at the welded junction, reducing tensile strength. MWCNT concentration was varied from 0.25 wt percent to 1.0 wt%, and an 8-second microwave heating duration was used to evaluate the effect of MWCNT concentration on dispersion. The tensile strength of the welded samples increased as the MWCNT concentration increased from 0.25 wt% to 0.75 wt percent but decreased as the concentration increased to 1.00 wt%. The lower tensile strength of the sample created with a 1.00 wt% MWCNT dispersion was caused by MWCNT penetration into only one side of the HDPE plate, resulting in a weak-welded connection.

Kravchenko et al. [73] suggested a microwave-assisted thermoplastic welding approach employing carbon nanostructures (CNS), which are branching CNTs (carbon nanotubes). Spray-assisted deposition of suspensions containing 0.01wt % CNS on thermoplastics with varied molecular structures, such as polycarbonate, polyurethane, and high-density polyethylene, was employed. The CNS nanofillers served as the microwave susceptor material, melting the surrounding polymer with the application of clamp force to produce structural welds. Microwave radiation was produced using a household microwave oven with a 2.45 GHz frequency and 700 W of power. The produced bond line is electrically conductive due to the formation of a percolated conductive network of carbon nanoparticles. By adjusting the CNS and microwave energy levels to provide the highest bonding strength, the welding technique offers potential for significantly reducing processing time.

In a domestic oven operating at 800 W, Palanisamy et al. [74] joined Acrylonitrile-Butadiene-Styrene (ABS) substrates utilizing charcoal as a susceptor material. The joining process was carried out using an adhesive technique, a direct heating approach, and microwave irradiation for a time of 3 to 5 minutes. Finally, once the joining was completed, the strength of the joint was compared. They discovered that compared to adhesive joining, the microwave joining approach displayed greater mechanical strength. Additionally, it was shown that the mechanical strength and hardness of the joint made are directly proportional to the heating duration. The direct heating technique, however, produced the strongest joints. The pores and air voids created by the charcoal powder at the connecting interface may be the cause of this.

Sweeney et al. [75] demonstrated a method of welding 3D-printed PLA-based surfaces utilizing strong localized heating of multi-walled carbon nanotubes through microwave irradiation. The samples were irradiated using a microwave source operating at 2.45 GHz, and an infrared camera was utilized to capture the temperature response of the samples. The PLA film's CNT content ranged from 0.10 percent to 20 percent. They found that semicrystalline polymers, like PLA, benefit from the interface being above the polymer's melting point such that crystalline areas can melt, diffuse, and recrystallize across the weld line. The microwave irradiation of PLA.MWCNT

boosts the weld fracture strength by 275 percent when compared to 3D-printed objects without MWCNT coating.

Poyraz et al. [76] carried out microwave-assisted welding of polypropylene (PP) specimens using polypyrrole nanogranule coated carbon and ferrocene (PPy/ferrocene) as an implant material. A 1250 W Panasonic Inverter microwave oven was used to irradiate the specimens. Due to the vigorous interactions between microwaves and electromagnetic absorbent PPy nanogranule coating, the growth of multi-walled carbon nanotubes (MWCNTs) at the interface was observed. Finally, the as-grown MWCNTs transferred heat into the neighboring bulk PP, resulting in the creation of locally molten surface layers. The slight pressure applied to the joint during the heating process eventually pressed the molten layers together, resulting in a new weld. Within 30-35 seconds, they welded a PP dog bone specimen with an average welded area of 576 mm^2. When compared to their non-welded counterparts, the welded joint retained around 95-98% of the maximum stress.

Farahani et al. [77] prepared conductive films for the welding of thermoplastic coupons in a single lap shear fashion using multi-walled carbon nanotube (MWCNT) buckypapers and nanocomposite films made of MWCNTs and polyethylene polymer. The heating efficiency of the manufactured films to weld polyethylene coupons was evaluated using two distinct welding methods: microwave welding and induction welding. Lap-shear mechanical testing was used to assess the mechanical strength of the joints. In general, a thicker coating, with a higher conductivity, and a longer welding duration resulted in superior quality and mechanical strength. Due to the high rate of heat generation caused by the interaction of microwaves and CNTs, microwave welding proved to be a more effective approach than Induction Welding. The mechanical strength of the specimens that were microwave welded indicated a high value of 7.9 MPa, which is close to the mechanical strength of the polymer bulk.

Two polymethmethyacrylate (PMMA) substrates were joined together by Yussuf et al. [78] utilizing liquid polyaniline in a single-mode microwave which operated at 2.45 GHz. These rapidly welded samples were then subjected to shear testing to assess the joint strength as a function of the processing variables such as heating time, microwave power, applied pressure, and polyaniline amount. The amount of polyaniline used, microwave power, and heating duration were all proven to boost joint strength. Joint strength rose from 1.7 to 6.8 MPa with a 15-second heating period and an increase in power from 100 to 300 Watts.

Random glass fiber reinforced thermoplastic matrix composites were effectively microwave welded by Ku et al. [79] using Araldite as a gasket material. Thirty-three percent by weight random glass fiber reinforced polystyrene composite [PS/GF (33 percent)] and thirty-three percent by weight random glass fiber reinforced low-density polyethylene composite [LDPE/GF (33 percent)] are the two thermoplastic substrates that were utilized. The samples were exposed to microwave radiation at a fixed frequency of 2.45 GHz. The test components were subjected to microwave irradiation at two distinct power levels, 400W and 800W, for varying amounts of time. An infrared thermometer was used to detect the temperature, and volumetric heating in the samples was noticed.

Wise and Froment [80] employed a variety of microwave-sensitive implants to achieve microwave joining of thermoplastics (including carbon-based implants as well as ceramic, polymer, and metal powder-based implants). A 2.2 kW multimode cavity applicator was designed, conceptually resembling a household microwave oven. They reported that carbon-based implants are the most promising and cost-effective, requiring only 3-60 seconds to construct a joint.

For effective microwave welding of polypropylene, Sun et al. [81] employed graphite coating (GC) as an implant material (PP). The power source used was a microwave oven with a 2.45 GHz frequency operating at 1000 W. The graphite powder (GP) can effectively absorb microwave energy and convert it into a substantial amount of heat, resulting in a dramatic increase in

temperature that can rapidly melt the interface of PP substrates and build a new structure where the GP was coated. Thus, one molten PP substrate wraps around GP to create a GC/PP sample, and with a particular amount of pressure, the molten PP couples unite to create a PP/GC/PP sample. While the PP/GC/PP samples display strong bonding strength in tensile testing, the GC/PP samples exhibit good electrical conductivity.

Yarlagadda and Chai [82] explored the use of highly focused microwave radiation for welding engineering thermoplastics. To successfully create polymer butt joints, they created a microwave generator with a variable power output from 0 to 1950 W operating at a frequency of 2450 MHz. Using a priming agent (epoxy-based resin), specimens with a low dielectric loss factor were bonded. The bonding agent's functions include absorbing microwave energy, producing local heat at the butt joint's interface, and allowing the surrounding thermoplastic to pair with the microwaves at higher temperatures. When primers were utilized, welding times were reduced (2.9 times faster), and bond strength improved.

In a 2.45 GHz microwave unit, Wu and Benatar [83] used the microwave absorption capabilities of intrinsically conductive polyaniline polymer to weld microwave transparent HDPE bars. Within 10 seconds a temperature of 300°C was attained, and a successful butt joint with a tensile strength comparable to bulk HDPE was attained in 60 seconds.

Wang et al. [84] joined polycarbonate substrates using multi-walled carbon nanotubes. A domestic microwave oven operating at 0.8 kW was used for this purpose and it took only 10 seconds to join the substrates. The bonding strength of the joint was found to be higher than that of the original polymer.

2.7.2 Physical Modeling

Since microwave heating takes place in a closed environment, it is challenging to observe and comprehend the heat and moisture transport inside the cavity using traditional techniques [85]. The introduction of finite elements and other simulation techniques has increased the demand for microwave technologies by enabling the analysis of the reciprocal coupling connection between different physical fields [86]. Food [87], ceramic [88], polymer composite [26], biomass [89], rubber [90], coal [91], and metal [92] have all demonstrated strong microwave heating simulation performance using COMSOL Multiphysics (COMSOL Inc., Burlington, MA, USA). However, for modelling and simulation of the welded joint heated by microwaves, only limited technical literature is currently accessible [93].

Santhosi et al. [94] concentrated on microwave absorption applications of polymeric nanocomposite structures in the 8.2-12.4 GHz frequency range. As a microwave absorber material, a hybrid nanocomposite made of polyurethane (PU) and epoxy polymer structures reinforced with low graphene weight concentrations (0 to 2.5 wt. %) was considered. The shielding efficacy of single-layered structures was calculated numerically using finite element method (FEM) based COMSOL 5.0 software. Experiments were used to validate these findings. A PU/graphene/epoxy 2.5 wt% structure had the best microwave absorption performance, while a PU/epoxy reinforced with 2.5 wt% graphene nanocomposite structure had the best shielding effectiveness (SE). Furthermore, these results were tested by simulation results, which match with an average error of 2.79 percent.

Ali et al. [95] used microwave curing to make natural fiber-reinforced thermoplastic composites. Composites were made using two types of natural fibers, sisal and Grewia optiva, as well as two types of thermoplastic polymers, polypropylene, and ethylene vinyl acetate. Microwave power and exposure duration were tuned for thermoplastic composite curing efficacy. Tensile and flexural strength results of produced composites indicated improvements in characteristics when compared to neat polymers. Microwave curing process simulation was also completed using COMSOL Multiphysics (version 4.1). After 570 seconds of heating, the composite reached a temperature

range of 175 to 185°C. However, the software projected a somewhat smaller temperature range of 155 to 170°C for the same time length. They also discovered that power input and microwave exposure duration play a key influence in directing the curing process.

Pitchai et al. [96] designed a three-dimensional finite element model that combined electromagnetic and heat transfer physics modules to simulate the 6-minute heating of 550 g of frozen mashed potato. The model was validated in a microwave oven rated at 1250 W, with the mashed potato tray positioned in the center of the stationary turntable. Simulated temperature profiles of the models utilizing a frequency of 2.45 GHz were compared to experimental temperature profiles acquired at the conclusion of heating using a thermal imaging camera and five fiber-optic thermocouples. The model was built using mashed potato's temperature-dependent dielectric characteristics (dielectric constant and dielectric loss factor) and thermal properties (thermal conductivity and specific heat capacity). In a 2.45 GHz frequency simulation, the average root mean square error value for the transient temperature profile measurement was 13.1°C. They discovered that the simulated transient temperature profiles, like the real temperature profiles, had a phase-change impact in their trend (change in slope near the thawing zone).

Nuhiji et al. [97] devised an electromagnetic field model that can be used to simulate microwave processing of composites. COMSOL Multiphysics software was used to effectively incorporate and mesh an industrial Vötsch microwave cavity into computer models. The influence of electromagnetic frequency on field homogeneity and temperature distribution was observed, with lower frequencies providing a more homogenous field and higher frequencies producing improved thermal ramp rates inside the composite but decreased Electromagnetic (EM) field uniformity. They also observed that an electromagnetic field changes the dielectric characteristics of the composite material, and that heat is released during cure through chemical reactions that vary with temperature and time.

Using finite element based COMSOL Multiphysics software, Arshad et al. [89] simulated the heating behavior of empty fruit bunch biomass in both bed and pellet form. In a COMSOL interactive system, a geometric model of a 1 kW household multimode microwave system operating at 2.45 GHz was created. The 10 s heating profile was quantitatively validated by comparing the simulated temperature profile to the experimental temperature. The microwave heating behavior of biomass represents a complex dependency of electromagnetic fields, microwave power dissipated in the material, thermal and dielectric characteristics of materials, and temperature profiles. COMSOL Multiphysics program can predict temperature distribution, hot and cold spots, electric field intensity, and microwave power absorbed in biomass materials during microwave heating. It was discovered that the end point temperature is substantially influenced by the biomass loading height and the sample's specific heat capacity. The electric field in the cavity was also seen to change quantitatively and qualitatively as the biomass loading height changed.

Srinath et al. [92] demonstrated a model for bonding bulk copper using a microwave susceptible interface powder layer and a finite element simulation with the COMSOL Multiphysics software. The interface powders comprise of copper and copper oxide. The microwave chamber is a metallic box that houses a 1 kW, 2.45 GHz microwave source connected to a rectangular waveguide in the TE_{10} mode. Microwave-assisted welding was performed experimentally in 300s at a temperature of roughly 1144°C. In comparison, the models showed that a maximum temperature of 1019°C was reached after 300 seconds. Thus, an approximately 8% difference was ascertained between the simulated and experimental findings in copper junctions.

Using charcoal as the susceptor, Bajpai et al. [26] effectively carried out microwave-assisted joining of a wide range of natural fiber-reinforced polylactic acid (PLA, commonly known as polylactide) and polypropylene substrates. Microwave heating and adhesive bonding methods were used to create lap joints, and the bond strength was assessed. Lap joints were made in 200-250 seconds using a 0.9 kW household microwave. When compared to the strength of adhesively joined connections, the joint strength attained using microwave joining was greater. The

microwave heating process was also simulated using multi-physics finite element software to investigate the microwave heating mechanism of PLA. The joint was achieved experimentally in 200 seconds, and the simulation results were found to be quite close. Finally, modelling findings showed that the position of the specimen within the microwave cavity, power input, microwave exposure length, choice of an appropriate susceptor, and susceptor selection all significantly influence the joining process.

In the work of Singh et al. [98], the joint strength of adhesively bonded joints and microwave-based joints was compared, and it was shown that the samples joined via microwave irradiation had higher joint strength than those made by adhesive bonding. The joint tensile shear strength was experimentally determined, and it was discovered that the bond strength of adhesively bonded specimens (4.9% of the parent material strength) is significantly lower than that of microwave joined specimens (62.85% of the parent material strength). To predict the estimated time necessary for microwave joining, the entire microwave heating process was simulated using the COMSOL Multiphysics version 4.1 software tool. The software model, which was validated with experimental results, can forecast the exposure time necessary for connecting natural fiber-reinforced composites.

The review of the technical literature revealed a gap relating to microwave absorption properties of multifunctional graphene-based PLA at 2.45 GHz. PLA is a thermoplastic polymer that is extensively used in commercial and research settings, including industrial packaging, medicinal devices, automotive sectors, and agricultural applications [99], [100]. PLA polymer's disadvantages, such as poor electrical and thermal conductivities, low service temperature and crystallization, and weak gas barrier, may limit industrial uses [101]. GNP as reinforcement has several benefits, including enhanced processability [102]–[104], comparatively low cost [105], reduced thermal contact resistance [106], a larger surface area [107], and a planar structure that favors large interaction regions [108], [109]. Thus, this study explores the use of GNP to create multifunctional PLA-based composites for high microwave absorption.

Chapter 3: Experimental Procedure and Characterization

Aspects of the material discussed in this chapter have been presented in the proceedings of The Canadian Society for Mechanical Engineering (CSME) International Congress, University of Alberta, Edmonton, Canada, June 5 - 8, 2022 and published in the proceedings of The Canadian-International Conference on Composites (CANCOM) International Congress, Fredericton-Moncton, NB, Canada, July 12-15, 2022. The material processing route presented herein was initially developed by Zhang et al. [110], [111].

3.1 Materials

Graphene nanoplatelets (xGnP grade M15) were procured from XG Sciences (Lansing, MI, USA). Their average thickness ranges from 6 to 8 nm, and their lateral dimension is 15 μm. The volumetric mass density, and electrical conductivity were, correspondingly, 2.2 g/cm^3, and 10^7 S/m parallel and 10^2 S/m perpendicular to the platelet plane. The in-plane thermal conductivity was 3000 W/mK, while through-plane was 6 W/mK. PLA was supplied in the form of pellets from Filabot Lab (type 4043D, Barre, VT, USA). The PLA glass transition temperature (Tg), volumetric mass density, and melting temperature range, decomposition temperature was specified by the supplier as 55 to 60°C, 1.24 g/cm^3, 145 to 160°C, and ~250°C respectively. Reagent grade chloroform and other chemicals, as well as tannic acid (TA) for functionalized nanocomposites was supplied by Fisher Scientific (Ottawa, ON, Canada).

3.2 Sample Preparation

Pure graphene nanoplatelets (pGNP) and functionalized GNP (fGNP) were used to create multifunctional PLA nanocomposites. They were prepared as follows:

3.2.1 GNP/PLA Nanocomposites

The GNP/PLA nanocomposites were prepared by solution mixing method using chloroform as the solvent (Figure 5). Initially, PLA pellets and pristine GNP were dried in an oven at 80°C overnight.

The next day, PLA and GNP were added to chloroform solvent forming two mixtures. The GNP mixture was treated with an ultrasonic processor for 3 hours (Q500, Qsonica, Newtown, CT, USA). The PLA mixture was mechanically stirred using an impeller agitator (Calframo, Georgian Bluffs, ON, Canada). After ultrasonication of the GNP mixture, both the mixtures were combined, sonicated for 60 minutes in an ice bath, and then transferred into a steel mold. The material was left in a fume hood for 12 hours to evaporate the solvent. The resultant films were dried in an oven at 120°C for 12 hours to eliminate any remnant solvent. Finally, the produced material was compression molded into plates.

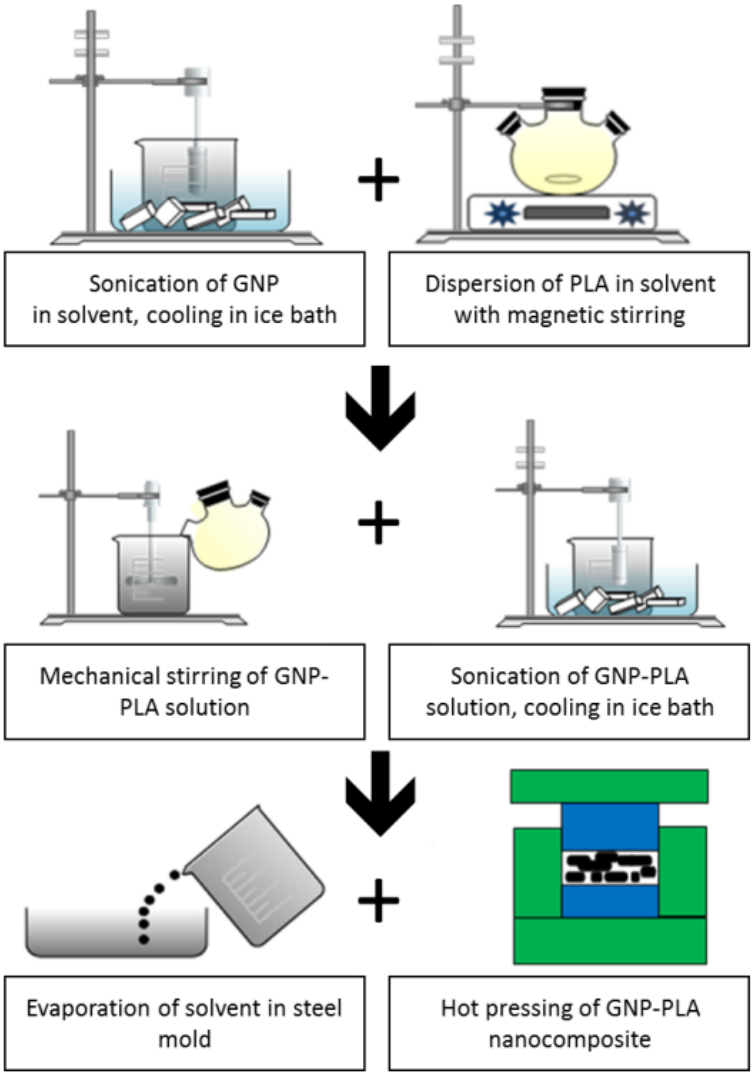

Figure 11: Solution Mixing Process to produce pGNP/PLA Nanocomposites (used with permission of ASME, from [111]; permission conveyed through with Copyright Clearance Center, Inc)

3.2.2 fGNP/PLA Nanocomposites

First, magnetic stirring was used to disperse GNP platelets in chloroform. Under strong magnetic stirring, TA was added to a GNP/chloroform solution with a mass ratio of 5:1. The mixture was then ultrasonically processed, sonicated, and magnetically stirred. The resulting suspension was vacuum filtered before being dried overnight at 80°C, resulting in the creation of non-covalent functionalized GNP (fGNP), as illustrated in Figure 12.

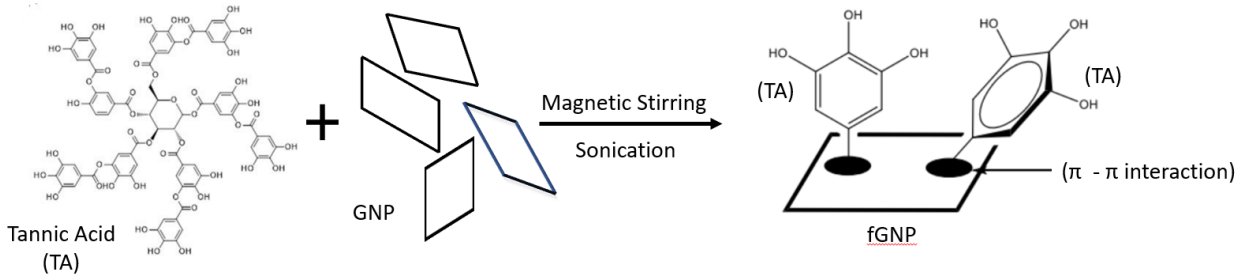

Figure 12: Fabrication of fGNP with tannic acid (TA)

Further details of the nanocomposite fabrication process can be found in [110] and [111]. Square test samples were cut with length and width of 25 mm and thickness of 1.8 mm, as shown in Figure 13 (A). For comparison, neat PLA samples were fabricated using comparable processes (Figure 13 (B)). Seven types of materials with different GNP and fGNP concentrations were prepared for testing as per Table 1. It should be noted that all samples were kept in a glass beaker separated by a paper towel (Figure 13 (C)). After that, the beakers were put in a desiccator (Figure 13 (D)) for about 21 days. This was done to prevent moisture from interfering with the absorption of microwave radiation.

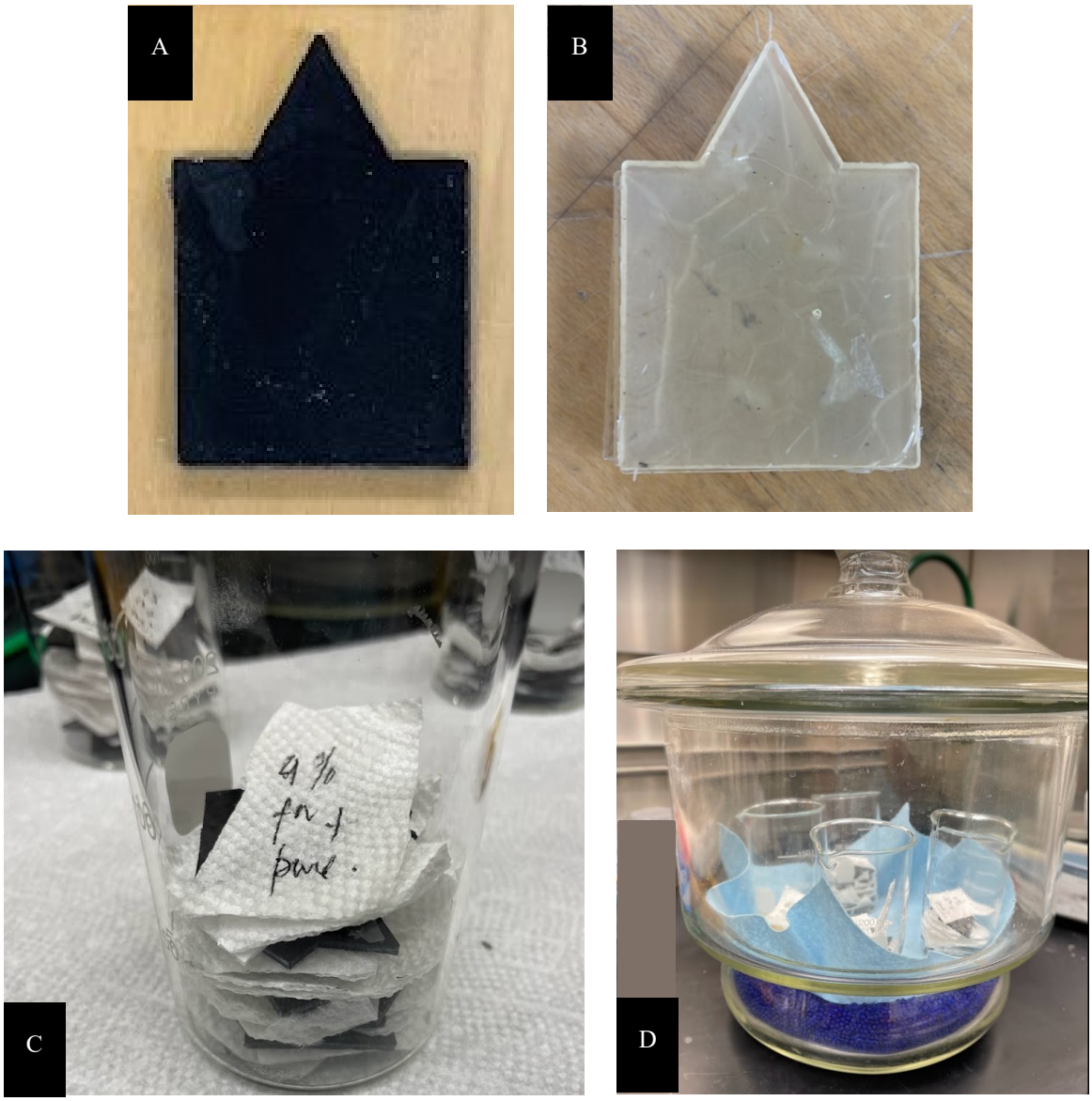

Figure 13: (A) GNP/PLA Nanocomposites, (B) Neat PLA Samples, (C) Samples Placed in Beaker, and (D) Samples Placed in Desiccator

3.3 Experimental Set-up

A 2.45 GHz fixed frequency multimode applicator (NNST67KS, Panasonic, Osaka, Japan) with a maximum power output of 1.2 kW was used. The microwave chamber dimensions are 525 x 310 x 401 mm.

Table 1: Composition of the nanocomposites

pGNP loading (wt%)	0	1	4	8
Material identifier	PLA	1-pGNP/PLA	4-pGNP/PLA	8-pGNP/PLA
fGNP loading (wt%)	1	4	8	-
Material identifier	1-fGNP/PLA	4-fGNP/PLA	8-fGNP/PLA	-

3.3.1 Inverter Technology

The microwave employed in this investigation makes use of inverter technology. Power is supplied to a conventional microwave via a transformer, which turns the power on and off, allowing the food to distribute heat. In this case, if the microwave is set to deliver 50% power, it will go through cycles of producing 100% power followed by a period of no power to achieve 50% power (Figure 14 (A)). In an inverter microwave, on the other hand, power is supplied through an inverter circuit to provide a steady and constant amount of power throughout the cooking time without cutting in and out. So, if 50% power is selected, the microwave will deliver 50% power throughout (Figure 14 (B)). Thus, inverter microwaves provide a consistent supply of power and accurate temperature control throughout the cooking duration to minimize overheating.

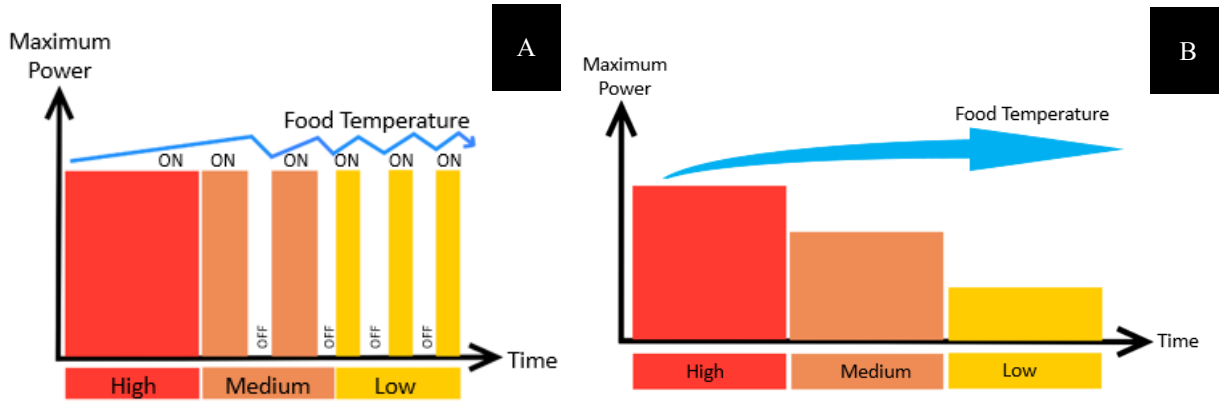

Figure 14: Microwave Output Image (A) Non-Inverter Technology, and (B) Inverter Technology

3.3.2 Hotspot Location

Temperature uniformity can be monitored directly during processing using many sensors, or indirectly in separate tests by seeing a visible change in a temperature sensitive material. Thermal paper is a common approach for indirect thermography since it is inexpensive and easy to use.

Despite being thermally sensitive, thermal paper does not absorb microwave radiation [112], [113]. However, when used in conjunction with a microwave absorbing substance, such as water, the thermal paper experiences a single, permanent color change when it reaches a specified trigger temperature. This mapping approach is time sensitive; exposure for too long may result in total blackening of the thermal paper, while exposure for too short a period would give the mistaken appearance of poor uniformity. High temperature regions of a damp thermal paper turn black, while colder sections stay white. The temperature range of 100-150°C was shown to cause the thermal paper to become black [112]. Thermal paper is exclusively used in the literature to explain the dispersion of microwaves in oven cavities when placed at various heights in the microwave chamber with a microwave absorbing substance [113].

The hotspot location in the present research was found utilizing microwave susceptible damp thermal paper. The thermal paper was positioned at three different heights parallel to the microwave's base. The damp thermal paper was then heated for 60 seconds at 1.2 kW power in all cases, and the experiment was repeated three times. In terms of sample location and energy input, this setup is meant to produce reproducible findings.

As seen in Figure 15 (A), when damp paper was placed at the bottom, heat patterns were found to be negligible. However, when positioned in the middle (Figure 15 (B)) and top (Figure 15 (C)) of the microwave, a significant number of hotspots were detected. As a result, it is preferable to position the samples as close to half the length of the microwave as feasible.

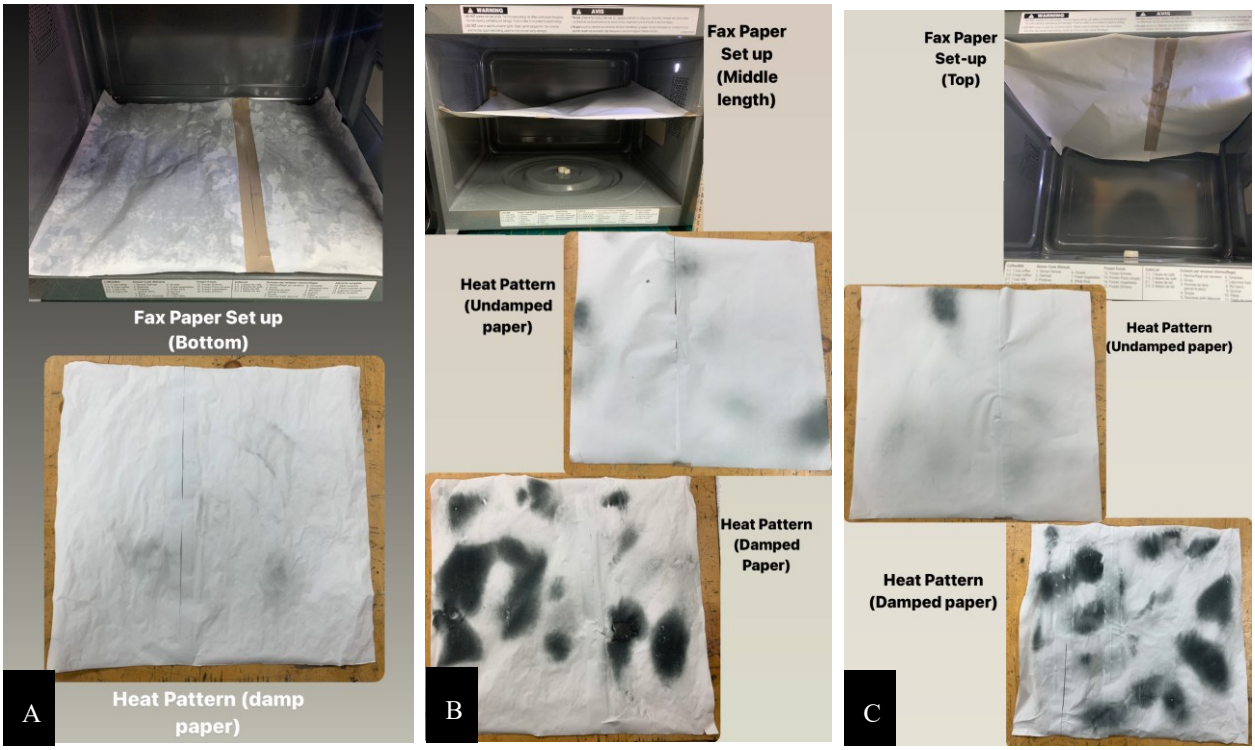

Figure 15: Hot-Spot Location: (A) Bottom of Microwave, (B) Mid - length of the microwave, and (C) Top of Microwave

3.3.3 Microwave Heating Set-Up

A stationary glass plate, as shown in Figure 16, was placed inside the chamber on four ceramic supports at the corners, 40.5 mm above the oven's base. The glass plate was set at that height from the oven base because 40.5 mm long ceramic supports were available.

After this, a damp thermal paper and an infrared (IR) camera (X8500sc, Teledyne FLIR, Wilsonville, OR, USA) were employed to determine the location on the glass plate with the highest temperature:

1) The damp thermal paper was laid on the glass plate and microwaved at 1.2 kW power for 1 minute. Figure 16 (A) depicts the hot spots identified.

2) A glass plate at room temperature was then heated under the same circumstances and put in front of the IR camera. The maximum temperature was discovered at the blue square depicted in Figure 16. (A).

The hot spot location in both the cases appear to overlap, and therefore, specimens in a PTFE dish were positioned at always the same hot-spot location on the glass plate within the chamber, as illustrated in Figure 16 (B). Glass plates and PTFE dishes were exchanged between tests to ensure the same thermal conditions for each test. Figure 16 (C) shows a GNP/PLA sample that thermally degraded when kept at that same position beyond initial melting.

3.3.4 Microwave Heating Methodology

Bajpai et al. [26] reported that microwave power input, exposure time, susceptor selection, and specimen location inside the microwave cavity all play important roles in determining microwave interaction with a material. Susceptor and specimen positions have been fixed in the present work. It has also been observed that the two key microwave parameters, power, and exposure duration, have a considerable impact on the mechanical characteristics of the produced composites and must thus be tuned for different polymers [24]. Thus, the influence of altering microwave power and duration on the melting of GNP/PLA specimens was considered in the current work.

All specimen types were irradiated at two different power levels, i.e., 0.6 kW and 1.2 kW. Microwave irradiation was halted after durations ranging from 3 to 180 seconds, or when melting of a specimen was observed. Following irradiation, the specimen with PTFE dish was removed rapidly from the chamber and placed on a wooden holder (Figure 17). The infrared camera was used to measure the specimen temperature distribution. For a given irradiation time and power level, single samples were tested for pure PLA, 1-fGNP/PLA, and 1-pGNP/PLA, while tests were conducted in triplicate for 4-fGNP/PLA, 4-pGNP/PLA, 8-fGNP/PLA, and 8-pGNP/PLA.

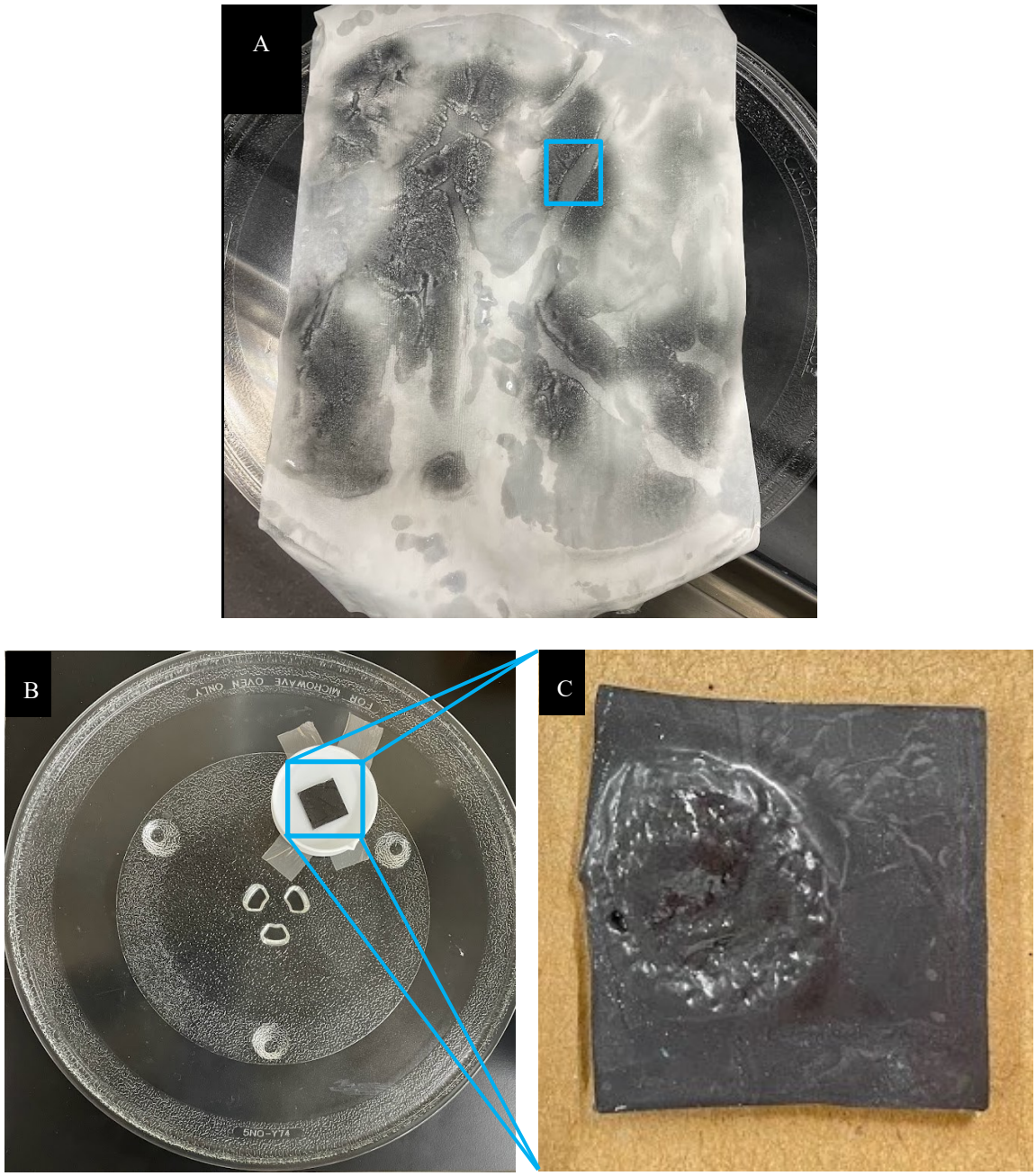

Figure 16: (A) Hotspots found using damp thermal paper, (B) Sample position on the glass plate, and (C) Specimen irradiation by the microwaves

3.4 Characterization

3.4.1 Thermal Properties

The specific heat capacity (*Cp*) of the materials was measured by differential scanning calorimeter (model Q100, TA Instruments New Castle, DE, USA). Note that determining *Cp* is a necessary step for assessing the anisotropic thermal conductivity of the materials. Samples with a mass of 5 to 10 mg, prepared in platinum pans, were heated from 0°C to 200°C at a rate of 10°C/min under dry nitrogen flow (50 mL/min), in accordance with ASTM E1269-11 [114]. One test was conducted per filler weight fraction.

Figure 17: Microwave heating of nanocomposites examined using thermal imaging

The anisotropic thermal conductivity of the materials was measured using a TPS2500S device (Thermtest, Fredericton, NB, Canada) with a Kapton sensor (type 5501, Thermtest). The sensor was sandwiched between two stacks of three samples of the same kind, as shown in Figure 18 (A)

and (B). Three test runs were conducted for each filler weight fraction, using a measurement duration and heating power set in accordance with IS0 22007-2 [115].

3.4.2 Electrical Conductivity

Material samples with a thickness and diameter of correspondingly 1 mm and 30 mm were prepared for electrical (volume) conductivity testing in dry air at room temperature. Samples with an electrical conductivity greater than 10^{-4} S/cm were examined by placing a four-pin probe at 90 V connected to a Loresta-GP resistivity meter (model MCP-T610, Mitsubishi Chemical, Osaka, Japan). For sample electrical conductivities less than 10^{-4} S/cm, a Hiresta-UP resistivity meter and UR type probe were used at 1000 V (Mitsubishi Chemical). One sample was tested for each filler loading.

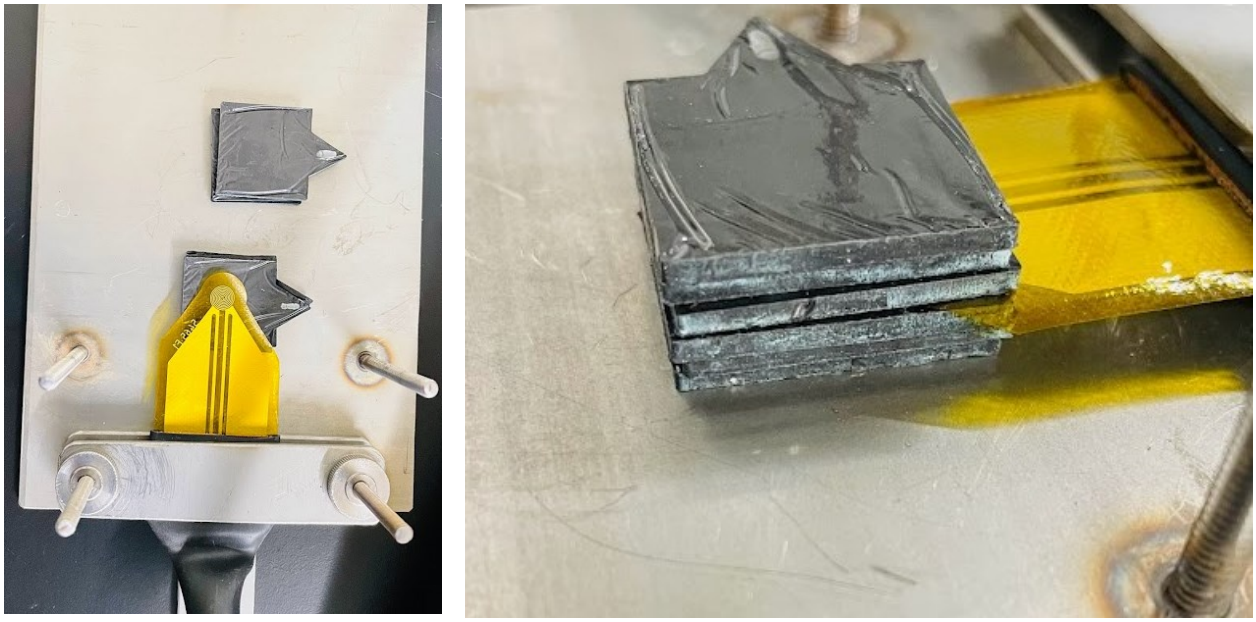

Figure 18: Stacking of samples for thermal conductivity measurement

3.4.3 Complex Permittivity

A vector network analyzer (ZVA67 Vector Network Analyzer, Rohde & Schwarz, Munich, Germany) operating in a frequency range of 2.35 to 2.45 GHz connected to an open-ended coaxial probe was used to obtain the complex permittivity for each sample type. The stages of the open-ended coaxial technique calibration used were: 'open circuit in air', 'short circuit with metal', and 'load in distilled water'. After complete calibration, PTFE was used as the standard material to confirm the calibration prior to the start of a sample characterization, as shown in Figure 19 (A). The sample to be measured was placed beneath the probe in such a manner that the probe tip was in direct contact with the sample without any air gap (Figure 19 (B)). Every sample was examined eight times, and the average value is reported.

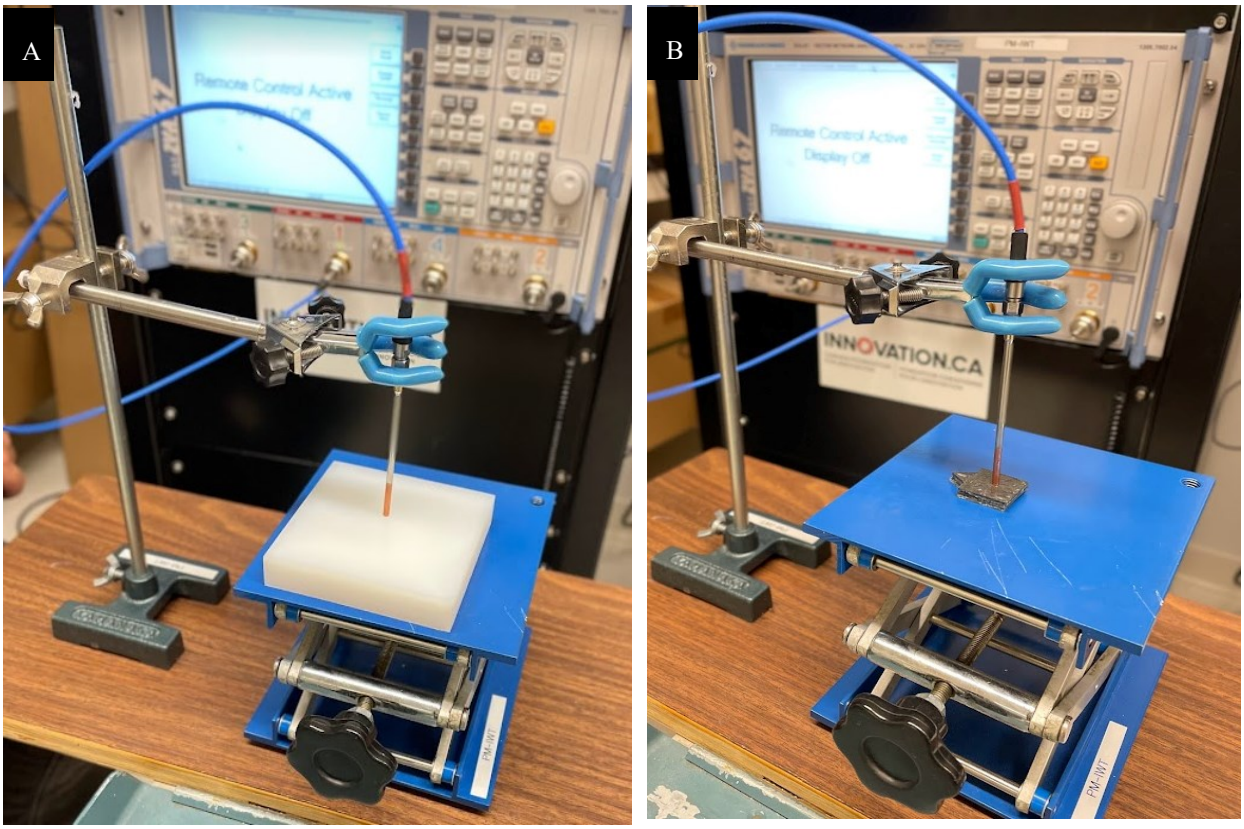

Figure 19: Complex Permittivity Measurement: (A) Using PTFE and (B) GNP/PLA Sample

Chapter 4: Numerical Modeling

Aspects of the material discussed in this chapter have been presented in the proceedings of The Canadian Society for Mechanical Engineering (CSME) International Congress, University of Alberta, Edmonton, Canada, June 5 - 8, 2022.

4.1 Model Definition

Using the COMSOL Multiphysics FEM-based software tool (version 5.5), a 3D finite element model of the microwave-assisted heating process of the specimens was developed. As shown in Figure 20 (A), the cylindrical glass plate, which has a radius of 113.5 mm and a height of 6 mm, the rectangular waveguide, which has dimensions of 50 mm in width, 78 mm in depth, and 18 mm in height, the microwave cavity, and the sample size were all selected in accordance with the actual experimental setup. The cylindrical glass plate with a specimen placed on top of the hotspot (as described in Section 3.3.4) was positioned at a height of 44.5 mm from the bottom of the oven (Figure 20 (B)).

Microwaves at 2.45 GHz were modelled to enter the microwave cavity through a rectangular waveguide operating in the TE_{10} mode from the port. The waveguide was placed at the centre of the cavity, as in the household microwave system. The electromagnetic waves, frequency-domain interphase was used to solve for the time-harmonic wave equation for the electric field distribution, which was then followed by a transient heat transfer simulation to illustrate how heat redistributes throughout the specimen (Figure 20 (C)). Meshing was done using the Physics-controlled mesh sequence type, with a normal element size, as shown in Figure 21. The simulation was performed using a custom-built computer equipped with an Intel Core i7-8700 3.20 GHz CPU, 16 GB RAM memory, and a 64-bit Windows 10 Education operating system.

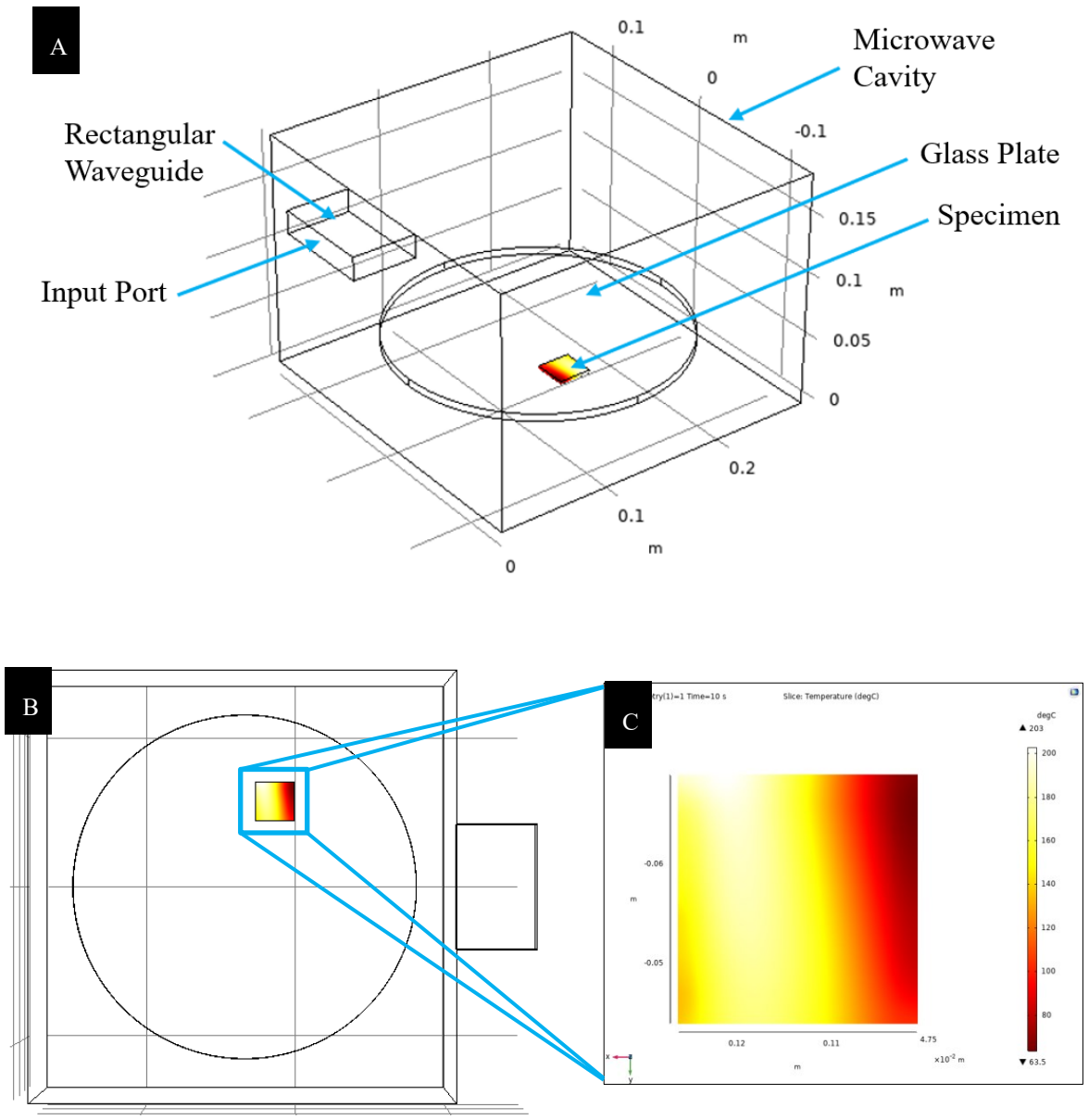

Figure 20: 3D Numerical model (A) microwave oven cavity, (B) specimen at hot spot, and (C) simulation of a melting specimen

4.2 Modeling Process

The numerical modeling process involves the following steps:

1) Choosing the appropriate Multiphysics interface(s)
2) Defining component variables and parameters in the ‘Definitions’ branch
3) Building the component geometry in the ‘Geometry’ branch
4) Assigning material properties to the geometry in the ‘Materials’ branch
5) Meshing the geometry in the ‘Mesh’ branch
6) Setting up the study and computational in the ‘Study’ branch
7) Analyzing and visualizing the results in the ‘Results’ branch

4.3 Governing Equations

The governing equations for Maxwell's equation based on boundary conditions, as utilised in the numerical model, are addressed in this section. Following that, the Electromagnetic Waves, Frequency Domain Interface, and Electric Losses are discussed. Finally, the interface for heat transfer is addressed.

4.3.1 Radio-frequency Interface Modeling

On a macroscopic level, electromagnetic analysis entails solving Maxwell's equations, as listed in Section 2.3.1 (Equations 3-6), depending on certain boundary conditions. The equations can be written in either differential or integral form. In the numerical model, the differential form is

preferable since it leads to differential equations that can be solved using the finite element method. The equation of continuity is another fundamental equation that can be expressed as:

$$\nabla \times J = \frac{-\partial \rho}{\partial t} \tag{12}$$

where, J = current density (A/m^2)

The constitutive relations characterising the macroscopic features of the medium are incorporated to produce a closed system [116]. They are provided as

$$D = \varepsilon_0 E + P_v \tag{13}$$

$$B = \mu_0 (H + M) \tag{14}$$

$$J = \sigma E \tag{15}$$

where, D = electric displacement (C/m^2)

P_v = electric polarization vector

B = magnetic flux density (T)

M = magnetization vector

σ = electrical conductivity (S/m)

When an electric field E is present, the polarization of the material is described by P_v. It is typically a function of E and may be read as the volume density of electric dipole moments. Even in the

absence of an electric field, some materials can have a nonzero P_v. M defines how the material is magnetized in the presence of a magnetic field H. It is commonly regarded as the volume density of magnetic dipole moments and is a function of H. Permanent magnets, on the other hand, have a nonzero M even when no magnetic field is present.

In terms of the electrical scalar potential '*Ve*' and the magnetic vector potential '*A*', the electric field and the magnetic flux density are described as follows:

$$B = \nabla \times A \tag{16}$$

$$E = -\nabla Ve - \frac{\partial A}{\partial t} \tag{17}$$

The magnetic vector potential's defining equation is a direct result of the magnetic Gauss' law. Faraday's law gives rise to the electric potential. Microwave is an electromagnetic energy, and the electric and magnetic energies are specified separately as:

$$W_e = \int_V \left(\int_0^D E \cdot dD \right) \cdot dV \tag{18}$$

$$W_m = \int_V \left(\int_0^B H \cdot dB \right) \cdot dV \tag{19}$$

The electric and magnetic power are the time derivatives of the electric and magnetic fields, respectively.

$$P_e = \int_V E \frac{\partial D}{\partial t} dV \tag{20}$$

$$P_m = \int_V H \frac{\partial B}{\partial t} dV \tag{21}$$

where, P_e = electric power (W)

P_m = magnetic power (W)

Poynting's theorem connects P_e, P_m, W_e, and W_m (Equations 18-21) to resistive and radiative energy loss [117].

$$-\int_V \left(E \cdot \frac{\partial D}{\partial t} + H \cdot \frac{\partial B}{\partial t}\right) dV = \int_V J \cdot E dV + \oint_S (E \times H) \cdot n \, dS \tag{22}$$

where, V = computation domain

S = closed boundary of computation domain

n = unit normal to the surface

Resistive losses are represented by the first term of the Equation 22. These losses result in heat dissipation in a material. The second term in Equation 22 represents the radiative losses.

$$P_h = \int_V J \cdot E \, dV \tag{23}$$

$$P_r = \oint_S (E \times H) \cdot n \, dS \tag{24}$$

where, P_h = resistive loss (W/m^3)

P_r = radiative loss (W/m^3)

S_P is the Poynting Vector and is represented by:

$$S_P = E \times H \tag{25}$$

4.3.2 Electromagnetic Waves, Frequency Domain Interface

Maxwell-Ampère and Faraday's laws can be used to derive equations for high-frequency waves.

$$\nabla \times H = \sigma E + \frac{\partial \varepsilon E}{\partial t} \tag{26}$$

$$\nabla \times E = -\frac{\partial H}{\partial t} \tag{27}$$

Assuming sinusoidal excitation and linear medium, the fields in time-harmonic form can be written as:

$$H(x,y,z,t) = E(x,y,z)e^{j\omega t} \tag{28}$$

$$E(x,y,z,t) = E(x,y,z)e^{j\omega t} \tag{29}$$

Equations 26-29 can be combined to provide a time harmonic equation for the electric field and magnetic field equations:

$$\nabla \times (\mu^{-1}\nabla \times E) - \omega^2 \varepsilon^* E = 0 \tag{30}$$

$$\nabla \times \left(\varepsilon^{*-1}\nabla \times H\right) - \omega^2 \mu E = 0 \tag{31}$$

The key feature node for the Electromagnetic waves, frequency domain interface is 'Wave Equation, Electric'. The Equation 30 is the governing equation for the same.

In a microwave oven, an electric wave without an electric field component in its direction of propagation, known as a transverse electric (TE) wave, excites the rectangular port. The TE_{10} mode is the only one that can propagate through the rectangular waveguide at an excitation frequency of 2.45 GHz. Thus, in the Port node, under the Port Mode Settings, a rectangular waveguide with a mode type TE is chosen. The cut-off frequencies (f_c) for the various modes as [118]:

$$(f_c)_{mn} = \frac{c}{2}\sqrt{\left(\frac{m_1}{a}\right)^2 + \left(\frac{n_1}{b}\right)^2} \tag{32}$$

where, m_1 and n_1 = mode numbers (for the TE_{10} mode, m_1 is 1 and n_1 is 0)

c = speed of light

The TE_{10} mode is the only mode able of propagating at frequencies between 1.92 GHz and 3.84 GHz, with dimensions of a = 7.8 cm and b = 1.8 cm.

A propagation constant, β, is necessary for the port condition, and for frequency f, it is provided by the expression:

$$\beta = \frac{2\pi}{c}\sqrt{f^2 - f_c^2} \tag{33}$$

The Equation 30 is solved for the electric field vector *E* within the waveguide and oven with the specified excitation at the rectangular port.

4.3.3 Electric Loss in the Frequency Domain

The frequency domain equation, represented by Equation 30, allows for the addition of electric losses in the form of finite conductivity, complex permittivity, and loss tangent [116]. In the present study, the complex permittivity approach has been used. In this, all the losses are given by ε''.

Resistive losses, on the other hand, represent the amount of energy converted into heat from microwave energy. Equation 23 represents the formula of resistive losses.

4.3.4 Transient, Heat Transfer in Solids Interphase

The electromagnetic losses from the electromagnetic waves are added by the multi-physics couplings as a heat source, and the characteristics of the electromagnetic materials can change with temperature. The Heat Transfer in Solids interface includes tools for simulating heat transfer by conduction, convection, and radiation. On all domains, the Heat Transfer in Solids model is enabled by default. In solid domains, the temperature equation corresponds to the differential form of Fourier's law, which may include other contributions such as heat sources [116].

Equation 34 was used to determine the thermal and heat transport conditions for the sample. This equation combines the electromagnetic heating module of COMSOL with the heat transfer equation of Fourier's energy balance as follows:

$$\rho c_p \frac{\partial T}{\partial t} = \nabla \cdot (k \nabla T) + Q \tag{34}$$

where, ρ = density of the sample (kg/m^3)

k = Thermal Conductivity of the sample (W/m^{-2}K^{-1})

T = Temperature (K)

Q = Heat Source (W/m^3)

The Electromagnetic Heat Source node represents electromagnetic losses. Because these losses act as a heat source in the model's heat transfer interphase, Q is referred to as a heat source.

$$Q = Q_{rh} + Q_{ml} \tag{35}$$

where, Q_{rh} = Resistive losses (W/m^3)

Q_{ml} = Magnetic losses (W/m^3)

Resistive losses have been represented by equation 23. The specimen is the only source of resistance inside the cavity under assumed ideal conditions. Therefore, due to resistive losses and deformation in electric field, non-uniform localized heating occurs which results in the hot spots in the specimen [26].

4.4 Boundary and interface Conditions

Due to the absence of surface currents at the interface between two medias, the following boundary conditions are always fulfilled.

$$n_2 \times (E_1 - E_2) = 0 \tag{36}$$

$$n_2 \times (B_1 - B_2) = 0 \tag{37}$$

where, n_2 = outward normal from medium

The first condition is automatically satisfied since the tangential component of the electric field is always continuous while E is being solved for. The second requirement is identical to the natural boundary condition and so met as well.

In terms of boundary conditions, the cavity walls were treated as 'Perfect Electric Conductor'. This boundary condition sets the tangential component of the electric field to zero. The governing equation for the Perfect Electric Conductor is:

$$n \times E = 0 \tag{38}$$

The following equation describes the impedance boundary condition, which was taken into account the metal body or walls of the microwave oven where it is known that the field penetrates only a short distance outside the boundary [116]:

$$\sqrt{\left(\frac{u_0 u_r}{\varepsilon_0 \varepsilon_r} - \frac{j\sigma}{\omega}\right)} n \times H + E - (n \cdot E)n = (n \cdot E_s)n - E_s \tag{39}$$

where, μ_r = relative permeability (/)

ε_r = relative permittivity (/)

E_s = source electric field (V/m)

The properties such as ε_r, u_r and σ are dependent on the material being irradiated by the microwaves.

4.5 Meshing strategy

In the process of finite element modelling, meshing is a crucial stage. By lowering the degree of freedom from infinite to finite by meshing, it is feasible to do computations at finite places. The data is then extrapolated throughout the whole domain. The finite element approach uses a basic shape function that might be constant, linear, or of higher order to approximate the solution within each element. To resolve the solution, a finer or coarser mesh is needed depending on the element order in the model. Necessary mesh resolution in case of a radio-frequency modeling is dependent on the following problem-dependent factors:

1) **Geometrical Factors:** In the finite element modeling, the variation in the solution is brought on by geometrical elements. In areas with a lot of fine geometrical characteristics, the mesh generator automatically creates a mesh that is more finely detailed.

2) **Penetration Depth:** From the conductivity, permeability, and frequency, the skin depth may be calculated with ease. To accurately record the variance of the fields, at least two linear components per penetration depth are needed.

3) **Wavelength:** It takes around 10 linear elements per wavelength to adequately resolve a wave. The local qualities of the material affect the wavelength.

4.5.1 Physics-Controlled Mesh

The domains are discretized by the mesh generator into tetrahedral, hexahedral, prism, or pyramid mesh elements, whose faces, edges, and corners are referred to as mesh faces, mesh edges, and mesh vertices, respectively. The software automatically sets up the meshing sequences for the pre-set physics-controlled meshes.

When the mesh type is not specified, a free (unstructured) mesh containing tetrahedral components is constructed automatically. The geometry, as well as several factors, determine the number of tetrahedral mesh elements. Swept meshing creates a structured mesh in the direction of the sweep using prism or hexahedral components in the case of 3D structured meshes. Boundary layer meshing creates structured layers of pieces that integrate into an existing structured or unstructured mesh. When the Physics-controlled mesh option is chosen in the Sequence type list of a Mesh node's Settings window, COMSOL Multiphysics generates a mesh that is tailored to the model's current physics interface settings.

In the present study, a physics-controlled mesh type was used for all specimens. For the microwave heating study in the present work, a parameter for the maximum mesh element size in open space

is activated. For the Electromagnetic Waves, Frequency Domain interface, the maximum mesh element size should be a fraction of the wavelength. However, as the wavelength changes in different dielectric and magnetic areas, the physics-controlled mesh automatically adjusts the maximum mesh element size. Then, the domain size that may be simulated increases in accordance with the amount of computer memory available and the wavelength [116].

The mesh on the specimen and the glass plate is finer than the oven walls, as can be observed in Figure 21(A), (B), and (C). This is owing to the shift in wavelength caused by the dielectric characteristics of the specimen, glass plate, and oven walls. The maximum wavelength is always kept as a maximum value of 1/5 of the smallest wavelength. A sweeping mesh with triangular prisms is automatically created for the completely matched layer domains (cavity walls and waveguide). For the glass plate and specimen, however, a free tetrahedral mesh is created. The maximum and minimum element sizes for glass plate and specimen are 0.01533 m and 4.598E-4 m, 0.01284 m and 3.853E-4 m, respectively.

4.6 Assumptions

Even though computational software has advanced rapidly to offer accurate findings that may be utilised in engineering, numerical problems caused by improper discretization of the time and space domains may occur [89], [119]. As a result, assumptions must carefully be made to achieve a sufficiently simple model and shorten the computing time. For the current simulation study, the following assumptions were made:

1) There was no consideration for heat transport in the glass plate, surrounding cavity, or atmosphere.

2) The simulation was run using a single magnetron frequency of 2.45 GHz.

3) The mass and momentum transport of moisture and chemical species were not considered.

4) The specimens' starting temperatures were thought to be homogenous.

5) The specimen's deformation, shrinkage, or collapse are not considered.

6) The specimen is assigned orthotropic material characteristics.

7) The specimen is presumed to be surrounded by air, which has no dielectric losses.

8) The chemical interaction between the air and the sample is minimal, if at all.

9) Heat transport equations were solved at constant dielectric and thermal conductivity parameters, with no values altered during the time step. This implies that these attributes were assumed to be temperature and time independent.

10) Throughout the simulation, the ambient temperature is assumed to be constant.

4.7 Parameters Required for Numerical Simulation

In the present study, the microwave power absorbed and temperature distribution in the heat source (sample material) were calculated by simultaneously solving the Maxwell's equations in the stationary, frequency-domain electromagnetic analysis and the transient heat transfer equation. Thus, the parameters required for numerical simulation of microwave heating are:

4.7.1 Complex Permeability

The addition of GNPs to PLA has shown no effect on its magnetic permeability but considerably increased its electrical permittivity [120]. Thus, in the present work the value for magnetic permeability for all the materials was considered as unity.

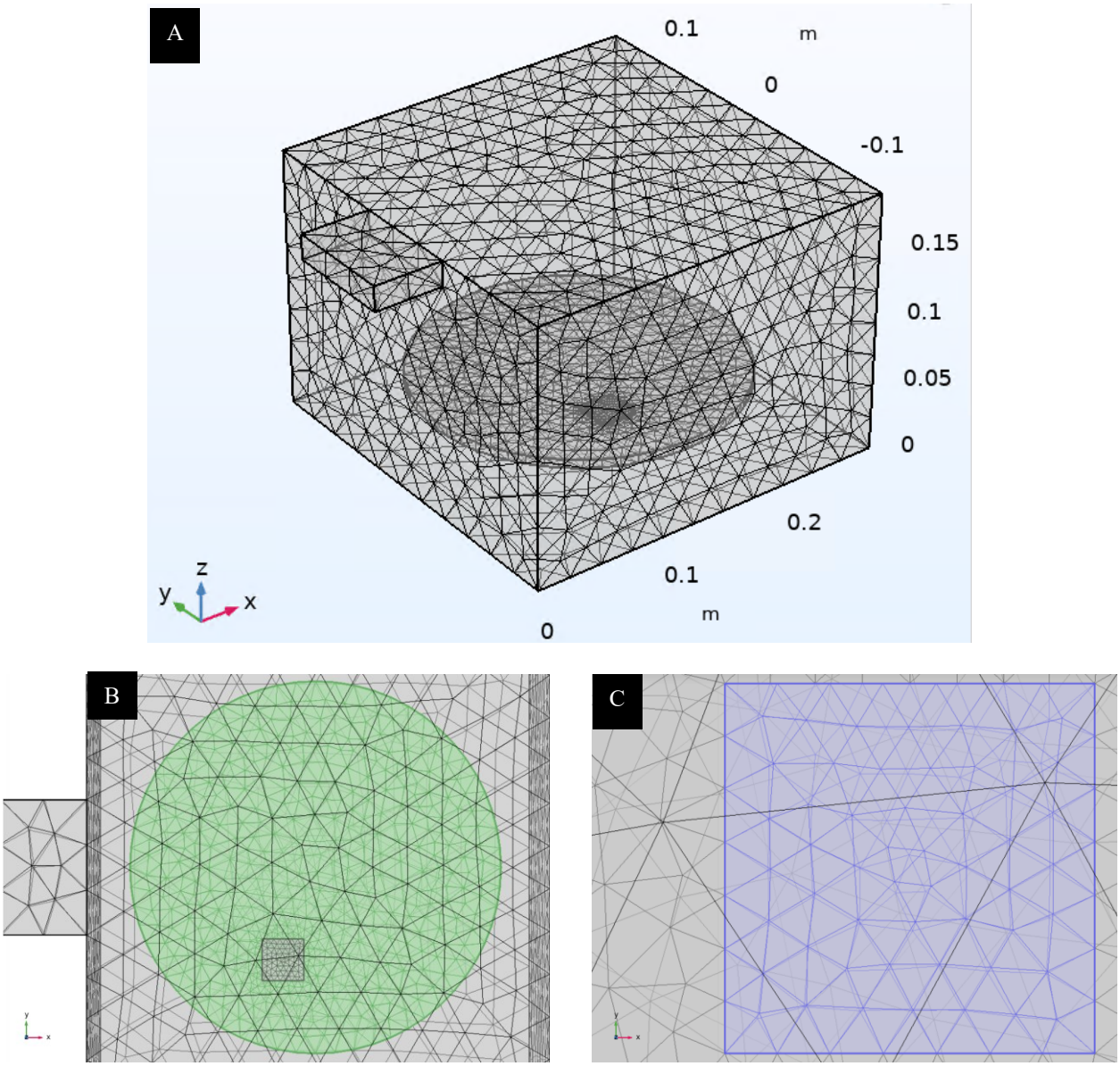

Figure 21: Meshing of (A) 3D microwave cavity, (B) Glass Plate, and (C) Specimen

4.7.2 Density

Taking the value of density of the matrix (PLA) and filler (GNP) as 1.24 g/cm^3 and 2.2 g/cm^3, respectively (from Section 3.1), the density of the nanocomposites (ρ_c) was calculated theoretically using the "rule of mixtures for density":

$$\rho_c = \frac{1}{\frac{w_f}{\rho_f} + \frac{w_m}{\rho_m}} \tag{40}$$

where, w_f = weight fraction of the filler

ρ_f = density of fillers

w_m = weight fraction of the matrix

ρ_m = density of matrix

4.7.3 Electrical Conductivity, Specific Heat, Thermal Conductivity and Complex Permittivity

The experimental setup used to compute the values of Electrical Conductivity, Specific Heat, Thermal Conductivity, and Complex Permittivity is described in Sections 3.4.1 to 3.4.3. The modification of all these properties with respect to GNP loading is addressed in the next chapter.

Chapter 5: Results and Discussion

Aspects of the material discussed in this chapter have been presented in the proceedings of The Canadian Society for Mechanical Engineering (CSME) International Congress, University of Alberta, Edmonton, Canada, June 5 - 8, 2022 and published in the proceedings of The Canadian-International Conference on Composites (CANCOM) International Congress, Fredericton-Moncton, NB, Canada, July 12-15, 2022.

5.1 Thermal Properties

Table 2 shows that the results from the differential scanning calorimetry. Specific heat capacity improved by 35.8 and 49.2 %, over the pure PLA matrix, respectively, when 8 wt% of pGNP and 8 wt% of fGNP were added. It is important to note that the experimental assessment of the specific heat capacity was made without taking into account the temperature dependency of density. Particularly at higher temperatures, this can have an impact on the measurement. Figures 22 (A) and (B) depict the thermal conductivity variation in pGNP/PLA and fGNP/PLA samples, respectively. The isotropic thermal conductivity of neat PLA is 0.12 W/mK, which is comparable with values reported in the technical literature [121], [122].

Table 2: Specific heat capacity of PLA composites with different GNP filler weight fractions

Material	**Filler loading (wt%)**	0	1	4	8
GNP	**Specific heat capacity (MJ/m^3K)**	1.87	2.1	2.45	2.54
fGNP	**Specific heat capacity (MJ/m^3K)**	-	2.41	2.69	2.79

In terms of thermal conductivity, adding more pGNP and fGNP filler significantly increased thermal conductivity, especially in the in-plane direction of the pGNP/PLA and fGNP/PLA samples, leading to significant anisotropy. For instance, in 8-pGNP/PLA samples, the in-plane thermal conductivity peaked at 1.05 W/mK, but the through-thickness direction only

reached 0.26 W/mK. Similarly, the in-plane and through-plane thermal conductivities of the 8-fGNP/PLA samples were 1.52 W/mK and 0.41 W/mK, respectively. Notably, the in-plane thermal conductivity of 8-pGNP/PLA and 8-fGNP/PLA nanocomposites was enhanced by a factor of approximately 7.5 and 12, respectively, when compared to pure PLA. It is also observed that the fGNP/PLA composites had greater thermal conductivity than pGNP/PLA composites with the same nanofiller concentration.

The rise in thermal conductivity is ascribed to GNP's extraordinarily high thermal conductivity relative to the polymeric matrix, as well as probable network development and interaction between graphene platelets as filler concentration increases, resulting in heat conduction channels. The latter can result in decreased phonon scattering effects between polymer chains and filler particles [110], [111], [123], [124]. In the case of fGNP/PLA samples, Tannic acid brings about non-covalent modification. Non-covalent modification has shown improvement in interfacial adhesion between functionalized filler and matrix, thereby promoting more uniform dispersion of functionalized filler in the matrix as compared to unfunctionalized filler [110], [125]. Better bonding and dispersion may further reduce phonon scattering between the fGNP-PLA interface and promote easier phonon transit between fGNP nanofillers, resulting in improved thermal conductivity [110], [124], [126]. The much increased in-plane thermal conductivity, compared to the through-thickness direction, may be explained by in-plane stacking effects of high-aspect ratio graphene platelets in the GNP/PLA nanocomposites. Similar patterns were seen in [111], [127].

5.2 Electrical Conductivity

Two processes lead to electrical conductivity in polymers: (i) contact between particles creates paths for the conduction of electrical charge known as leakage current; and (ii) sufficiently close proximity of particles (at the nanometer scale) enables the quantum mechanical phenomenon of electron tunnelling to occur, allowing the conduction of electrical charge via a tunnelling current [128], [129]. Furthermore, filler particle aspect ratio and filler dispersion state, as well as filler-matrix and filler-filler interactions, all influence electrical conductivity in polymer nanocomposites [44]. Additionally, in polymer nanocomposites with electrically conductive filler there is a

considerable increase in electrical conductivity at a threshold proportion of conductive particles. The percolation threshold is the least amount of nanofillers necessary to cause this abrupt change.

Electrical conductivity of pGNP/PLA and fGNP/PLA nanocomposites varied significantly as a function of GNP loading, as seen in Figures 23 (A) and (B). The electrical conductivity of neat PLA, 1-pGNP/PLA, and 1-fGNP/PLA samples was below 10^{-15} S/cm, indicating that they were insulators. However, the electrical conductivity of the 4-pGNP/PLA and 8-pGNP/PLA nanocomposites increased by many orders of magnitude to ~10^{-9} S/cm and ~10^{-3} S/cm, respectively. For the 4-fGNP/PLA and 8-fGNP/PLA, the value rose to ~10^{-9} S/cm and ~10^{-2} S/cm, respectively. Thus, the 8-pGNP/PLA and 8-fGNP/PLA nanocomposites can be classified as a semiconductor rather than an insulator. The percolation threshold is also defined as the point at which an insulator transitions to a conductor owing to the development of a conductive network [130], [131]. Thus, the transition of PLA-based nanocomposites from insulator to semi-conductor indicates that percolation threshold has been reached in this study.

The incorporation of graphene sheets into polymer matrices improves free electron and charge carrier mobility [131]. Thus, with rising GNP concentrations, leakage and tunnelling currents increase due to increased physical contacts and reduced spacing between platelets, respectively. Leakage current is more likely to contribute to charge conduction than tunnelling current [132]. However, conductive routes are limited at low pGNP and fGNP concentrations because the distance between nanofillers is greater than the tunnelling distance. Thus, polymer chains envelop and separate nanoparticles. As a result, conductivity increases by a very little amount up to 6 wt% pGNP and fGNP loading. With the addition of pGNP and fGNP, the nanocomposite reached a critical concentration between 6 wt% and 8 wt%, with a three to four orders of magnitude rise. This dramatic increase in electrical conductivity might be attributed mostly to an increase in electron migrating and hopping [133]. It has thus assumed that the percolation threshold has been reached, supporting the aforementioned hypotheses. As a result, the PLA's electron conduction networks were developed at pGNP and fGNP weight fractions between 6 and 8 % [110], [111]. In

other studies, it was discovered that percolating happened when GNP concentration rose from 7 to 8 wt% [129] and 6 to 9 wt% [132].

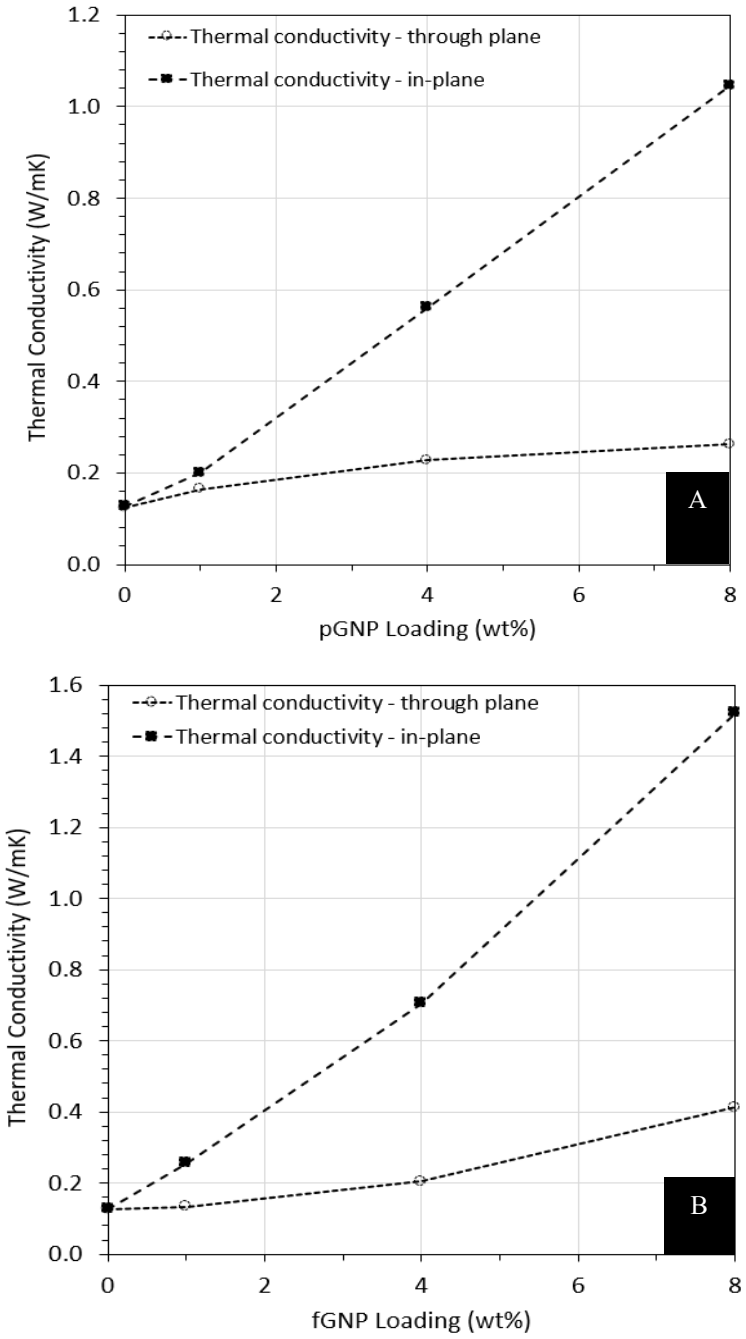

Figure 22: Thermal conductivity for PLA composites with (A) different pGNP filler weight fractions and (B) different fGNP filler weight fractions

Moreover, when compared to the same nanofiller loading, fGNP/PLA had greater electrical conductivity than pGNP/PLA, which is due to improved dispersion of fGNP within the polymeric matrix and increased contact area between the overlapping surfaces of fGNP [110]. As a result, more linked electron conduction networks may emerge, facilitating electron transmission.

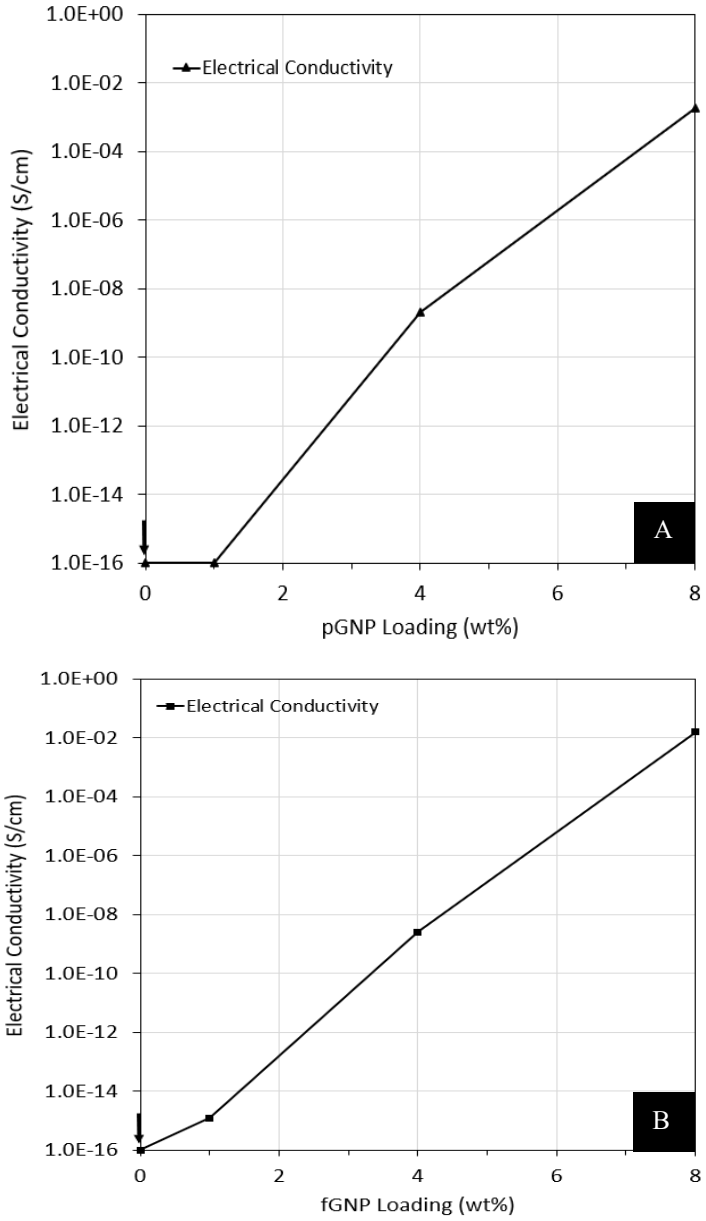

Figure 23: Electrical conductivity for PLA composites with (A) different pGNP filler weight fractions and (B) different fGNP filler weight fractions

5.3 Complex Permittivity

A material's permittivity can be affected by the polarisation of its internal charges [131]. Permittivity in polymers is normally low; but, by adding conductive fillers, it may be greatly raised [131], [134]. In filled polymers, matrix polarisation, conductive filler particles used, filler weight percent and its dispersion, the matrix/filler interface interaction, frequency, and temperature can all affect the composite's total permittivity [131], [132]. Due to the different relaxation durations of the matrix and the filler, a current flowing across their interface may lead to a buildup of charges at the interface, increasing the permittivity [132].

The variation of dielectric constant, ε', and dielectric loss factor, ε'', of pGNP/PLA and fGNP/PLA nanocomposites with respect to GNP loading is shown in Figures 24 (A) and (B), respectively. The data demonstrate that pGNP and fGNP concentration has a significant impact on the complex permittivity of PLA nanocomposites. Both ε' and ε'' show similar growth patterns with increasing pGNP and fGNP loading. For pGNP/PLA nanocomposites, the values of ε' and ε'' climbed from 2.5 to 5.91 and 0.04 to 0.67 from neat PLA to 8-pGNP/PLA samples, respectively. ε' and ε'' rose from 2.5 to 6.23 and 0.04 to 0.51 from neat PLA to 8-fGNP/PLA samples, respectively.

The experimental results and the technical literature are in agreement. According to [135], adding a conductive GNP filler to PLA nanocomposites boosts their conductivity and dipole moment, which significantly improves their permittivity. Similar increases in ε' and ε'' with increased pristine GNP loading were noted in other studies ([129], [132], [136]). For instance, for a 4 vol% GNP/epoxy nanocomposite at 1 GHz, ε' and ε'' were 8.5 and 0.9, respectively [136]. The main disadvantage of using pristine polymer/graphene composites for energy storage applications is their high energy dissipation, high dielectric loss, high current leakage at the percolation threshold, and a high tendency for graphene sheet agglomeration in the polymer matrix. These limitations can be overcome by introducing functionalized graphene sheets [131].

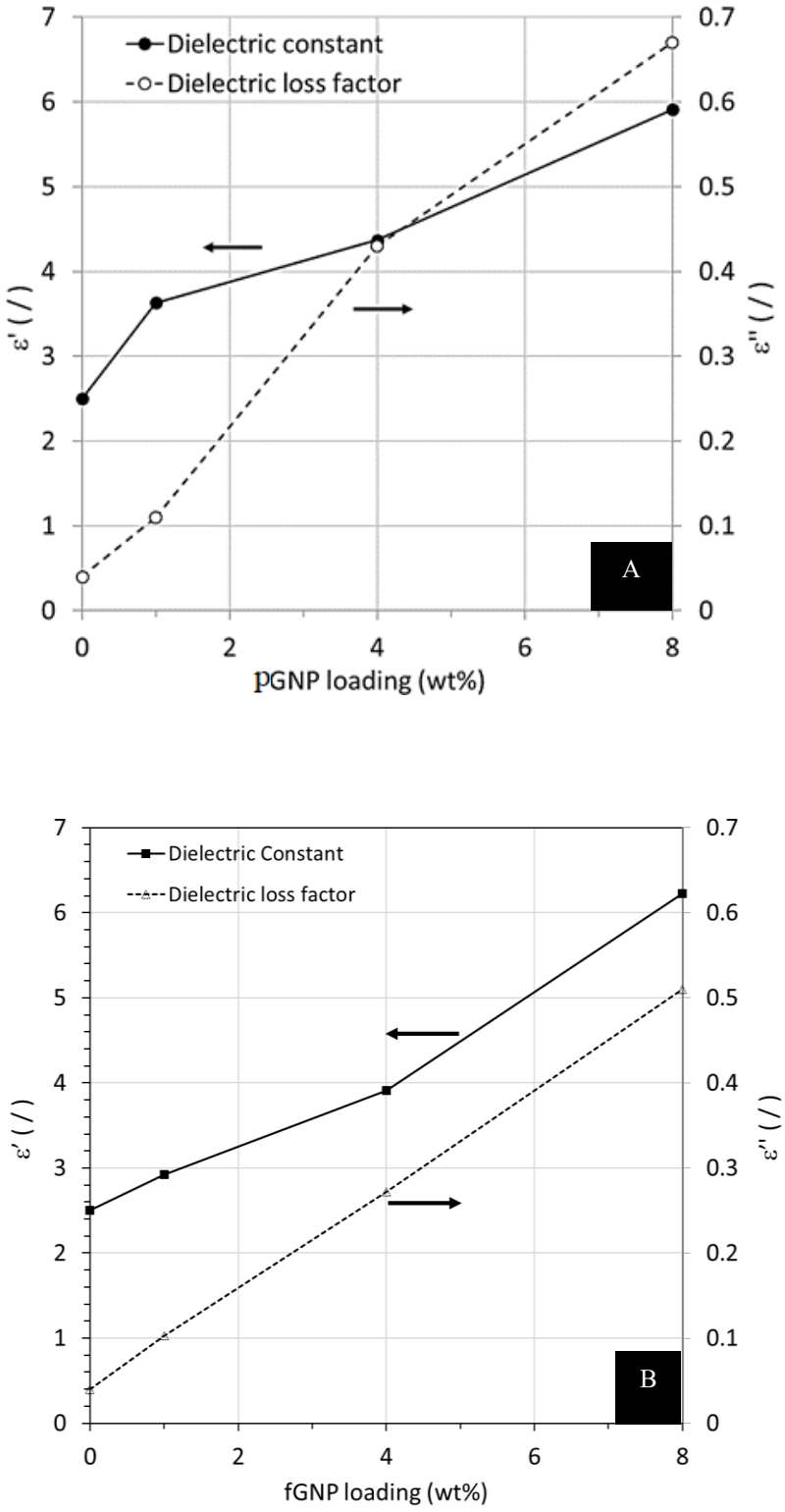

Figure 24: Complex permittivity, i.e., dielectric constant ε' and dielectric loss factor ε'', for PLA composites with (A) different pGNP filler weight fractions and (B) different fGNP filler weight fractions

Presumably due to better interfacial contact between graphene sheets and the polymer matrix [137] and the production of several micro-capacitors [138], functionalized graphene sheets improve the dielectric performance of polymers. However, in the current study it was observed that fGNP/PLA showed overall lower complex permittivity than pGNP/PLA at the same nanofiller loading. The functionalized graphene/polymer composites' low values of complex permittivity and energy dissipation are ascribed to a restriction on the high mobility of free electrons, delocalized π-orbital electrons, and current leakage [131], [139] due to the wrapping of the fillers by polymer matrix.

5.4 Microwave Heating

Figure 25 (A) depicts a 1-pGNP/PLA sample that has melted, and Figure 25 (B) shows a thermograph for the same sample after heating at 1.2 kW for 60 seconds. The thermograph as well as the melted sample show the anticipated volumetric heating of the nanocomposite material, with sample interior temperatures reaching their highest levels. It is clear that the location of the high temperature, also known as ‘hotspots’, is the same in both situations. The maximum temperatures for the different pGNP/PLA and fGNP/PLA samples after being exposed to radiation for the specified durations at 0.6 kW and 1.2 kW are shown in Figures 25 (C) and 26, respectively. Appendices A and B provide melted sample images and thermographs, respectively.

The graph shows that even after 180 seconds of irradiation, the melting temperature (160°C) of pure PLA when heated at 0.6 kW was not attained. The pure PLA sample did, however, reach the melting point in 180 seconds at 1.2 kW. For the pGNP-based nanocomposites, at the low and high-power levels, the 1-pGNP/PLA samples melted after 180 and 80 seconds, respectively. For the fGNP-based nanocomposites, at 0.6 kW and 1.2 kW power level, the 1-fGNP/PLA samples showed no signs of melting within 180 seconds. Notably, the melting points of the 4-pGNP/PLA, 4-fGNP/PLA, 8-pGNP/PLA, and 8-fGNP/PLA samples were achieved for both power levels within 15 seconds. Observations made from these plots are discussed in the following section.

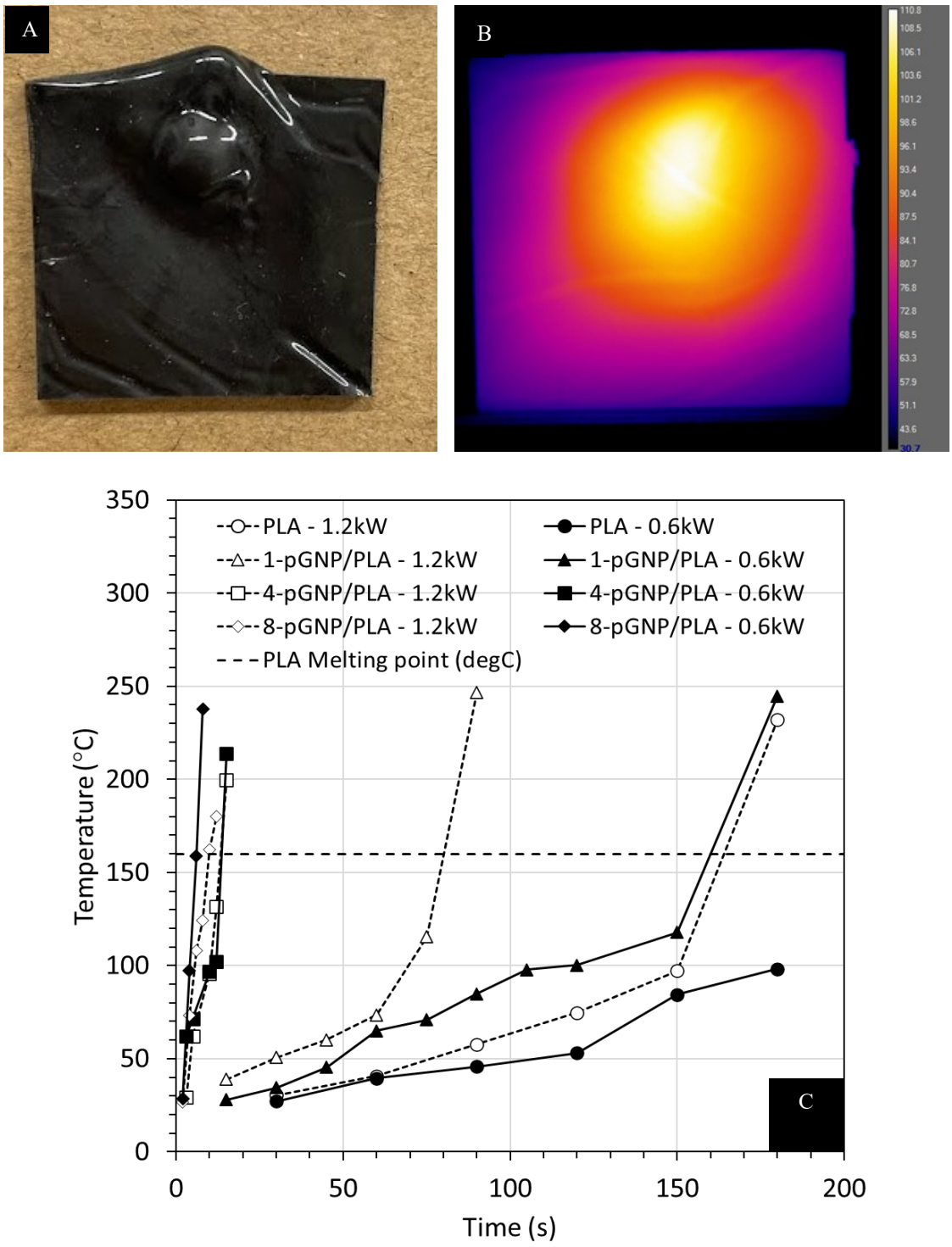

Figure 25: 1-pGNP/PLA sample (A) Melted after microwave heating, (B) thermograph when irradiated with microwaves at 1.2kW for 60 seconds, and (C) measured maximum temperatures at different microwave irradiation durations for samples with different pGNP filler weight fractions

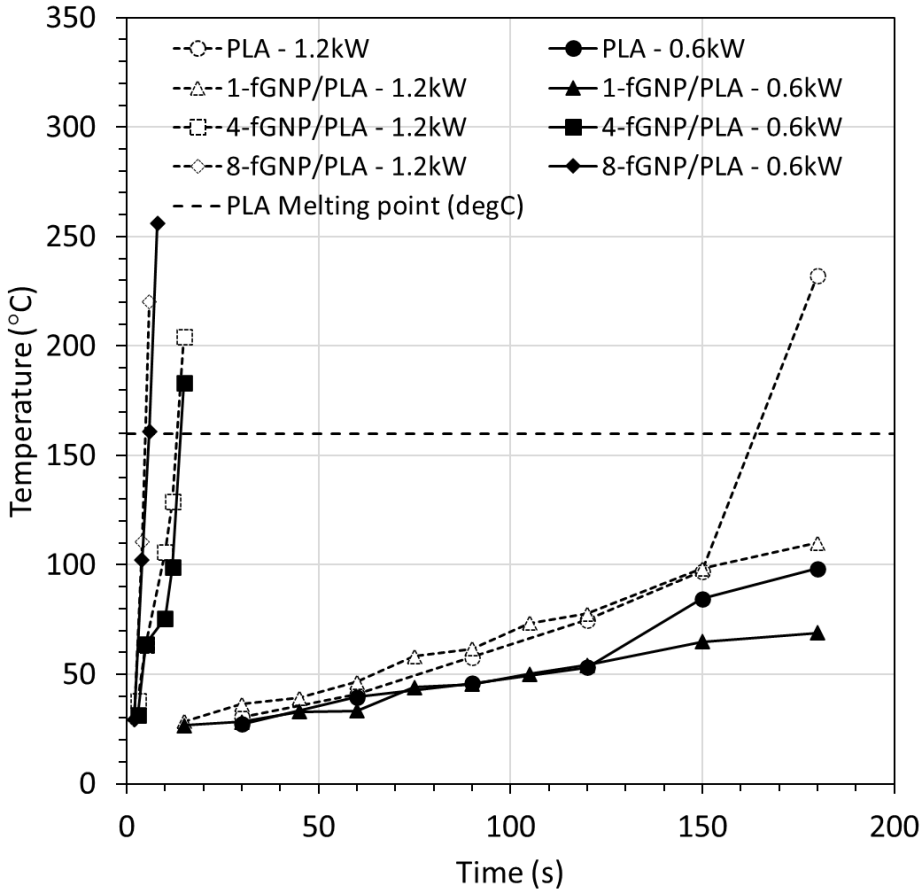

Figure 26: Measured average temperatures at different microwave irradiation durations for samples with different fGNP filler weight fractions

5.4.1 Effect of GNP Addition

It is evident from Figures 25 (C) and 26, that when electromagnetic wave absorbing pGNP and fGNP are added to the PLA matrix, the time required to melt the material decreases drastically. Clearly, as GNP loading increases, the nanocomposite shielding effectiveness improves, as does electrical (and thermal) conductivity and permittivity [129], [140]. Similar findings were made in [127], where it was shown that at a given hot table temperature for the same heating period, the surface temperatures of GNP-based polymethyl methacrylate nanocomposites with high filler weight fractions were considerably greater than those with low filler weight fractions. They concluded that this was because the sample with higher GNP loading had a more complete heat conduction network and pathway than the sample with lower loading. Di-electric loss has also been

identified as the cause of the improvement in the microwave absorption of GNP-based composites [141], [142]. A conductive composite's free electric charges will interact strongly with outside microwave radiation and convert that energy to heat. This would aid to significant improvement in microwave absorption [141]. In the present study, the dielectric loss of 8-pGNP/PLA and 8-fGNP/PLA was greater than that of other samples, hence these samples melted first.

5.4.2 Data Scatter

As seen in Figures 27 (A) and (B), there was substantial data scatter for the 4-pGNP/PLA and 8-pGNP/PLA samples, with standard deviations approaching 100K in certain instances. For microwave related experiments to be accurate and repeatable, steady power and uniform heating are needed [143]. The type of microwave source used in this study, a domestic microwave, is seen to be primarily responsible for the observed significant data scatter. Similar issues of uneven heating when using a domestic oven have been reported in [96], [143]–[145]. A household microwave oven's heating chamber is a sealed metal space where the microwaves will be completely reflected. A microwave standing wave distribution, characterised by a non-uniform spatial distribution of the electric field, would occur in the heating chamber following repeated reflections on the metal surface [145]. Inevitably, the inhomogeneous spatial distribution of the microwave radiation causes the microwave chamber to heat unevenly. It has also been demonstrated that this microwave type produces uneven radiation power [143]. Due to all of this, values vary significantly. It is advised that future experimental research employ a single-mode microwave source, which is more suited to maintaining controlled power and homogenous heating.

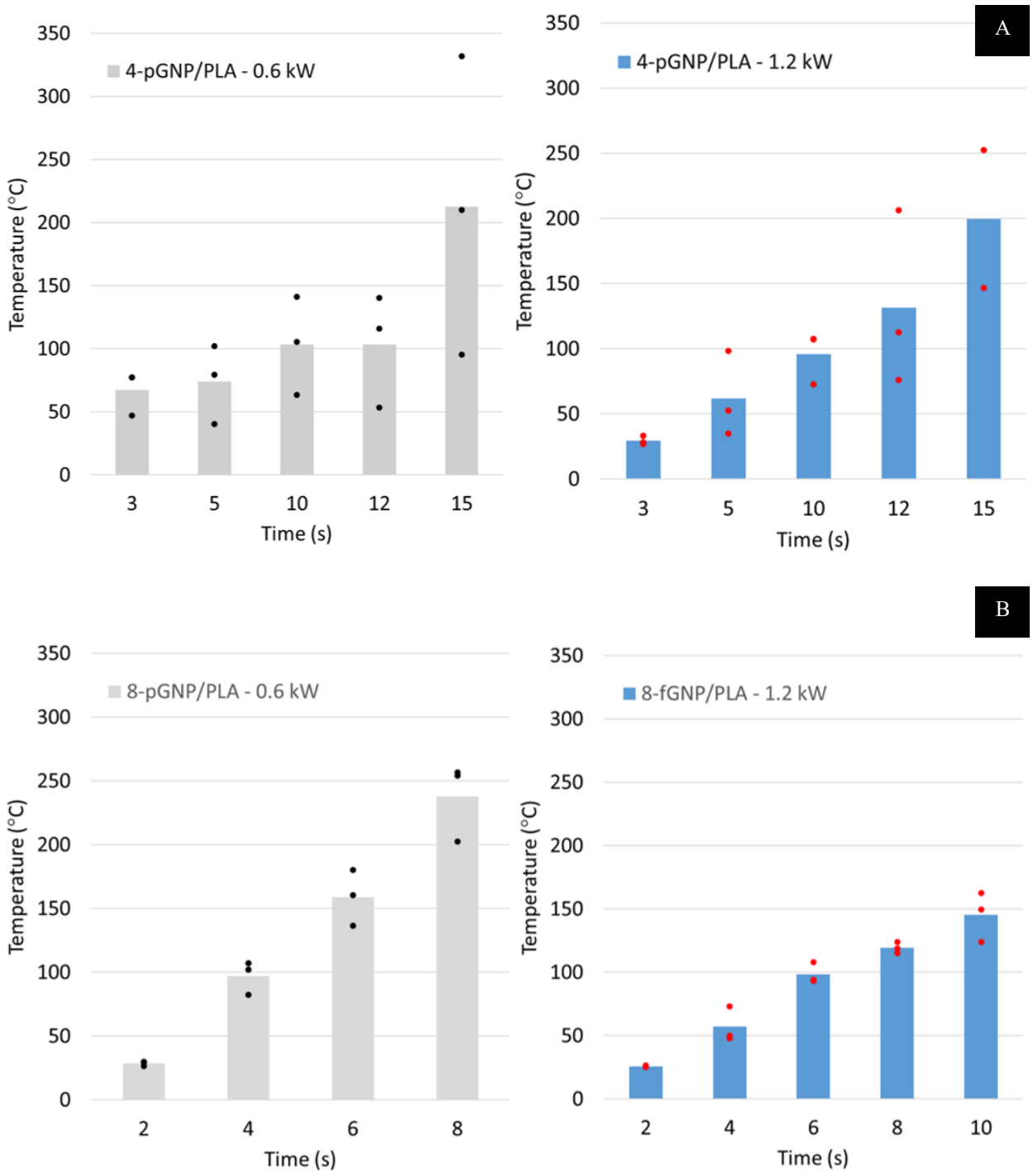

Figure 27: Standard variation in (A) 4-pGNP/PLA and (B) 8-pGNP/PLA when irradiated with microwaves at 0.6 kW and 1.2 kW

5.4.3 Rapid Increase Close to Melting Point

As depicted in Figure 25 (C), a somewhat linear temperature increase was noticed for neat PLA and 1-pGNP/PLA samples up until a sharp spike in temperature was noticed close to the melting point. A similar sudden rise close to melting point is seen in Figures 28 (A) and (B) for 4-pGNP/PLA, 4-fGNP/PLA, 8-pGNP/PLA and 8-fGNP/PLA. The observed rapid rise in temperature towards the melting point might be due to the fact that composite dielectric loss increases with temperature [146]–[148] while thermal diffusivity decreases [149], boosting heat generation. The effect of varying temperature on the microwave energy absorption has been discussed in Sections 2.5.1 and 2.5.2. As a result, if the sample temperature is sufficiently high (close to the melting point), the heat generation rate surpasses the sample's heat dissipation capability. Under these conditions, heat accumulates in the specimen, resulting in continual and rapid temperature rise [149]. Therefore no data in shown in Figure 27 (B) for the melting of 8-pGNP/PLA when heated for 10 seconds at 0.6 kW. Another possibility for this sudden spike is the presence of thermal transition effects. The p-GNP/PLA specimens had a glass transition temperature between 66.7 and 69.4 °C [110]. When heated at 0.6 kW and 1.2 kW, the heating rate of the PLA and 1-pGNP/PLA specimens changes abruptly around these temperatures, as shown in Figure 25 (C). This indicates that the specimen has changed from hard and brittle to soft and pliable. For thermoplastic-based polymer composites, the effect of threshold temperature (which may be glass transition) and rapid heating is discussed in Section 2.6.1. In the work of Bajpai et. al [26], the authors employed microwaves to join natural fiber reinforced PLA. They discovered that when the temperature of the joint is higher than the matrix's glass transition temperature, a suitable bond between the matrix and the gasket material is formed. The influence of glass transition temperature on microwave-aided material processing has been employed in fracture healing [150]. The polymer chains melt as a result of the heat generated in the area surrounding the microwave absorber filler. If these chains are well above their glass transition temperature, they can diffuse into each other and repair the crack.

When heated at 0.6 kW and 1.2 kW, the samples melted in 8 and 10 seconds, respectively. It is thought that when heated at 1.2 kW, rather than 0.6 kW, the 8-pGNP/PLA material reached the

phase transition temperature quickly, and the heat generated was unable to travel to lower temperature areas, diminishing temperature uniformity and slowing the melting process. Moreover, in case of microwave-assisted heating, uniform heating is only possible when the frequency and penetration depth match the thickness of the materials [151]. If the thickness of the material is very large (with respect to penetration depth) and the frequency is insufficient, just the surface of the material gets heated, and not the entire material.

5.4.4 'Diminishing Return' Beyond 4 wt% pGNP and fGNP

An intriguing observation is a 'diminishing return' in pGNP and fGNP loading, i.e., beyond 4-pGNP/PLA and 4-fGNP/PLA heating a nanocomposite to the melting point happens in only seconds, as seen in Figures 28 (A) and (B). This may offer process control issues to avoid overheating. These effects might be attributed to the presence of filler agglomerates and percolated particle clusters exceeding 6 wt% pGNP loading [111], as discussed in Section 5.2. Agglomerates and interconnected particles are formations that have a greater aspect ratio but a lower effective conductivity. When the concentration of filler approaches the percolation threshold, agglomerates or arrays of linked particles begin to have lateral dimensions similar to the whole specimen. The description of electromagnetic processes in agglomerates is a challenging problem that may be tackled using percolation theory and Monte Carlo simulation [152]. However, percolation often impacts the imaginary component of the dielectric permittivity while influencing the real part to only a minor extent [153]. Thus, the diminishing return beyond 4 wt% GNP can be due to the drastic change in dielectric loss factor of samples close to the percolation threshold at 6 wt % GNP. The variation of dielectric loss factor with GNP loading has been discussed in Section 5.3.

Similar findings were obtained in [75], where microwave heating was used to weld 3D-printed carbon nanotube/ PLA composites. The authors discovered a substantial link between electrical percolation and film heating response, with a significant increase in heating rate over the percolation threshold. They also found that there is a minimum filler loading that is required to obtain a quick heating response (which in the present case is 4 wt% GNP). At greater filler loadings, the thermal response decreases and becomes less uniform. This unexpected outcome

occurs because, as loading increases, the films become more reflective and hence less absorbent to incident microwaves. This explains the diminishing return beyond 4 wt% GNP. Thus, optimizing both heating rate and uniformity requires a narrow range of loadings with a robust interaction between the electromagnetic field and the composite.

5.4.5 Comparison of Functionalized and Pristine GNP Nanocomposites

Figures 29 (A) and 29 (B) show the fluctuation of maximum temperature with time for pure and functionalized GNP-based nanocomposites. When heated at 0.6 kW for 180 seconds, 1-pGNP/PLA and 1-fGNP/PLA did not melt. 4-pGNP/PLA and 4-fGNP/PLA, as well as 8-pGNP/PLA and 8-fGNP/PLA, show comparable temperature rises over time. When heated at 1.2 kW, 1-fGNP/PLA did not melt. However, 1-pGNP/PLA melted in 80 seconds. 4-pGNP/PLA and 4-fGNP/PLA demonstrated similar responses to temporal variation. In contrast, the 8-fGNP/PLA samples melted quicker than the 8-pGNP/PLA samples.

Microwave heating is the formation of heat because of interactions between the material and microwaves, and it is a consequence of the electric field strength, frequency, and dielectric loss qualities of the medium. The dielectric characteristics of composites with a filler are affected by the filler type, concentration, and shape, as well as the sample preparation procedure. As a result, in a continual microwave treatment condition, the material with higher dielectric loss produces a higher temperature [150], [151]. Moreover, with reference to Figure 6, materials with low dielectric loss factors have been discovered to be transparent to microwaves due to a high penetration depth and low energy absorption. The dielectric loss of 1-pGNP/PLA is greater than that of 1-fGNP/PLA, as mentioned in Section 5.3. This explains why 1-fGNP/PLA does not melt when heated at 0.6 and 1.2 kW. Furthermore, rapid melting was seen when microwaves were irradiated at 1.2 kW, owing to the fact that increasing microwave power results in higher temperatures [154]. The effect of increasing microwave power on microwave energy absorption has been discussed in Section 2.5.4.

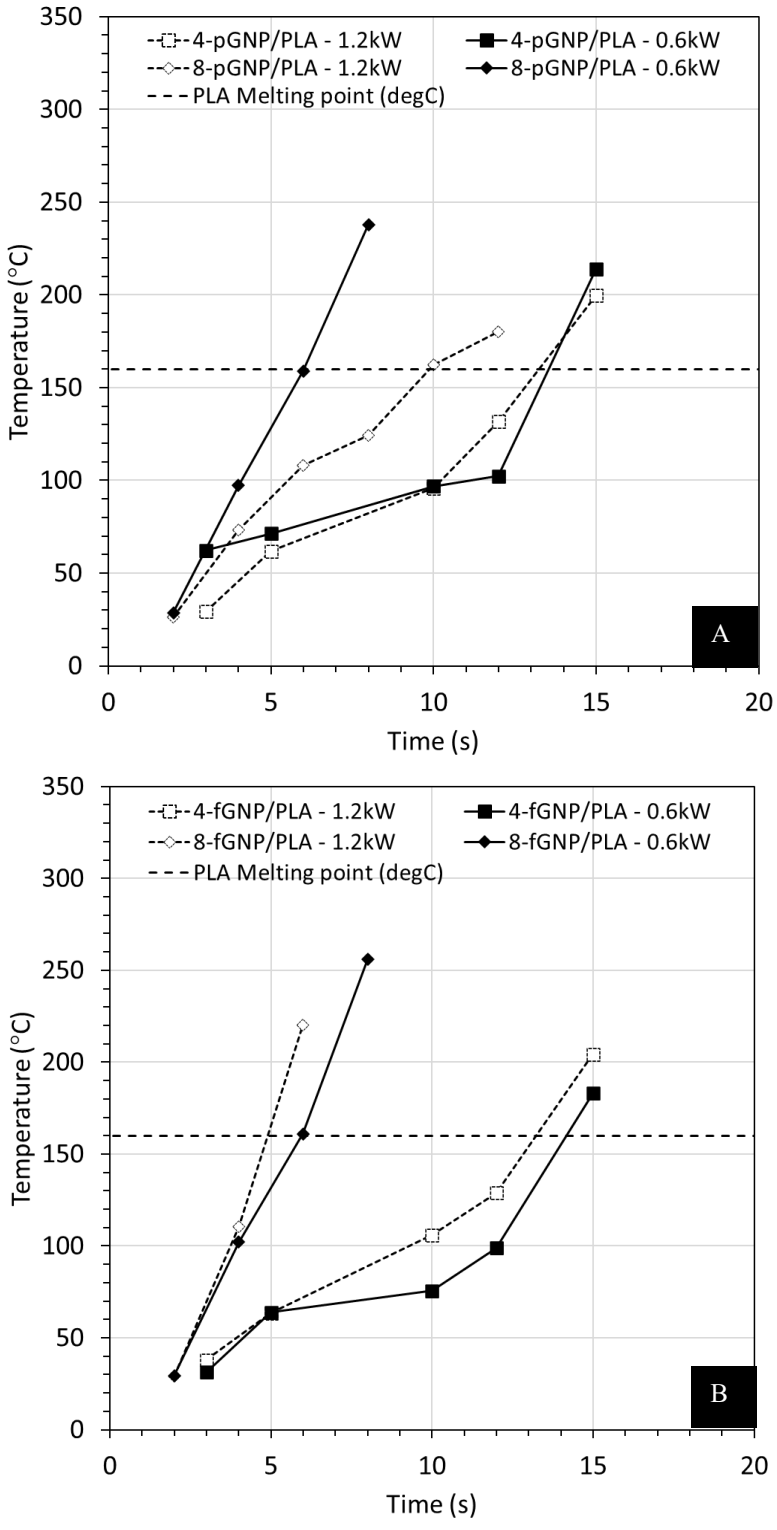

Figure 28: Diminishing Return Beyond 4 wt% (A) pGNP and (B) fGNP

The limited thermal conductivity of a polymer matrix prevents heat from passing through the specimen [150]. The heat conductivity in the through-plane direction of 4-fGNP/PLA composites is greater than that of 4-pGNP/PLA composites. Section 5.1 includes a detailed discussion on this subject. The dielectric loss of 4-pGNP/PLA, however, is greater than that of 4-fGNP/PLA. This means that while the 4-pGNP/PLA absorbs microwaves better, the 4-fGNP/PLA has superior heat conduction in the specimen after heating. It is postulated that for each of these samples, this leads to a nearly identical temporal prediction.

As discussed in [155], the addition of functionalized graphene oxide to a polymer matrix may be one of the reasons for the improvement in graphene filler particle dispersion. This results in consistent heating hotspots [156], better electromagnetic waves absorption [155] and a uniform increase in temperature [150]. This is seen to be the rationale for the superior heating and melting properties of 8-fGNP/PLA over 8-pGNP/PLA.

5.5 Numerical Model Predictions

The numerical model predictions were compared to the experimental findings for all samples when exposed with microwaves at 0.6 and 1.2 kW. The following section discusses the comparison between maximum temperature and time, as well as microwave energy absorbed and time.

5.5.1 Maximum Temperature

Figures 30 and 31 show the variance in measured and experimental maximum temperatures for samples irradiated with microwaves at 0.6 kW and 1.2 kW with varying pGNP and fGNP filler weight percentages. The modeled maximum temperature values matched the experimental data quite well. It is also observed that the simulated temperature profile increased linearly over time. All the plots, however, have one issue in common: the numerical model failed to account for the substantial increase in maximum temperature around the melting point. Similar findings were observed in [89], [95], [96], [157], [158].

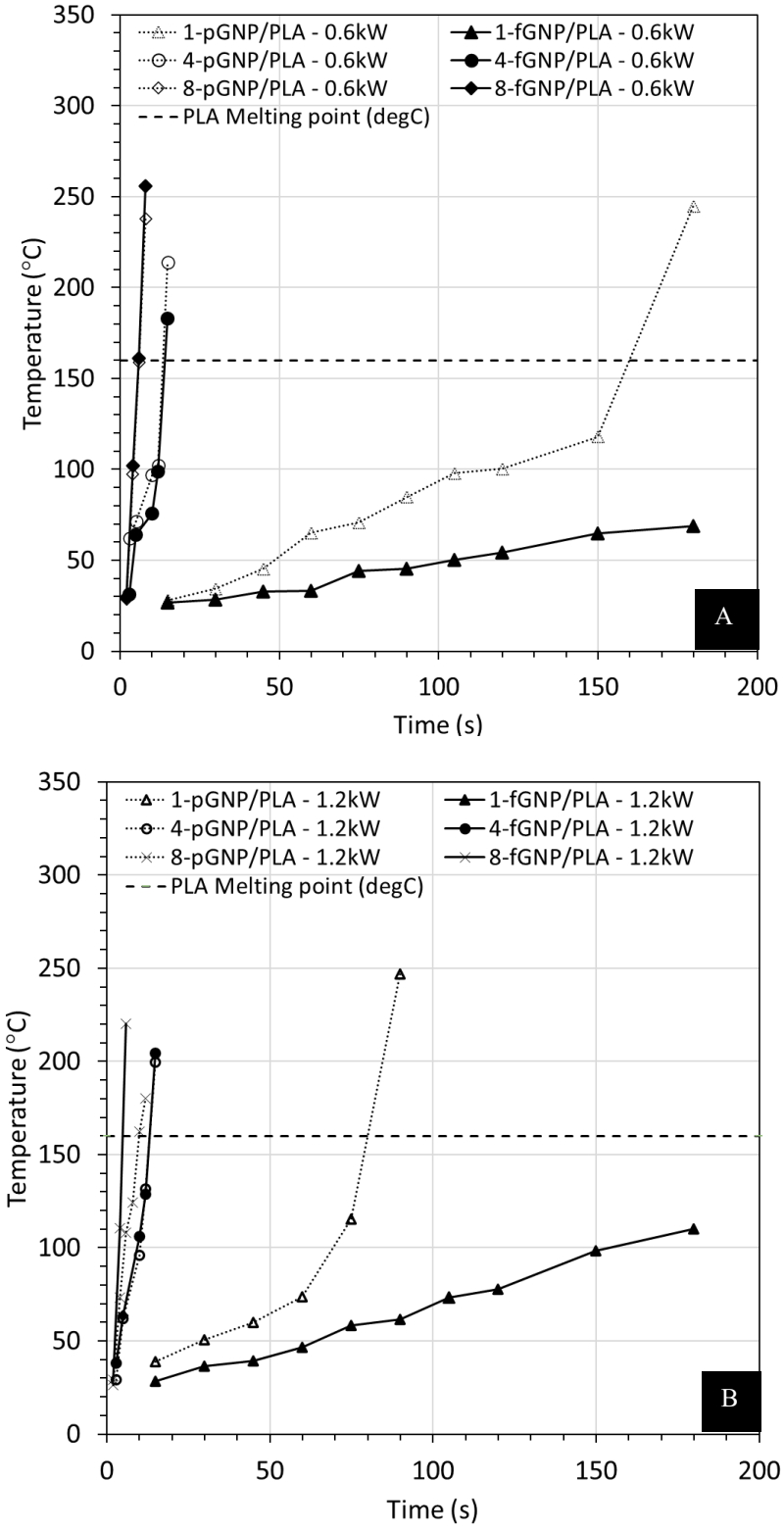

Figure 29: Temperature rise in functionalized and pristine nanocomposites when irradiated with microwaves at (A) 0.6 kW and (B) 1.2 kW

In actuality, due to changes in material characteristics as a function of temperature, the temperature of a material heated in a microwave may not vary linearly with time [158]. Section 2.5.1 explore this concept in depth. Furthermore, because no moisture mass and momentum transfer were incorporated in the present simulation study, a linear increase in the simulated temperature profile was predicted. Also, the simulation's used a constant specific heat value, which is a major factor for why the predicted temperature profile shows a linear rise over time. Another cause might be that the samples' dielectric characteristics are assumed to be constant. However, in the actual samples, these qualities are subject to change with time and temperature. Neglecting intraparticle resistance to heat and mass transfer may also lead to temperature discrepancies from experimental results [89]. The inherent (microscopic) characteristics of the material that the simulation physics treats macroscopically also contribute to the observed deviation between the simulated and measured behavior [159].

Moreover, changes in a magnetron's frequency can also have a significant impact on the distribution of the electric field and the pace of heating [96]. A typical magnetron is said to diverge from its fundamental frequency by roughly 50 MHz [160]. The position of the hot and cold areas was discovered to shift when the magnetron frequency changed [119]. As a result, an inaccurate frequency input may be the cause of the difference in temperature between expected and observed values. The effect of varying frequency on microwave energy absorption has been discussed in Section 2.5.2. Additionally, it has been observed that the core of a material dries quickest when heated with a microwave because of the volumetric heating feature. The heat from the core is then transferred to the outer layers via steam. The model cannot account for the fluctuation in electromagnetic characteristics caused by this occurrence [118].

It should be noted that the numerical model more effectively predicted the conditions for the 1-pGNP/PLA and pure PLA samples when heated at 0.6 kW for the p-GNP-based nanocomposites. Similar to this, when subjected to 0.6 kW of microwave radiation, the behavior of 1-fGNP/PLA material was found to be predicted with reasonable accuracy. This might be due to the fact that

when samples were heated at 0.6 kW, temperature rose at a reduced rate, causing material properties to change slowly as well with temperature and time, resulting in a fair approximation.

Conversely, when heated at 1.2 kW, superior predictions were established for the 4-pGNP/PLA, 8-pGNP/PLA, 4-fGNP/PLA, and 8-fGNP/PLA. The reason for this is because under increased microwave power irradiation, the 4 and 8 wt% GNP samples exhibit a quick rise in characteristics due to a rapid increase in material properties with regard to temperature and time, resulting in an almost linear increase in temperature rise. As a result, a more accurate estimate is provided. Section 2.5.4 explains the effect of microwave power on microwave energy absorption.

Overall, the maximum temperature of the fGNP/PLA samples was predicted with reasonable accuracy. At the microscopic level, functionalized nanocomposites have greater filler dispersion, but the numerical model did not account for these characteristics. Furthermore, as compared to pure specimens, the functionalized specimens had a greater value of electrical conductivity. High electrical conductivity has been demonstrated to cause interface impedance mismatch, which can enhance surface reflection while decreasing microwave absorption [161]. The numerical model does not incorporate this information. Additionally, at the same nanofiller loading, pGNP/PLA samples demonstrated lesser thermal conductivity. Thus, the fGNP/PLA nanocomposites may have conducted more heat from the PTFE dish and glass plate than the pGNP/PLA nanocomposites did. The numerical model did not account for these factors.

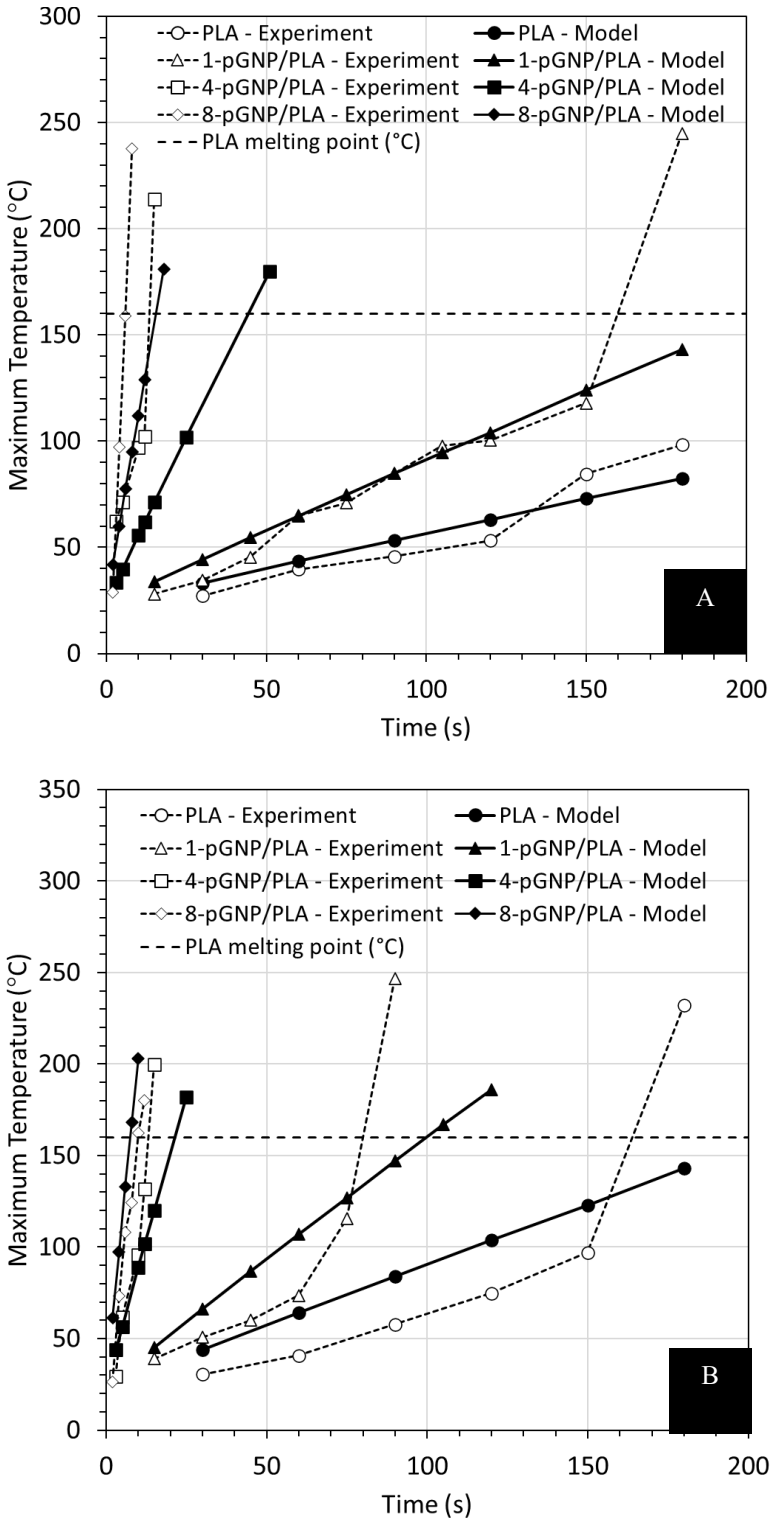

Figure 30: Measured and experimental maximum temperatures for samples with different pGNP filler weight fractions when irradiated with microwaves at (A) 0.6 kW and (B) 1.2 kW

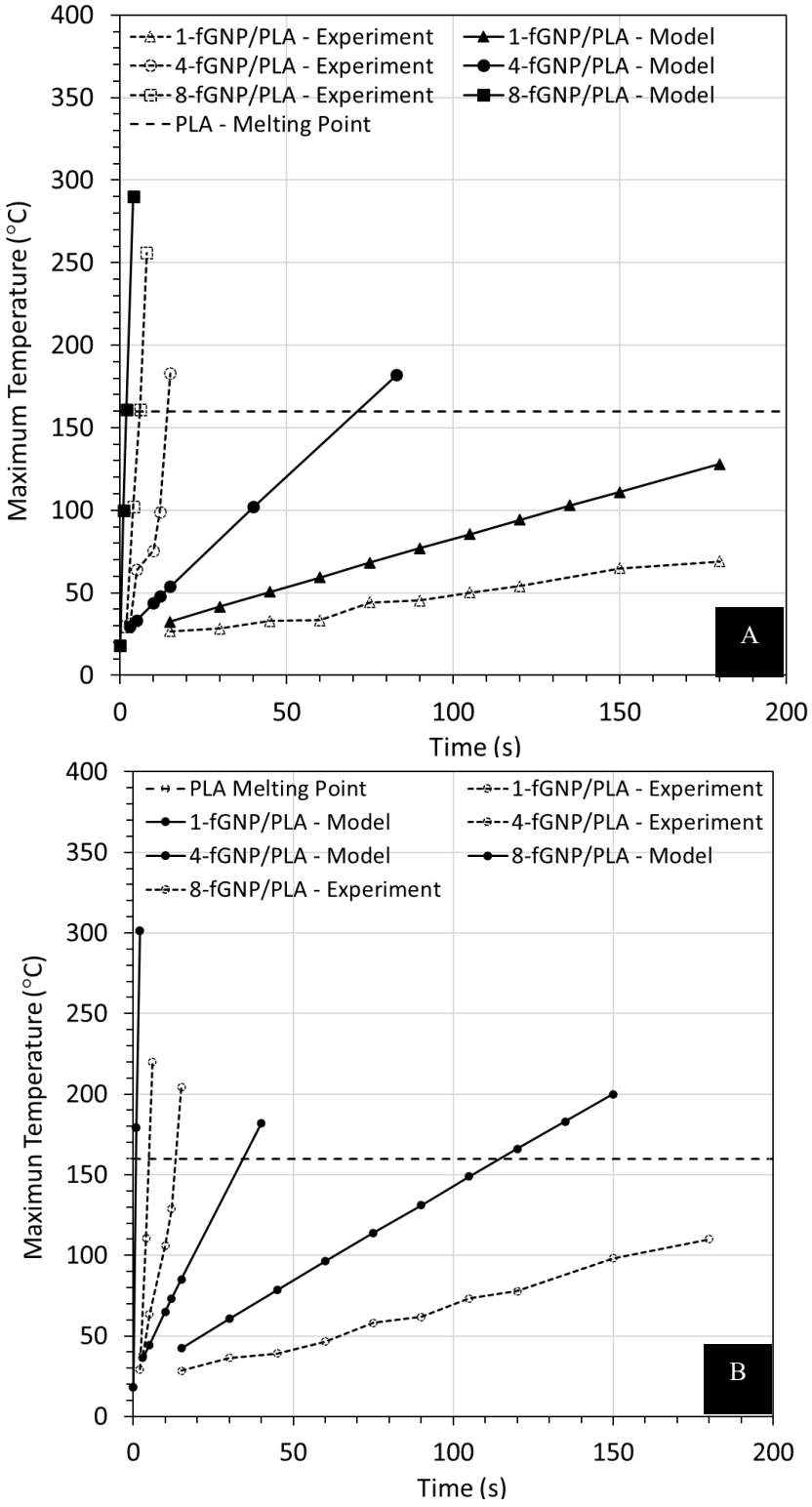

Figure 31: Measured and experimental maximum temperatures for samples with different fGNP filler weight fractions when irradiated with microwaves at (A) 0.6 kW and (B) 1.2 kW

5.5.2 Microwave Energy Absorbed

One way for measuring the microwave's effect on the given material is to assess the microwave power that is absorbed by a specimen when using a laboratory-scale microwave device [162]. The computed electromagnetic power density was integrated over the entire specimen domain in the numerical model to determine the microwave power absorbed. Similar studies have been published in [96], [163]–[165].

The simulated microwave energy absorbed (*Js*) with respect to time was then computed by:

$$J_S = P \times t \tag{41}$$

where, P = microwave power absorbed (Watt)

The experimental microwave energy absorbed (J_e) was determined as follows:

$$J_e = m \cdot c_p \cdot \Delta T \tag{42}$$

The quantity of microwave power absorbed is determined by the material's dielectric characteristics [165]. Microwaves are absorbed by materials with the largest dielectric losses at room temperature, whereas microwaves propagate through materials with lower losses. The absorbing medium transfers heat and energy to the transparent material.

Figures 32 and 33 illustrate the time-dependent change of experimental and theoretical microwave energy absorbed when irradiated with microwaves at 0.6 and 1.2 kW, respectively. In Section 5.3,

a rise in dielectric loss was seen in response to GNP concentration. Accordingly, as GNP concentration rises, so does the amount of microwave radiation that the samples are able to absorb.

The experimental and theoretical values of microwave energy absorbed are in good agreement up until the steep rise in experiment values is observed. As discussed in Sections 5.4.3 and 5.5.1, this sharp increase is the result of the increase in dielectric characteristics with regard to temperature (also explained in Section 2.5.1) and time. As a result, as the sample gets closer to the melting point, the rate at which heat is generated rapidly outpaces the sample's capacity to dissipate heat, and the microwave energy absorbed suddenly increases. Because the numerical model has not been equipped with the change in dielectric characteristics with regard to time and temperature, the predicted absorbed energy fails to include this abrupt rise in absorption.

A linear increase in microwave energy absorption is seen, which is consistent with the maximum temperature prediction in Section 5.5.1. There may be a variety of causes for this implausible trend. This includes not taking into account the change in material characteristics with time and temperature, intraparticle resistance to heat and mass transfer [89], as well as moisture mass and momentum transfer. Not accounting for the changes in specific heat and dielectric properties with time and temperature can potentially be a significant factor.

The fluctuations in electric and magnetic field strengths with temperature and time make experimental measurements of microwave power absorbed inside a material extremely challenging [11]. Furthermore, as seen in equation 10, power absorbed is affected by frequency and electric field. As discussed in Section 5.5.1, magnetron frequency diverges by approximately 50 MHz, which affects the electric field [96] and hence hotspot position [160]. As a result, an incorrect frequency might be the source of the temperature disparity between predicted and observed values. Section 2.5.2 discusses the influence of frequency variation on microwave energy absorption. Furthermore, functionalized nanocomposites have better filler dispersion at the microscopic level, but the numerical model cannot account for these properties.

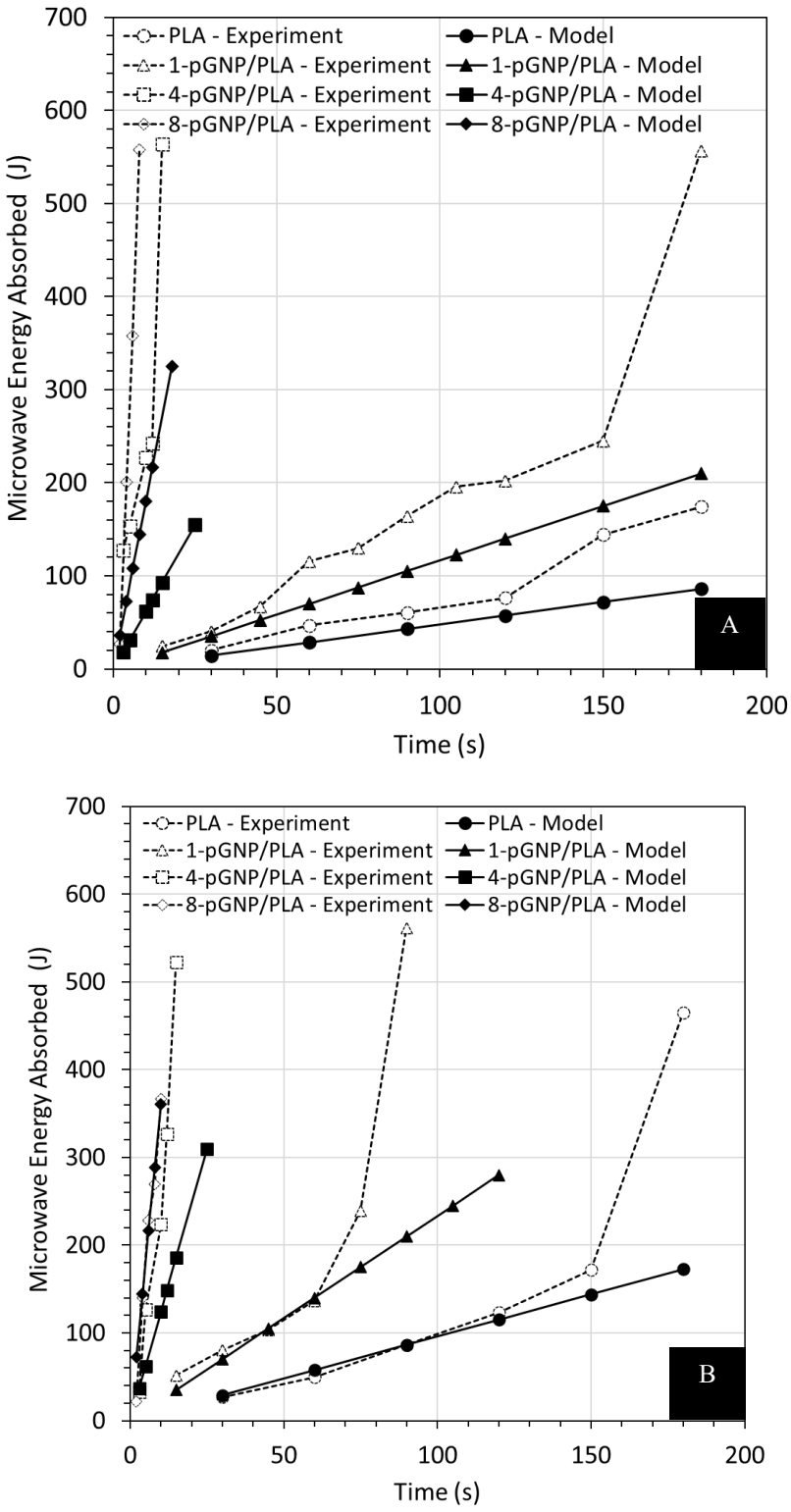

Figure 32: Microwave Energy Absorbed for samples with different pGNP filler weight fractions when irradiated with microwaves at (A) 0.6 kW and (B) 1.2 Kw

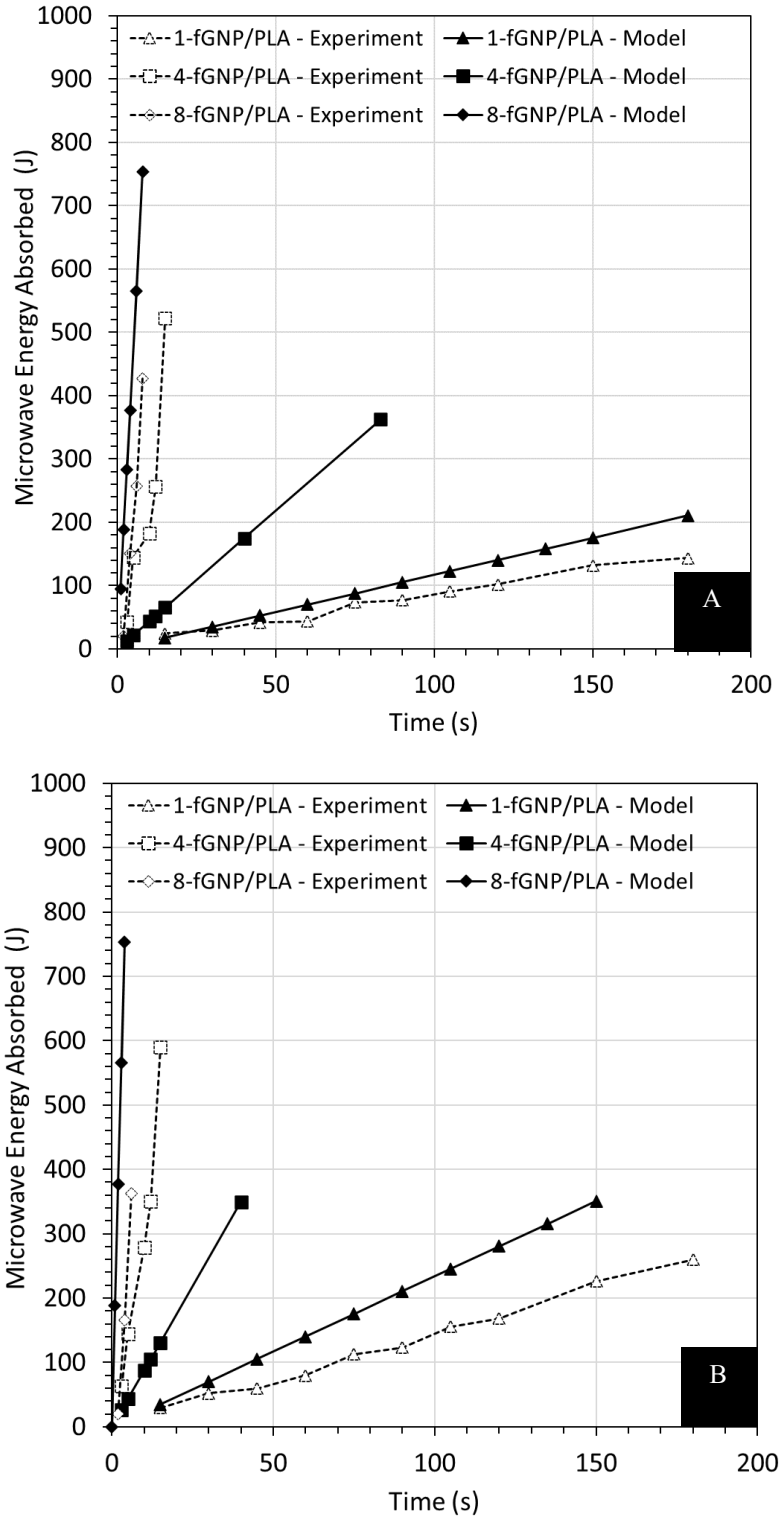

Figure 33: Microwave Energy Absorbed for samples with different fGNP filler weight fractions when irradiated with microwaves at (A) 0.6 kW and (B) 1.2 kW

Chapter 6: Conclusion and Future Work

6.1 Conclusion

Multifunctional GNP/PLA nanocomposite samples with various pGNP and fGNP concentrations were fabricated in this work. Their thermal and electrical properties, complex permittivity, and microwave heating behavior as a function of microwave power and filler concentration, were studied.

The results revealed that increasing pGNP and fGNP loading from nil to 8 wt% enhanced the specific heat capacity by 35.8% and 49.2%, respectively. The pGNP/PLA and f-GNP/PLA nanocomposites exhibited anisotropic thermal behaviour, with the in-plane thermal conductivity of 8-pGNP/PLA and 8-fGNP/PLA nanocomposites improving by a factor of almost 7.5 and 12, respectively, over pure PLA. In terms of electrical conductivity, pure PLA, with a value of less than 10^{-15} S/cm, was confirmed to be an insulator. In contrast, electrical conductivity for the 8-pGNP/PLA and 8-fGNP/PLA nanocomposites increased several orders of magnitude (10^{-3} S/cm and 10^{-3} S/cm), indicating that they are semiconductor materials. The complex permittivity parameters, ε' and ε'', rose from 2.5 to 5.91 and 0.04 to 0.67, respectively, from the neat PLA to 8-pGNP/PLA samples. ε' and ε'' rose from 2.5 to 6.23 and 0.04 to 0.51, respectively, from neat PLA to 8-fGNP/PLA samples, respectively. At the same nanofiller loading, fGNP/PLA had better thermal and electrical conductivity and lower complex permittivity than pGNP/PLA.

When heated in a 2.45 GHz fixed frequency multimode applicator at 0.6 kW, the 8-pGNP/PLA and 8-fGNP/PLA nanocomposites melted in mere 8 seconds, while pure PLA remained notably below the melting point even after 180 seconds or irradiation. The study revealed that increasing pGNP and fGNP filler loading to 4 wt% and 8 wt% substantially reduced the microwave heating time by over an order of magnitude compared to the pure polymer. The temperature rise was observed to be rapid, with poor reproducibility in test findings. Also, a sudden spike in temperature was noticed close to the specimen melting point. However, a decreasing return in filler loading

appears to exist beyond 4 wt%. Lastly, it was noted that when heating at 600W, 8-pGNP/PLA reached the melting point somewhat faster than when heating at 1200W.

When comparing the experimental temporal variations of functionalized and pristine GNP nanocomposites, it was discovered that when heated at 0.6 kW for 180 seconds, 1-pGNP/PLA and 1-fGNP/PLA did not melt. The temperature rises in the 4-pGNP/PLA and 4-fGNP/PLA, as well as the 8-pGNP/PLA and 8-fGNP/PLA, are comparable over time. 1-fGNP/PLA did not melt when heated to 1.2kW. 1-pGNP/PLA, on the other hand, melted in 80 seconds. 4-pGNP/PLA and 4-fGNP/PLA responded similarly to temporal variation. The 8-fGNP/PLA samples, on the other hand, melted faster than the 8-pGNP/PLA ones.

The numerical model predictions for maximum temperature and microwave energy absorbed matched the experimental data well. The simulated temperature profile increased linearly over time. However, all results have one issue in common: the numerical model failed to account for the significant rise in maximum temperature and microwave energy absorbed close to the melting point. It should be observed that when heated at 0.6 kW, the numerical model more accurately predicted the temperatures for the 1-pGNP/PLA, 1-fGNP/PLA, and pure PLA samples. Superior predictions were established when heated at 1.2 kW for the 4-pGNP/PLA, 8-pGNP/PLA, 4-fGNP/PLA, and 8-fGNP/PLA. Furthermore, it was discovered that as GNP concentration increases, so does the quantity of microwave radiation that the samples can absorb.

In summary, the produced multifunctional GNP nanocomposites were shown to afford high microwave absorption and hence rapid heating, owing to their considerably raised thermal and electrical conductivity and complex permittivity. This indicates that thermoplastic GNP nanocomposites are a suitable choice for gasket materials that enable fusion bonding via microwave irradiation in thermoplastic-based components such as in piping systems. In the experiments, imaging using a thermal camera not only revealed the temperature distribution but also the volumetric heating of the microwave-assisted heated samples. The developed numerical

model enabled predicting the maximum temperature and microwave energy absorbed in the heated specimens. However, the modeling approach, using constant material properties, was unable to predict a sharp increase in temperature close to the material melting point. Additionally, the model indicated a linear temperature rise over time, which deviates from experimental observations. The model could be augmented to incorporate temperature-dependent properties to capture the non-linear effects.

6.2 Future Work

This study offers a vast avenue for further exploration. Future work includes the following:

1) Incorporating a single-mode microwave in lieu of a multi-mode configuration. Single-mode microwaves have demonstrated quick and uniform, and reproducible heating results.

2) The fluctuation of material characteristics with reference to temperature can be taken into account when simulating experimental results using a numerical model.

3) The experimental values of density and complex permeability can be used in future numerical models.

4) Experiments can be repeated at multiple frequencies to observe the behaviour of materials at different frequencies.

5) Specimens of various shapes and sizes can be included, and their microwave absorption patterns can be investigated.

6) Specimens can be placed in the domestic oven at different spots and heights to study microwave absorption.

7) Specimens may be further characterised using scanning electron microscopy and Fourier transform infrared spectroscopy to examine GNP dispersion and surface chemical parameters, respectively. The transmission, reflection, and absorption spectra of the specimen can also be examined to better understand a material's behaviour when exposed to microwaves.

Bibliography

[1] "Key World Energy Statistics 2020 – analysis," IEA. (n.d.). [Online]. Available: https://www.iea.org/reports/key-world-energy-statistics-2020. [Accessed: April 04, 2022]

[2] Yu, K., Morozov, E. V., Ashraf, M. A., & Shankar, K. (2017). A review of the design and analysis of reinforced thermoplastic pipes for offshore applications. *Journal of Reinforced Plastics and Composites*, *36*(20), 1514-1530.

[3] Avery, A., & Martin, S. (2003, January). Reinforced Thermoplastic Pipe: Innovative technology for onshore field developments. In *International Conference on Offshore Mechanics and Arctic Engineering* (Vol. 36835, pp. 787-794).

[4] Thattaliyath Kadumberi, A. P., O'Leary, R., & Gachagan, A. (2012). Ultrasonic imaging of electrofusion welded polythene pipes employed in utilities industry.

[5] Starostin, N. P., & Tikhonov, R. S. (2022, February). Thermoelastic state during electrofusion welding of polyethylene pipes at different ambient temperatures. In *IOP Conference Series: Earth and Environmental Science* (Vol. 991, No. 1, p. 012011). IOP Publishing.

[6] Sarambale, D. S., & Shinde, D. K. (2017). Electro-Fusion Joint Failure Polyethylene Pipes Analysis and its Simulation using Finite Element Analysis. *International Journal of Mechanical and Production Engineering*, *5*(12), 51-55.

[7] Tutunchi, A., Eskandarzade, M., Aghamohammadi, R., Masalehdan, T., & Osouli-Bostanabad, K. (2022). Risk assessment of electrofusion joints in commissioning of polyethylene natural gas networks. *International Journal of Pressure Vessels and Piping*, *196*, 104627.

[8] Doan, H. G. (2019). Development of Automated Tape Winding Setup for Thermoplastic Fibre Reinforced Polymer Composites and Bi-Axial Creep Testing Setup for Tubular Coupons.

[9] Chandrasekaran, S., Ramanathan, S., & Basak, T. (2013). Microwave food processing—A review. *Food research international*, *52*(1), 243-261.

[10] Naik, T. P., Singh, I., & Sharma, A. K. (2022). Processing of polymer matrix composites using microwave energy: A review. *Composites Part A: Applied Science and Manufacturing*, 106870.

[11] Mishra, R. R., & Sharma, A. K. (2016). Microwave–material interaction phenomena: Heating mechanisms, challenges and opportunities in material processing. *Composites Part A: Applied Science and Manufacturing*, *81*, 78-97.

[12] Clark, D. E., Folz, D. C., & West, J. K. (2000). Processing materials with microwave energy. *Materials Science and Engineering: A*, *287*(2), 153-158.

[13] Matli, P. R., Shakoor, R. A., Amer Mohamed, A. M., & Gupta, M. (2016). Microwave rapid sintering of Al-metal matrix composites: a review on the effect of reinforcements, microstructure and mechanical properties. *Metals*, *6*(7), 143.

[14] Cheng, J., Agrawal, D., Zhang, Y., & Roy, R. (2002). Microwave sintering of transparent alumina. *Materials Letters*, *56*(4), 587-592.

[15] Singh, A., & Sharma, A. K. (2020). On microwave drilling of metal-based materials at 2.45 GHz. *Applied Physics A*, *126*(10), 1-11.

[16] Lautre, N. K., Sharma, A. K., Kumar, P., & Das, S. (2014). Microwave drilling with Litz wire using a domestic applicator. *Bonfring International Journal of Industrial Engineering and Management Science*, *4*(3), 125-131.

[17] George, T. J., Sharma, A. K., & Kumar, P. (2014). Experimental Study and Simulation on Microwave Drilling of Metals and Glasses. *microwaves*, *12*, 13.

[18] Zafar, S., & Sharma, A. K. (2014). Development and characterisations of WC–12Co microwave clad. *Materials Characterization*, *96*, 241-248.

[19] Gupta, D., & Sharma, A. K. (2011). Development and microstructural characterization of microwave cladding on austenitic stainless steel. *Surface and Coatings Technology*, *205*(21-22), 5147-5155.

[20] Mishra, R. R., & Sharma, A. K. (2016). On mechanism of in-situ microwave casting of aluminium alloy 7039 and cast microstructure. *Materials & Design*, *112*, 97-106.

[21] Mishra, R. R., & Sharma, A. K. (2016). A review of research trends in microwave processing of metal-based materials and opportunities in microwave metal casting. *Critical Reviews in Solid State and Materials Sciences*, *41*(3), 217-255.

[22] Srinath, M. S., Sharma, A. K., & Kumar, P. (2011). A new approach to joining of bulk copper using microwave energy. *Materials & Design*, *32*(5), 2685-2694.

[23] Srinath, M. S., Sharma, A. K., & Kumar, P. (2011). Investigation on microstructural and mechanical properties of microwave processed dissimilar joints. *Journal of Manufacturing Processes*, *13*(2), 141-146.

[24] Naik, T. P., Singh, I., & Sharma, A. K. (2022). Processing of polymer matrix composites using microwave energy: A review. *Composites Part A: Applied Science and Manufacturing*, 106870.

[25] Singh, M. K., & Zafar, S. (2020). Influence of microwave power on mechanical properties of microwave-cured polyethylene/coir composites. *Journal of Natural Fibers*, *17*(6), 845-860.

[26] Bajpai, P. K., Singh, I., & Madaan, J. (2012). Joining of natural fiber reinforced composites using microwave energy: Experimental and finite element study. *Materials & Design*, *35*, 596-602.

[27] Metaxas, A. A., & Meredith, R. J. (1983). *Industrial microwave heating* (No. 4). Institution of Electrical Engineers (IET).

[28] McQuarrie, D. A., & Simon, J. D. (1997). *Physical chemistry: a molecular approach* (Vol. 1). Sausalito, CA: University science books.

[29] Osepchuk, J. M. (1984). A history of microwave heating applications. *IEEE Transactions on Microwave theory and Techniques*, *32*(9), 1200-1224.

[30] Agazzi, A., & Pirola, C. (2000). Fundamentals, methods and future trends of environmental microwave sample preparation. *Microchemical Journal*, *67*(1-3), 337-341.

[31] Kubrakova, I. V., & Toropchenova, E. S. (2008). Microwave heating for enhancing efficiency of analytical operations. *Inorganic Materials*, *44*(14), 1509-1519.

[32] Robinson, J., Kingman, S., Irvine, D., Licence, P., Smith, A., Dimitrakis, G., ... & Kappe, C. O. (2010). Understanding microwave heating effects in single mode type cavities—theory and experiment. *Physical Chemistry Chemical Physics*, *12*(18), 4750-4758.

[33] Mello, P. A., Barin, J. S., & Guarnieri, R. A. (2014). Microwave heating. In *Microwave-Assisted Sample Preparation for Trace Element Analysis* (pp. 59-75). Elsevier.

[34] Vollmer, M. (2004). Physics of the microwave oven. *Physics Education*, *39*(1), 74.

[35] Loharkar, P. K., Ingle, A., & Jhavar, S. (2019). Parametric review of microwave-based materials processing and its applications. *Journal of Materials Research and Technology*, *8*(3), 3306-3326.

[36] Varith, J., Noochuay, C., Netsawang, P., Hirunstitporn, B., Janin, S., & Krairiksh, M. (2007, December). Design of multimode-circular microwave cavity for agri-food processing. In *2007 Asia-Pacific Microwave Conference* (pp. 1-4). IEEE.

[37] Jeon, S., Kim, J., & Yang, D. (2022). Design of Large-Scale Microwave Cavity for Uniform and Efficient Plastic Heating. *Polymers*, *14*(3), 541.

[38] Franzi, M., Wang, J., Dolgashev, V., & Tantawi, S. (2016). Compact rf polarizer and its application to pulse compression systems. *Physical Review Accelerators and Beams*, *19*(6), 062002.

[39] Kwak, M., Robinson, P., Bismarck, A., & Wise, R. (2011, August). Curing of composite materials using the recently developed hephaistos microwave. In *18th international conference on composite materials* (pp. 21-26).

[40] Kwak, M., Robinson, P., Bismarck, A., & Wise, R. (2015). Microwave curing of carbon–epoxy composites: penetration depth and material characterisation. *Composites Part A: applied science and manufacturing*, *75*, 18-27.

[41] Chaturvedi, P. K. (2018). *Microwave, Radar & RF Engineering: With Laboratory Manual*. Springer.

[42] Rana, K. K., & Rana, S. (2014). Microwave reactors: A brief review on its fundamental aspects and applications. *Open Access Library Journal*, *1*(6), 1-20.

[43] Gupta, M., & Eugene, W. W. L. (2011). Microwaves—Theory. *Microwaves and Metals; John Wiley & Sons (Asia) Pte Ltd.: Singapore*, 25-41.

[44] Mishra, R. R., & Sharma, A. K. (2016). Microwave–material interaction phenomena: Heating mechanisms, challenges and opportunities in material processing. *Composites Part A: Applied Science and Manufacturing*, *81*, 78-97.

[45] Clarricoats, P. J. B. (1967). Foundations for microwave engineering. *Electronics and Power*, *13*(1), 29.

[46] Zhang, H., & Datta, A. K. (2003). Microwave power absorption in single-and multiple-item foods. *Food and bioproducts processing*, *81*(3), 257-265.

[47] Ku, H. S., Siu, F., Siores, E., Ball, J. A. R., & Blicblau, A. S. (2001). Applications of fixed and variable frequency microwave (VFM) facilities in polymeric materials processing and joining. *Journal of Materials Processing Technology*, *113*(1-3), 184-188.

[48] Sturm, G. S. J., Stefanidis, G. D., Verweij, M. D., Van Gerven, T. D. T., & Stankiewicz, A. I. (2010). Design principles of microwave applicators for small-scale process equipment. *Chemical Engineering and Processing: Process Intensification*, *49*(9), 912-922.

[49] Thostenson, E. T., & Chou, T. W. (1999). Microwave processing: fundamentals and applications. *Composites Part A: Applied Science and Manufacturing*, *30*(9), 1055-1071.

[50] Cha-um, W., Rattanadecho, P., & Pakdee, W. (2009). Experimental analysis of microwave heating of dielectric materials using a rectangular wave guide (MODE: TE10) (Case study: Water layer and saturated porous medium). *Experimental Thermal and Fluid Science*, *33*(3), 472-481.

[51] Saltiel, C., & Datta, A. K. (1999). Heat and mass transfer in microwave processing. In *Advances in heat transfer* (Vol. 33, pp. 1-94). Elsevier.

[52] Yang, H. W., & Gunasekaran, S. (2001). Temperature profiles in a cylindrical model food during pulsed microwave heating. *Journal of Food Science*, *66*(7), 998-1004.

[53] Ayappa, K. G., Davis, H. T., Davis, E. A., & Gordon, J. (1991). Analysis of microwave heating of materials with temperature-dependent properties. *Aiche journal*, *37*(3), 313-322.

[54] Moulson, A. J., & Herbert, J. M. Electroceramics: materials, properties, applications, 2003.

[55] Sparks, M., Loudon, R., & Kittel, C. (1961). Ferromagnetic relaxation. I. Theory of the relaxation of the uniform precession and the degenerate spectrum in insulators at low temperatures. *Physical Review*, *122*(3), 791.

[56] Bizzi, C. A., Barin, J. S., Hermes, A. L., Mortari, S. R., & Flores, É. M. (2011). A fast microwave-assisted procedure for loss on drying determination in saccharides. *Journal of the Brazilian Chemical Society*, *22*, 376-381.

[57] Meir, Y., & Jerby, E. (2012). Localized rapid heating by low-power solid-state microwave drill. *IEEE transactions on microwave theory and techniques*, *60*(8), 2665-2672.

[58] Zlotorzynski, A. (1995). The application of microwave radiation to analytical and environmental chemistry. *Critical Reviews in Analytical Chemistry*, *25*(1), 43-76.

[59] Machmudah, S., Kanda, H., & Goto, M. (2017). Hydrolysis of biopolymers in near-critical and subcritical water. In *Water Extraction of Bioactive Compounds* (pp. 69-107). Elsevier.

[60] Museok, K. (2016). Microwave curing of carbon-epoxy composites: Process development and material evaluation. *London: Imperial College London, Department of Aeronautics*, *150*.

[61] Ku, H., Chan, W. L., Trada, M., & Baddeley, D. (2007). An evaluation of fracture toughness of vinyl ester composites cured under microwave conditions. *Journal of Materials Engineering and Performance*, *16*(6), 741-745.

[62] Boey, F. Y. C. (1995). Humidity and autoclave pressure effect on the interfacial shear strength of a microwave cured epoxy-glass fibre composite. *Polymer testing*, *14*(5), 471-477.

[63] Naik, T. P., Rana, R. S., Singh, I., & Sharma, A. K. (2021). Microwave Processing of Polymer Matrix Composites: Review of the Understanding and Future Opportunities. *Recent Advances in Mechanical Engineering*, 517-529.

[64] Chen, M., Siochi, E. J., Ward, T. C., & McGrath, J. E. (1993). Basic ideas of microwave processing of polymers. *Polymer Engineering & Science*, *33*(17), 1092-1109.

[65] Zong, L., Zhou, S., Sgriccia, N., Hawley, M. C., & Kempel, L. C. (2003). A review of microwave-assist polymer chemistry (MAPC). *Journal of microwave power and electromagnetic energy*, *38*(1), 49-74.

[66] Dua, M., & Mertiny, P. (2021, June). Comparison of the Elastic Modulus of Elastomer Clay Nanocomposites Predicted by Various Mechanical Models. In Canadian Society for Mechanical Engineering International Congress (Volume 4).

[67] Singh, A. P., Sharma, M., & Singh, I. (2013). A review of modeling and control during drilling of fiber reinforced plastic composites. *Composites Part B: Engineering*, *47*, 118-125.

[68] Asim, M., Jawaid, M., Saba, N., Nasir, M., & Sultan, M. T. H. (2017). Processing of hybrid polymer composites—a review. *Hybrid polymer composite materials*, 1-22.

[69] Chaitanya, S., Singh, I., & Song, J. I. (2019). Recyclability analysis of PLA/Sisal fiber biocomposites. *Composites Part B: Engineering*, *173*, 106895.

[70] Lila, M. K., Komal, U. K., & Singh, I. (2021). Thermal post-processing of bagasse fiber reinforced polypropylene composites. *Composites Communications*, *23*, 100546.

[71] Li, N., Li, Y., Jelonnek, J., Link, G., & Gao, J. (2017). A new process control method for microwave curing of carbon fibre reinforced composites in aerospace applications. *Composites Part B: Engineering*, *122*, 61-70.

[72] Mohamadi, M., Kowsari, E., Yousefzadeh, M., Chinnappan, A., & Ramakrishna, S. (2020). Highly-efficient microwave absorptivity in reduced graphene oxide modified with PTA@ imidazolium based dicationic ionic liquid and fluorine atom. *Composites Science and Technology*, *188*, 107960.

[73] Kravchenko, O. G., Solouki Bonab, V., & Manas-Zloczower, I. (2019). Spray-Assisted Microwave Welding of Thermoplastics Using Carbon Nanostructures with Enabled Health Monitoring. *Polymer Engineering & Science*, *59*(11), 2247-2254.

[74] Palanisamy, C., Selearajen, S. K., & Siva, K. (2018). Comparative Study on Microwave and Conventional Joining of Thermoplastic. In *Solid State Phenomena* (Vol. 280, pp. 277-283). Trans Tech Publications Ltd.

[75] Sweeney, C. B., Lackey, B. A., Pospisil, M. J., Achee, T. C., Hicks, V. K., Moran, A. G., ... & Green, M. J. (2017). Welding of 3D-printed carbon nanotube–polymer composites by locally induced microwave heating. *Science advances*, *3*(6), e1700262.

[76] Poyraz, S., Zhang, L., Schroder, A., & Zhang, X. (2015). Ultrafast microwave welding/reinforcing approach at the interface of thermoplastic materials. *ACS applied materials & interfaces*, *7*(40), 22469-22477.

[77] Farahani, R. D., Tavares, J., & Dubé, M. (2015, July). Carbon Nanotube-Based Conductive Films for Welding of Thermoplastic Polymers. In 20th International Conference on Composite Materials (pp. 19–24).

[78] Yussuf, A. A., Sbarski, I., Hayes, J. P., Tran, N., & Solomon, M. (2004). Rapid microwave welding of two polymethylmethacrylate (PMMA) substrates. In *ANTEC conference proceedings* (Vol. 1, pp. 1256-1260). Society of Plastics Engineers.

[79] Ku, H. S., Lee, K. F., & Li, C. W. (2003). Thermal analysis comparison between two random glass fibre reinforced thermoplastic matrix composites bonded by adhesives using microwaves: preliminary results. *Journal of electromagnetic waves and applications*, *17*(6), 901-919.

[80] Wise, R. J., & Froment, I. D. (2001). Microwave welding of thermoplastics. *Journal of materials science*, *36*(24), 5935-5954.

[81] Sun, X., Wu, G., Yu, J., & Du, C. (2018). Efficient microwave welding of polypropylene using graphite coating as primers. *Materials Letters*, *220*, 245-248.

[82] Yarlagadda, P. K., & Cheok, E. C. (1999). Study on the microwave curing of adhesive joints using a temperature-controlled feedback system. *Journal of materials processing technology*, *91*(1-3), 128-149.

[83] Wu, C. Y., & Benatar, A. (1997). Microwave welding of high density polyethylene using intrinsically conductive polyaniline. *Polymer Engineering & Science*, *37*(4), 738-743.

[84] Wang, C. Y., Chen, T. H., Chang, S. C., Cheng, S. Y., & Chin, T. S. (2007). Strong carbon-nanotube–polymer bonding by microwave irradiation. *Advanced Functional Materials*, *17*(12), 1979-1983.

[85] Gangurde, L. S., Sturm, G. S., Devadiga, T. J., Stankiewicz, A. I., & Stefanidis, G. D. (2017). Complexity and challenges in noncontact high temperature measurements in microwave-assisted catalytic reactors. *Industrial & engineering chemistry research*, *56*(45), 13379-13391.

[86] Yang, H., Yan, B., Meng, L., Jiao, X., Huang, J., Gao, W., ... & Fan, D. (2022). Mathematical modeling of continuous microwave heating of surimi paste. *Journal of Food Engineering*, *315*, 110797.

[87] Campañone, L. A., Paola, C. A., & Mascheroni, R. H. (2012). Modeling and simulation of microwave heating of foods under different process schedules. *Food and Bioprocess Technology*, *5*(2), 738-749.

[88] Vaz, R. H., Pereira, J. M., Ervilha, A. R., & Pereira, J. C. (2014). Simulation and uncertainty quantification in high temperature microwave heating. *Applied Thermal Engineering*, *70*(1), 1025-1039.

[89] Salema, A. A., & Afzal, M. T. (2015). Numerical simulation of heating behaviour in biomass bed and pellets under multimode microwave system. *International Journal of thermal sciences*, *91*, 12-24.

[90] Chen, H., Li, T., Wang, Z., Ye, R., & Li, Q. (2020). Effect of dielectric properties on heat transfer characteristics of rubber materials via microwave heating. *International Journal of Thermal Sciences*, *148*, 106162.

[91] Lin, B., Li, H., Chen, Z., Zheng, C., Hong, Y., & Wang, Z. (2017). Sensitivity analysis on the microwave heating of coal: A coupled electromagnetic and heat transfer model. *Applied Thermal Engineering*, *126*, 949-962.

[92] Srinath, M. S., Murthy, P. S., Sharma, A. K., Kumar, P., & Kartikeyan, M. V. (2012). Simulation and analysis of microwave heating while joining bulk copper. *International Journal of Engineering, Science and Technology*, *4*(2), 152-158.

[93] Thakur, A., & Bedi, R. (2022). Influence of process parameters on microwave joining of the similar/dissimilar materials: A review. *Materials Today: Proceedings*.

[94] Santhosi, B. V. S. R. N., Ramji, K., Rao, N. M., Nagaraju, D., & Naidu, M. K. (2022). Microwave absorption analysis of graphene-based hybrid nanocomposites: experimental, numerical and component level testing studies. *Plastics, Rubber and Composites*, 1-16.

[95] Ali, S., Bajpai, P. K., Singh, I., & Sharma, A. K. (2014). Curing of natural fibre-reinforced thermoplastic composites using microwave energy. *Journal of Reinforced Plastics and Composites*, *33*(11), 993-999.

[96] Pitchai, K., Chen, J., Birla, S., Jones, D., & Subbiah, J. (2016). Modeling microwave heating of frozen mashed potato in a domestic oven incorporating electromagnetic frequency spectrum. *Journal of Food Engineering*, *173*, 124-131.

[97] Nuhiji, B., Bower, M. P., Swait, T., Phadnis, V., Day, R. J., & Scaife, R. J. (2021). Simulation of carbon fibre composites in an industrial microwave. *Materials Today: Proceedings*, *34*, 82-92.

[98] Singh, I., Bajpai, P. K., Malik, D., Madaan, J., & Bhatnagar, N. (2012). Microwave joining of natural fiber reinforced green composites. In *Advanced materials research* (Vol. 410, pp. 102-105). Trans Tech Publications Ltd.

[99] Jonoobi, M., Harun, J., Mathew, A. P., & Oksman, K. (2010). Mechanical properties of cellulose nanofiber (CNF) reinforced polylactic acid (PLA) prepared by twin screw extrusion. *Composites Science and Technology*, *70*(12), 1742-1747.

[100] Farah, S., Anderson, D. G., & Langer, R. (2016). Physical and mechanical properties of PLA, and their functions in widespread applications—A comprehensive review. *Advanced drug delivery reviews*, *107*, 367-392.

[101] Xue, B., Ye, J., & Zhang, J. (2015). Highly conductive Poly (L-lactic acid) composites obtained via in situ expansion of graphite. *Journal of Polymer Research*, *22*(6), 1-9.

[102] Asmatulu, R., Khan, W. S., Reddy, R. J., & Ceylan, M. (2015). Synthesis and analysis of injection-molded nanocomposites of recycled high-density polyethylene incorporated with graphene nanoflakes. *Polymer Composites*, *36*(9), 1565-1573.

[103] Wang, F., Drzal, L. T., Qin, Y., & Huang, Z. (2015). Mechanical properties and thermal conductivity of graphene nanoplatelet/epoxy composites. *Journal of materials science*, *50*(3), 1082-1093.

[104] Nieto, A., Lahiri, D., & Agarwal, A. (2012). Synthesis and properties of bulk graphene nanoplatelets consolidated by spark plasma sintering. *Carbon*, *50*(11), 4068-4077.

[105] Gu, J., Yang, X., Lv, Z., Li, N., Liang, C., & Zhang, Q. (2016). Functionalized graphite nanoplatelets/epoxy resin nanocomposites with high thermal conductivity. *International Journal of Heat and Mass Transfer*, *92*, 15-22.

[106] Mehrali, M., Latibari, S. T., Mehrali, M., Mahlia, T. M. I., Metselaar, H. S. C., Naghavi, M. S., ... & Akhiani, A. R. (2013). Preparation and characterization of palmitic acid/graphene nanoplatelets composite with remarkable thermal conductivity as a novel shape-stabilized phase change material. *Applied Thermal Engineering*, *61*(2), 633-640.

[107] El Achaby, M., & Qaiss, A. (2013). Processing and properties of polyethylene reinforced by graphene nanosheets and carbon nanotubes. *Materials & Design*, *44*, 81-89.

[108] Botlhoko, O. J., Ramontja, J., & Ray, S. S. (2017). Thermally shocked graphene oxide-containing biocomposite for thermal management applications. *RSC advances*, *7*(54), 33751-33756.

[109] Selvam, C., Mohan Lal, D., & Harish, S. (2017). Thermal conductivity and specific heat capacity of water–ethylene glycol mixture-based nanofluids with graphene nanoplatelets. *Journal of Thermal Analysis and Calorimetry*, *129*(2), 947-955.

[110] Zhang, Q. (2020). *Fabricating and Characterizing Multifunctional Graphene Nanoplatelets-based Polylactide Nanocomposites*. [Master's thesis, University of Alberta]. Education and Research Archive (ERA)

[111] Zhang, Q., & Mertiny, P. Effect of Graphene Nanoplatelet Addition on the Conductive Behavior of Solution Mixing Processed Polylactide Biopolymer Nanocomposites. In *ASME 2019 International Mechanical Engineering Congress and Exposition*. American Society of Mechanical Engineers Digital Collection.

[112] Bradshaw, S., Delport, S., & Wyk, E. V. (1997). Qualitative measurement of heating uniformity in a multimode microwave cavity. *Journal of microwave power and electromagnetic energy*, *32*(2), 87-95.

[113] Kalinke, I., Kubbutat, P., Taghian Dinani, S., Ambros, S., Ozcelik, M., & Kulozik, U. (2022). Critical assessment of methods for measurement of temperature profiles and heat load history in microwave heating processes—A review. *Comprehensive reviews in food science and food safety*.

[114] ASTM International. (2011. Reapproved, 2018). *Standard test method for determining specific heat capacity by differential scanning calorimetry* (ASTM E1269-11). Retrieved from https://www.astm.org/e1269-11r18.html

[115] International Organization for Standardization (ISO), Switzerland. (2015). *Plastics – determination of thermal conductivity and thermal diffusivity – Part 2: transient plane heat source (hot disc) method* (ISO 22007-2: 2015). Retrieved from https://www.iso.org/standard/61190.html

[116] *RF Module User's Guide.* (2017). COMSOL Multiphysics.

https://doc.comsol.com/5.3/doc/com.comsol.help.rf/RFModuleUsersGuide.pdf

[117] James, J. R. (1991). The Principles of Electromagnetic Theory. *Electronics & Communication Engineering Journal*, *3*(6), 290-290.

[118] *Microwave Oven*. COMSOL Multiphysics.

https://cds.comsol.com/model/download/953961/models.rf.microwave_oven.pdf?__gda__=1659600706_8a7750178d249ad119a98a574f8036ef&fileExt=.pdf

[119] Pitchai, K., Birla, S. L., Subbiah, J., Jones, D., & Thippareddi, H. (2012). Coupled electromagnetic and heat transfer model for microwave heating in domestic ovens. *Journal of Food Engineering*, *112*(1-2), 100-111.

[120] Kashi, S., Gupta, R. K., Baum, T., Kao, N., & Bhattacharya, S. N. (2016). Morphology, electromagnetic properties and electromagnetic interference shielding performance of poly lactide/graphene nanoplatelet nanocomposites. *Materials & Design*, *95*, 119-126.

[121] Haleem, A., Kumar, V., & Kumar, L. (2017). Mathematical modelling & pressure drop analysis of fused deposition modelling feed wire. *Int. J. Eng. Technol*, *9*(4), 2885-2894.

[122] Zmeskal, O., Marackova, L., Lapcikova, T., Mencik, P., & Prikryl, R. (2020, November). Thermal properties of samples prepared from polylactic acid by 3D printing. In *AIP Conference Proceedings* (Vol. 2305, No. 1, p. 020022). AIP Publishing LLC.

[123] Ruan, K., Guo, Y., & Gu, J. (2021). Liquid crystalline polyimide films with high intrinsic thermal conductivities and robust toughness. *Macromolecules*, *54*(10), 4934-4944.

[124] Lin, H., Pei, L., & Zhang, L. (2018). Enhanced thermal conductivity of PLA-based nanocomposites by incorporation of graphite nanoplatelets functionalized by tannic acid. *Journal of Applied Polymer Science*, *135*(26), 46397.

[125] Uyor, U. O., Popoola, A. P., Popoola, O., & Aigbodion, V. S. (2018). Energy storage and loss capacity of graphene-reinforced poly (vinylidene fluoride) nanocomposites from electrical and dielectric properties perspective: a review. *Advances in Polymer Technology*, *37*(8), 2838-2858.

[126] Guo, R., Ren, Z., Bi, H., Xu, M., & Cai, L. (2019). Electrical and thermal conductivity of polylactic acid (PLA)-based biocomposites by incorporation of nano-graphite fabricated with fused deposition modeling. *Polymers*, *11*(3), 549.

[127] Pan, Y., Yang, B., Jia, N., Yu, Y., Xu, X., Wang, Y., ... & Fang, Y. (2021). Enhanced Thermally Conductive and Microwave Absorbing Properties of Polymethyl Methacrylate/Ni@ GNP Nanocomposites. *Industrial & Engineering Chemistry Research*, *60*(33), 12316-12327.

[128] Chang, J., Liang, G., Gu, A., Cai, S., & Yuan, L. (2012). The production of carbon nanotube/epoxy composites with a very high dielectric constant and low dielectric loss by microwave curing. *Carbon*, *50*(2), 689-698.

[129] Kashi, S., Gupta, R. K., Baum, T., Kao, N., & Bhattacharya, S. N. (2016). Morphology, electromagnetic properties and electromagnetic interference shielding performance of poly lactide/graphene nanoplatelet nanocomposites. *Materials & Design*, *95*, 119-126.

[130] He, F., Lau, S., Chan, H. L., & Fan, J. (2009). High dielectric permittivity and low percolation threshold in nanocomposites based on poly (vinylidene fluoride) and exfoliated graphite nanoplates. *Advanced Materials*, *21*(6), 710-715.

[131] Ameli, A., Jung, P. U., & Park, C. B. (2013). Electrical properties and electromagnetic interference shielding effectiveness of polypropylene/carbon fiber composite foams. *Carbon*, *60*, 379-391.

[132] Kashi, S., Gupta, R. K., Baum, T., Kao, N., & Bhattacharya, S. N. (2016). Dielectric properties and electromagnetic interference shielding effectiveness of graphene-based biodegradable nanocomposites. *Materials & Design*, *109*, 68-78.

[133] Kashi, S., Gupta, R. K., Kao, N., Hadigheh, S. A., & Bhattacharya, S. N. (2018). Influence of graphene nanoplatelet incorporation and dispersion state on thermal, mechanical and electrical properties of biodegradable matrices. *Journal of materials science & technology*, *34*(6), 1026-1034.

[134] Phang, S. W., Tadokoro, M., Watanabe, J., & Kuramoto, N. (2008). Microwave absorption behaviors of polyaniline nanocomposites containing TiO2 nanoparticles. *Current Applied Physics*, *8*(3-4), 391-394.

[135] Gupta, A., & Choudhary, V. (2011). Electromagnetic interference shielding behavior of poly (trimethylene terephthalate)/multi-walled carbon nanotube composites. *Composites Science and Technology*, *71*(13), 1563-1568.

[136] Lee, S. E., Choi, O., & Hahn, H. T. (2008). Microwave properties of graphite nanoplatelet/epoxy composites. *Journal of Applied Physics*, *104*(3), 033705.

[137] Wu, Y., Lin, X., Shen, X., Sun, X., Liu, X., Wang, Z., & Kim, J. K. (2015). Exceptional dielectric properties of chlorine-doped graphene oxide/poly (vinylidene fluoride) nanocomposites. *Carbon*, *89*, 102-112.

[138] Chu, L., Xue, Q., Sun, J., Xia, F., Xing, W., Xia, D., & Dong, M. (2013). Porous graphene sandwich/poly (vinylidene fluoride) composites with high dielectric properties. *Composites science and technology*, *86*, 70-75.

[139] Wang, D., Zhou, T., Zha, J. W., Zhao, J., Shi, C. Y., & Dang, Z. M. (2013). Functionalized graphene–BaTiO 3/ferroelectric polymer nanodielectric composites with high permittivity, low dielectric loss, and low percolation threshold. *Journal of materials Chemistry A*, *1*(20), 6162-6168.

[140] Omran, M., Fabritius, T., Chen, G., & He, A. (2019). Microwave absorption properties of steelmaking dusts: effects of temperature on the dielectric constant (ε′) and loss factor (ε″) at 1064 MHz and 2423 MHz. *RSC advances*, *9*(12), 6859-6870.

[141] Wang, Z., Luo, J., & Zhao, G. L. (2014). Dielectric and microwave attenuation properties of graphene nanoplatelet–epoxy composites. *AIP Advances*, *4*(1), 017139.

[142] Littlefield, A. G., Bartolucci, S. F., & Maurer, J. A. (2018, May). Graphene-Peek Composites as Microwave-Activated High-Temperature Adhesives. In SAMPE's 2018 Spring Technical Conference and Exhibition.

[143] Han, Z., Li, Y., Luo, D. H., Zhao, Q., Cheng, J. H., & Wang, J. H. (2021). Structural variations of rice starch affected by constant power microwave treatment. *Food Chemistry*, *359*, 129887.

[144] Geedipalli, S. S. R., Rakesh, V., & Datta, A. K. (2007). Modeling the heating uniformity contributed by a rotating turntable in microwave ovens. *Journal of Food Engineering*, *82*(3), 359-368.

[145] Wang, S., Hu, Z., Han, Y., & Gu, Z. (2013). Effects of magnetron arrangement and power combination of microwave on drying uniformity of carrot. *Drying Technology*, *31*(11), 1206-1211.

[146] Hurayra–Lizu, K. A., Bari, M. W., Gulshan, F., & Islam, M. R. (2021). GO based PVA nanocomposites: tailoring of optical and structural properties of PVA with low percentage of GO nanofillers. *Heliyon*, *7*(5), e06983.

[147] Cao, M. S., Song, W. L., Hou, Z. L., Wen, B., & Yuan, J. (2010). The effects of temperature and frequency on the dielectric properties, electromagnetic interference shielding and microwave-absorption of short carbon fiber/silica composites. *Carbon*, *48*(3), 788-796.

[148] Z. Wang *et al.*, "Dielectric Studies of Al Nanoparticle Reinforced Epoxy Resin Composites," no. 14, 2018, doi: 10.1002/pc.24012.

[149] Liu, K., Xu, X., & Zhang, B. (2021). Characterization and simulation of the nonlinear thermal field of the aramid/bismaleimide composites caused by the dielectric heating effects of the microwave radiations. *Polymer Composites*, *42*(5), 2565-2573.

[150] Ghezghapan, S., (2022). *Graphene Oxide-Thermoplastic Nanocomposites: Fabrication and Properties*. [Doctoral dissertation, Clemson University]. TigerPrints.

[151] Devi, N., Kumar, R., & Singh, R. K. (2019). Microwave-assisted modification of graphene and its derivatives: Synthesis, reduction and exfoliation. In *Graphene Functionalization Strategies* (pp. 279-311). Springer, Singapore.

[152] Spinelli, G., Giustiniani, A., Lamberti, P., Tucci, V., & Zamboni, W. (2012). Numerical study of electrical behaviour in carbon nanotube composites. *International Journal of Applied Electromagnetics and Mechanics*, *39*(1-4), 21-27.

[153] Bychanok, D., Angelova, P., Paddubskaya, A., Meisak, D., Shashkova, L., Demidenko, M., ... & Kuzhir, P. (2018). Terahertz absorption in graphite nanoplatelets/polylactic acid composites. *Journal of Physics D: Applied Physics*, *51*(14), 145307.

[154] Xu, X., Wang, X., Cai, Q., Wang, X., Wei, R., & Du, S. (2016). Improvement of the compressive strength of carbon fiber/epoxy composites via microwave curing. *Journal of Materials Science & Technology*, *32*(3), 226-232.

[155] Galindo, B., Benedito, A., Gimenez, E., & Compañ, V. (2016). Comparative study between the microwave heating efficiency of carbon nanotubes versus multilayer graphene in polypropylene nanocomposites. *Composites Part B: Engineering*, *98*, 330-338.

[156] Mgbemena, C. O., Li, D., Lin, M. F., Liddel, P. D., Katnam, K. B., Thakur, V. K., & Nezhad, H. Y. (2018). Accelerated microwave curing of fibre-reinforced thermoset polymer composites for structural applications: A review of scientific challenges. *Composites Part A: Applied Science and Manufacturing*, *115*, 88-103.

[157] Salvi, D., Boldor, D., Aita, G. M., & Sabliov, C. M. (2011). COMSOL Multiphysics model for continuous flow microwave heating of liquids. *Journal of food engineering*, *104*(3), 422-429.

[158] Ivanov, E., Kotsilkova, R., Xia, H., Chen, Y., Donato, R. K., Donato, K., ... & Angelov, V. (2019). PLA/Graphene/MWCNT composites with improved electrical and thermal properties suitable for FDM 3D printing applications. *Applied Sciences*, *9*(6), 1209.

[159] Christie, M. A., Glimm, J., Grove, J. W., Higdon, D. M., Sharp, D. H., & Wood-Schultz, M. M. (2005). Error analysis and simulations of complex phenomena. *Los Alamos Science*, *29*(6).

[160] Yakovlev, V. V. (2006). Examination of contemporary electromagnetic software capable of modeling problems of microwave heating. In *Advances in Microwave and Radio Frequency Processing* (pp. 178-190). Springer, Berlin, Heidelberg.

[161] Bi, S., Su, X., Hou, G., Liu, C., Song, W. L., & Cao, M. S. (2013). Electrical conductivity and microwave absorption of shortened multi-walled carbon nanotube/alumina ceramic composites. *Ceramics International*, *39*(5), 5979-5983.

[162] Pickles, C. A. (2009). Microwaves in extractive metallurgy: Part 2–A review of applications. *Minerals Engineering*, *22*(13), 1112-1118.

[163] Akinwekomi, A. D., Yeung, K. W., Tang, C. Y., Law, W. C., & Tsui, G. C. P. (2020). Finite element simulation of hybrid microwave sintering based on power approach. *The International Journal of Advanced Manufacturing Technology*, *110*(9), 2503-2515.

[164] Cardenia, C., Balomenos, E., & Panias, D. (2020). Optimization of Microwave Reductive Roasting Process of Bauxite Residue. *Metals*, *10*(8), 1083.

[165] Borrell, A., & Salvador, M. D. (2018). Advanced ceramic materials sintered by microwave technology. *Sinter. Technol. Method Appl*, 3-24.

Appendices

This section includes images of melted samples and thermographs.

Appendix A : Melted Samples

Figure 34: Melted PLA sample

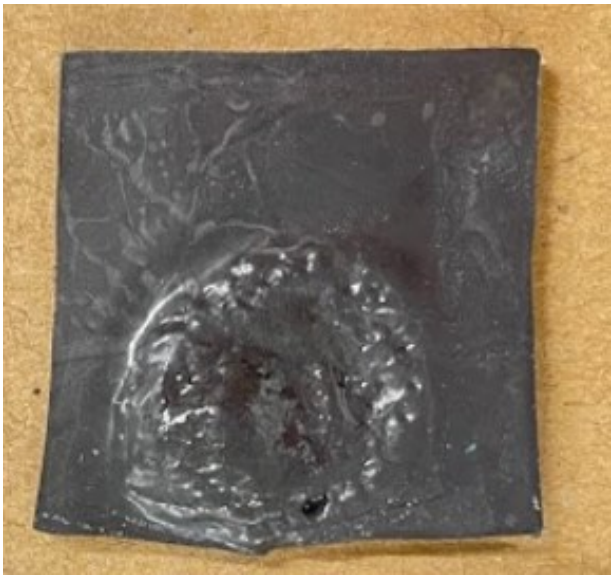

Figure 35: Melted 4-pGNP/PLA sample

Figure 36: Melted 8-pGNP/PLA sample

Figure 37: Melted 1-fGNP/PLA sample

Figure 38: Melted 4-fGNP/PLA sample

Figure 39: Melted 8-fGNP/PLA sample

Appendix B : Thermographs of Samples

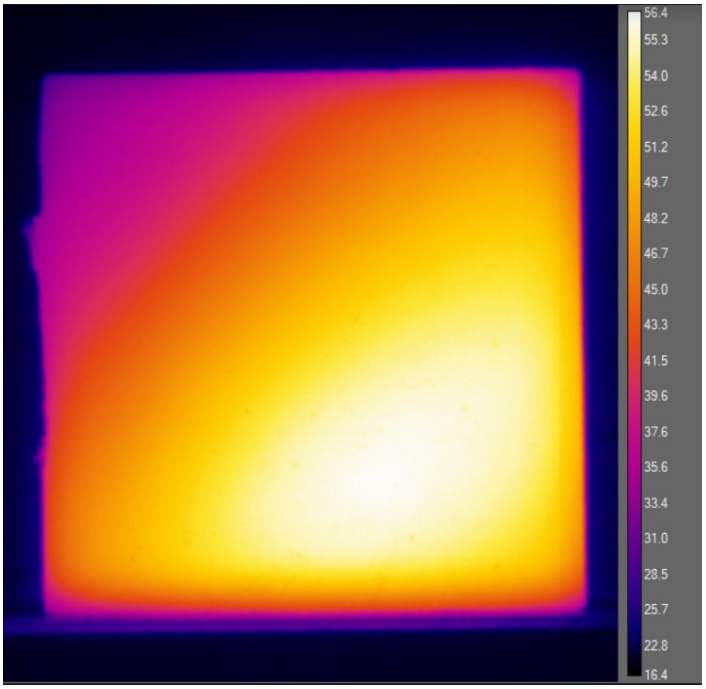

Figure 40: Thermograph of PLA sample when heated at 1.2 kW for 90 seconds

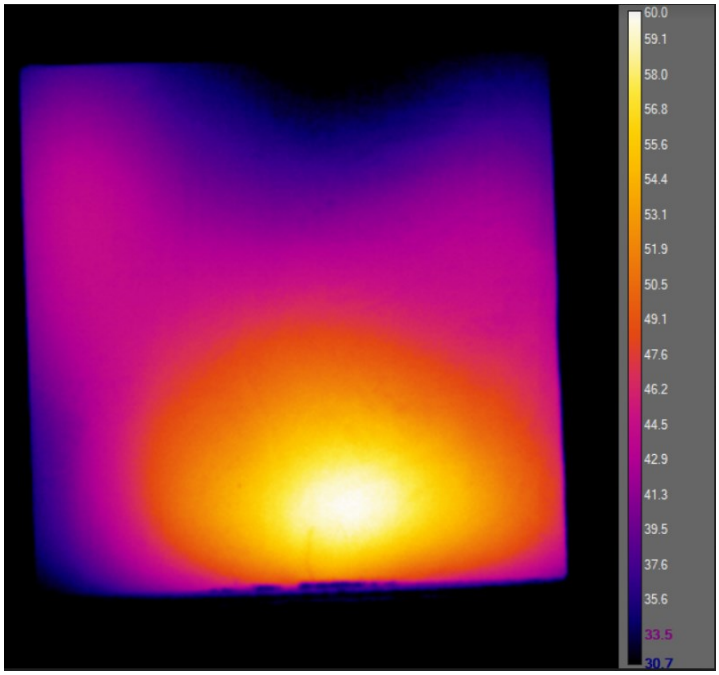

Figure 41: Thermograph of 4-pGNP/PLA sample when heated at 0.6 kW for 10 seconds

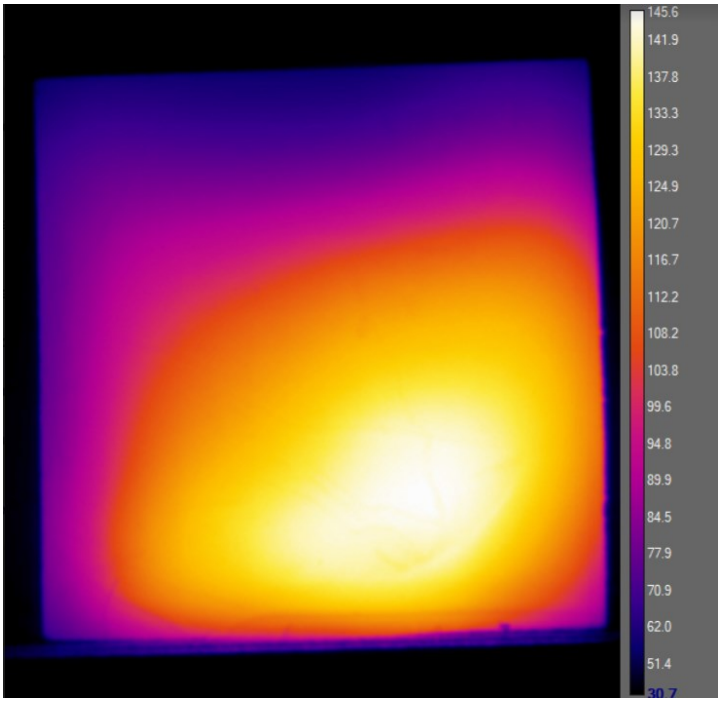

Figure 42: Thermograph of 4-fGNP/PLA sample when heated at 1.2 kW for 15 seconds

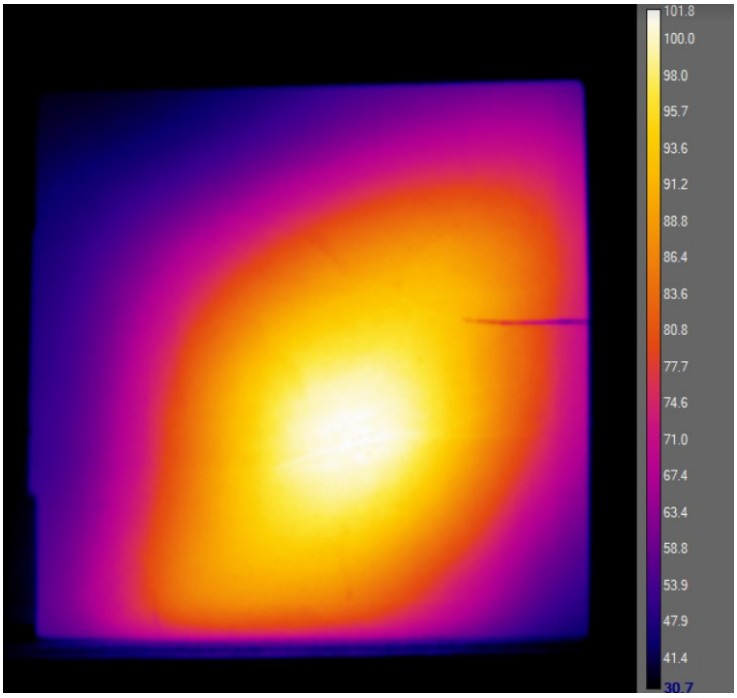

Figure 43: Thermograph of 8-pGNP/PLA sample when heated at 0.6 kW for 4 seconds

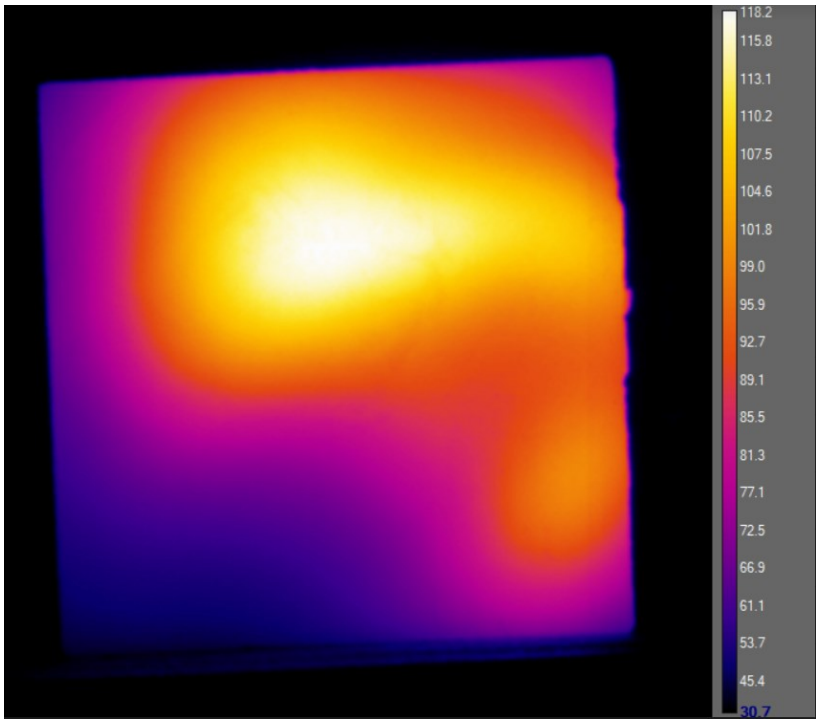

Figure 44: Thermograph of 8-fGNP/PLA sample when heated at 1.2 kW for 8 seconds